E-7111

NASA
Technical
Paper
3247

March 1993

Analytical and Experimental Studies of a Short Compact Subsonic Diffuser for a Two-Dimensional Supersonic Inlet

Chanthy Iek,
Richard R. Burley,
and Albert L. Johns

NASA

NASA
Technical
Paper
3247

1993

Analytical and Experimental Studies of a Short Compact Subsonic Diffuser for a Two-Dimensional Supersonic Inlet

Chanthy Iek,
Richard R. Burley,
and Albert L. Johns
Lewis Research Center
Cleveland, Ohio

NASA
National Aeronautics and
Space Administration
Office of Management
Scientific and Technical
Information Program

Summary

An experimental study of a two-dimensional supersonic inlet with a short compact subsonic diffuser, length to exit diameter (dl/d) ratio of 1.25, was conducted to (1) investigate the impact of the short diffuser on inlet performance at low speeds and (2) assess the diffuser subsonic performance for a simulated diffuser flow corresponding to high-speed inlet conditions near the design flight Mach number of 2.2.

For the low-speed testing, a drooped lip was employed to improve the inlet performance at a high angle of attack. For the simulated high-speed testing, air was blown through slots or discrete nozzles as an active boundary-layer control. The results from the low-speed performance test were compared with the results from a previous test program on the same inlet with a long subsonic diffuser (dl/d = 4.5). The comparison indicates that inlet recovery was not affected by the use of the short diffuser for either the baseline (no droop) or the drooped cowl lip configuration. However, the inlet baseline distortion for the short diffuser configuration was substantially higher than for the long diffuser. A comparison of the two configurations with a 70° drooped lip showed no significant difference in distortion. For the portion of the experimental program in which diffuser conditions for high-speed flight were simulated, diffuser-induced flow separation occurred. This separation was predicted from an analytical study that used the Hess potential flow panel method and the Herring two-dimensional boundary-layer analysis computer codes. The flow separated mainly on the diffuser ramp. Subsequent tests in which boundary-control systems were utilized showed that blowing with either slots or discrete nozzles could suppress the flow separation in the short subsonic diffuser, thereby substantially improving the diffuser performance.

Introduction

The development of a highly maneuverable supersonic tactical aircraft will require an advanced, lightweight inlet/diffuser system that gives high performance at static and low subsonic speeds with high angles of incidence as well as at supersonic speeds. As demonstrated in reference 1, when a long subsonic diffuser is used, drooping the cowl lip of a two-dimensional supersonic inlet results in high internal performance at static and low subsonic speeds with high angles of incidence. The inlet cowl lip would be set to the baseline (no droop) position to achieve high performance at supersonic speeds. However, although the long subsonic diffuser helps achieve high performance at supersonic speeds, it is very heavy. The requirement for light weight can be satisfied by using a short subsonic diffuser, but flow separation is more likely in a short diffuser. Such diffuser flow separation can be prevented with a boundary-layer control (BLC) technique such as tangential blowing.

This report presents the results of an experimental investigation to determine the internal performance of the two-dimensional supersonic inlet that was studied with a long diffuser in reference 1; however, in this study, the long subsonic diffuser was replaced by a short subsonic diffuser. The short diffuser was sufficiently short so that (without BLC) significant flow separation would occur when the diffuser was in its high-speed position. Therefore, a BLC tangential blowing system to prevent the flow separation was incorporated into the design of the short diffuser. The effectiveness of blowing through rectangular slots was compared with the effectiveness of blowing through a spanwide array of discrete nozzles. For it to be an effective alternative, the short diffuser must not degrade the high internal performance that was achieved by using the long diffuser at static and low speeds with high angles of attack. Therefore, the effect of the short diffuser on inlet performance at these conditions was also investigated. The two-dimensional inlet was a 43-percent scale model based on the General Electric (GE) F–404 engine.

The test was conducted in the NASA Lewis Research Center's 9– by 15–Foot Low Speed Wind Tunnel (LSWT). The tunnel vacuum system was used to induce airflow through the two-dimensional inlet. For the low-speed investigation, data were taken at static conditions as well as over a range of free-stream Mach numbers from 0.06 to 0.18, and angles-of-attack from 0° to 110°. The internal performance of the short diffuser in its supersonic position was investigated over a range of diffuser entrance Mach numbers from 0.57 to 0.88. A BLC blowing system was operated with blowing pressure ratios (blowing total pressure divided by free-stream total pressure) from 1.0 to 3.4 for slots and from 1.0 to 7.0 for discrete nozzles, and with a blowing temperature ratio (blowing total temperature divided by free-stream total temperature) of 1.0.

In addition, some results from a computational fluid dynamic analysis of the short diffuser are discussed briefly in this report. The computer codes used in this analysis were the Hess potential flow panel method program (ref. 2) and the Herring two-dimensional heat transfer and boundary-layer analysis program (ref. 3). These programs were used to

determine flow separation in the short subsonic diffuser in its high-speed position. Results are presented with no BLC as well as with BLC by tangential blowing.

Symbols

A	flow area, cm^2
BLC	boundary-layer control
C_f	skin friction coefficient
d	diffuser exit diameter, cm
dl	diffuser axial length, cm
H	height of total-pressure rake, cm
h	distance from inlet surface, cm
l	inlet axial length, cm
M	Mach number
NC	distance between the centerline through the nozzle base and the jet-exit plane, cm
ND	nozzle diameter, cm
NH	nozzle height from inlet surface to the centerline of the nozzle jet-exit plane, cm
NS	nozzle spacing between the center of one nozzle jet-exit plane and the center of an adjacent nozzle jet-exit plane, cm
P	pressure, Pa (N/m^2)
P_{T0}	free-stream total pressure, Pa (N/m^2)
P_{T1}	total pressure at the inlet throat, Pa (N/m^2)
P_{T2}	area-weighted engine-face average total pressure based on 104 measured total pressures, Pa (N/m^2)
$P_{T2,avg}$	area-weighted engine-face average total pressure based on 40 measured total pressures, Pa (N/m^2)
$P_{T2,rms}$	engine-face average value pressure turbulence based on eight measured dynamic pressures, Pa (N/m^2)
$P_{T2,avg}/P_{T0}$	engine-face total-pressure recovery
$\frac{P_{T2,max}-P_{T2,min}}{P_{T2,avg}}$	engine-face total-pressure distortion
$P_{T2,rms}/P_{T2}$	engine-face average turbulence
R	radial height of engine-face rake, cm
r	radial distance from the surface of the inlet center body (hub), cm
SH	slot height, cm
SW	slot width, cm
T_w	inlet throat width, cm
W	mass flow rate, kg/sec
X	axial location from inlet leading edge, cm
X_j	axial location from inlet throat to the blowing jet exit plane, cm
Y	vertical location, cm
Z	transverse location, cm
α	angle of attack, deg
β	sideslip angle, deg
ϕ	circumferential position, deg
θ	diffuser wall angle, deg

Subscripts:

avg	average
c	captured
j	blowing jet
max	maximum
min	minimum
rms	root mean square
s	local
T	total
0	free stream
1	inlet throat station
2	engine-face station

Apparatus and Procedure

Test Facility

A two-dimensional inlet with a short subsonic diffuser was tested in the NASA Lewis Research Center's 9– by 15– Foot Low-Speed Wind Tunnel, which is an atmospheric total-pressure facility with a free-stream velocity range to 75 m/sec. The facility is described in detail in reference 4.

Photographs of the inlet model installed in the test section are presented in figures 1 and 2. A photograph of the inlet with the long subsonic diffuser that was used in reference 1 is presented in figure 3. To vary the inlet angle of attack, the model rotated in a horizontal plane about a vertical support

post. The end of the post that came through the tunnel floor was mounted on a swivel joint. The other end of the post that came through the tunnel ceiling was connected to an external flow suction/ducting facility.

Model Geometry

Figure 4 shows a schematic of the model geometry. The two-dimensional inlet is a 43-percent scale model based on the GE F–404 engine. A cylindrical adaptor was inserted between the model and the facility model support rig in order to reduce flow interference that could be induced by the support column (fig. 4(a)). The model was mounted with the ramp leading edge in a vertical position, and the rig was rotated to place the model at any angle-of-attack position between 0° and 110°. The inlet cowl lip knee (fig. 4(b)) had the shape of a circular arc, which allowed the cowl lip to droop up to 70°. The inlet had two external compression ramps. The forward ramp was fixed at 6° from the horizontal axis (fig. 4(c)), and the second ramp could be manually varied from 0° to 15° relative to the first ramp (fig. 4(d)). The short subsonic diffuser incorporated a variable ramp geometry that allowed the diffuser ramp section to be positioned at the correct location relative to the inlet second ramp as shown in figures 4(c) and (d) for the low-speed and high-speed configurations, respectively. Between the inlet second ramp and the subsonic diffuser ramp, a bleed slot was incorporated to provide boundary-layer bleed for supersonic operation. For this test series, the free stream was subsonic even for the simulated high-speed conditions. Therefore, the slot was closed by a plug designed to bridge the two ramps (fig. 4(d)).

The inlet second ramp and the diffuser ramp were set at the maximum throat area for low-speed testing and at the minimum throat area for high-speed simulation testing as shown in figures 4(c) and (d), respectively. The high-speed simulation (Mach 2.2) ramp position, which is necessary to provide high performance at the high Mach number, also assured that flow separation would occur in the short diffuser unless some type of BLC was used. In the low-speed test, the cowl lip was set at three positions, including baseline (0°), 40°, and 70° droop angles. For the high-speed simulation test, a 20° drooped cowl lip was used with the inlet. The drooped lip with the inlet forward ramp formed a two-dimensional-type bellmouth entrance to provide a relatively uniform flow field at the diffuser entrance. Exhaust suction attached to the engine face was then used to set diffuser entrance or inlet throat Mach numbers to simulate conditions that would be obtained in supersonic flight.

Details of the short diffuser geometry are shown in figure 5. Figure 5(a) depicts the change of the diffuser ramp position from low-speed (flight Mach number less than 1.4) to high speed (flight Mach number greater than 1.4). Figures 5(b) and (c) show the variations of the short diffuser centerline and area distributions resulting from this change of the diffuser ramp position.

Figure 6 shows the design parameters of the blowing system used for BLC control. The blowing system, which included either slot or discrete nozzles, was connected to the facility high-pressure air-supply system. Details of the model parts used in the blowing system for the BLC study are presented in figure 7.

Instrumentation

Figures 8 and 9 depict instrumentation used to acquire data during low-speed testing. The inlet cowl lip had 20 static-pressure taps located along its internal and external centerline as shown in figure 8. A total-pressure rake with 10 probes and a static pressure were installed just downstream of the inlet throat section on the cowl side. Positions of individual static- and total-pressure probes are tabulated in table I. Model reference axes are shown in figure 4. Engine-face rakes (fig. 9) were located at the diffuser exit. Eight rakes were equally spaced with the 0° position designated to be the rake location on the cowl centerline. Each rake contained 13 total-pressure probes. Five of these probes were equally area weighted (standard arrangement). The remaining probes in each rake were located at the ends to better define the boundary layer. In addition, two dynamic pressure transducers were located on every other rake, as denoted by the square boxes in figure 9(a). Eight static-pressure taps were located around the inner ring (hub) and eight were located around the outer ring (tip). The engine-face rakes were used during all inlet testing.

Additional instrumentation that was used during the simulated high-speed testing is shown in figure 10. Static-pressure taps were installed on the ramp centerline from the first inlet ramp to the diffuser exit. Ten additional static-pressure taps were installed on each of the other three walls, from the diffuser entrance to its exit. Four total-pressure rakes with six probes per rake were installed at the inlet throat section to monitor the flow condition entering the diffuser (section A–A, fig. 10). At the diffuser section near the ramp aft pivot point, four total-pressure rakes with 10 probes per rake were used to survey the level of diffuser flow separation on the diffuser walls (section B–B, fig. 10). Table II lists the positions for the model static-pressure taps and total-pressure probes that were used during the high-speed simulation. Blowing pressure was measured by a total-pressure probe installed in each of the four blowing plenums. High-pressure blowing airflow was provided by four pressure supply lines connected to the facility high-pressure air system (fig. 10(b)). A valve was installed upstream of each flow line to the blowing plenum so that the blowing pressure and airflow could be regulated by a remote control. For each line, a turbine

flowmeter was installed downstream of the valve to measure the blowing mass flow rate.

Data Acquisition and Processing

For low-speed testing, tunnel Mach numbers were set at 0.06, 0.12, and 0.18. For each tunnel Mach number, the model was rotated to six angle-of-attack positions: 0°, 20°, 45°, 70°, 90°, and 110°. At the angle of attack of 0°, the model was tested to determine the effect of varying engine-face Mach numbers. With higher angle-of-attack positions, inlet performance data were obtained for an engine-face design Mach number of 0.533. Inlet performance data also were obtained for cowl lip droop angles of 0° and 70°. During testing of the inlet at low speeds, inlet flow was induced by the facility suction system. The suction capacity was regulated to provide engine-face Mach numbers from 0.25 to 0.67. This suction system also was used for the high-speed simulation testing.

In the simulated high-speed testing, the tunnel free-stream Mach number was set at 0.12, and the engine-face Mach number was varied between 0.3 and 0.42 to provide a range of simulated high-speed throat Mach numbers between 0.57 and 0.88. At each throat Mach number, the blowing pressure ratio (blowing-jet total pressure divided by the free-stream total pressure) was varied from 1.0 to 3.4 for the slots and from 1.0 to 7.0 for the discrete nozzles. The blowing-jet mass flow rate was normalized by the inlet mass flow to obtain the blowing mass flow ratio. The blowing temperature ratio (the blowing total temperature divided by the free-stream total temperature) was 1.0. Diffuser BLC blowing was used first on the ramp side, then on the ramp and cowl sides, and eventually on all four sides.

All steady-state pressures were measured with the facility Electronically Scanned Pressure (ESP) system. The blowing total pressures were measured with 500-psia transducers that had an accuracy of ±0.85 psi. All other pressures were measured with 15-psia transducers that had an accuracy of ±0.0025 psi. The outputs of the eight dynamic pressure transducers on the engine-face rakes were fed through an electronic low-pass filter with a cut-off frequency of 400 Hz; then they were processed by a root mean square (rms) module. This module integrated the zero-base fluctuation pressure over a 1-sec time interval.

The major performance parameters computed were total-pressure recovery, steady-state distortion, and average turbulence. Pressure recovery was calculated using 40 area-weighted total-pressure probes (see **Instrumentation** section) at the engine face which were averaged and divided by the free-stream total pressure. Steady-state distortion was obtained by determining the difference between the maximum and minimum values of the 40 total pressures and dividing this value by the area-weighted average value of the 40 total pressures. The dynamic pressure transducers on the engine-face rakes provided eight rms values, which were averaged. The engine-face average turbulence was then obtained by dividing this rms average value by the average value of all the engine-face total pressures.

The venturi flowmeter in the facility model flow-exhaust suction system measured the inlet mass flow. Note that the inlet mass flow rate for low-speed testing was the inlet-captured mass flow; but for the high-speed simulation testing with BLC blowing, it was the sum of the inlet-captured and blowing mass flow rates. The engine-face Mach number was determined from the inlet mass flow, the engine-face flow area, and the total pressure and total temperature at the engine-face station. The total pressure was the average of all the engine-face area-weighted total pressures. The total temperature was taken to be the free-stream total temperature. At a particular engine-face Mach number, the inlet throat Mach number was calculated from the inlet-captured mass flow rate, the throat area, and the total and static pressures and total temperature at the inlet throat station. The calculation was based on a one-dimensional flow analysis.

Results and Discussion

The two-dimensional inlet with a short subsonic diffuser was tested at low speeds (takeoff and approach conditions) and for diffuser flow conditions that simulated high-speed flight. Low-speed test results are shown in figures 11 to 14. Figure 15 compares the performance data of the inlet with the short diffuser with the performance data of the same inlet with a long diffuser (ref. 1). A photograph of the two-dimensional inlet with the long diffuser is shown in figure 3.

For the simulated high-speed flight, the diffuser was sufficiently short so that flow separation would occur. The effectiveness of BLC blowing was investigated, and the results are shown in figures 16 to 27.

Inlet Low-Speed Performance With Short Diffuser

Inlet performance for a variation of engine-face Mach numbers at an angle of attack of 0° is presented in figure 11. Figure 11(a) shows pressure recovery, distortion, and average turbulence versus engine-face Mach number for a range of free-stream Mach numbers. For each free-stream Mach number tested, an increase in the engine-face Mach number for the baseline inlet configuration adversely affected the inlet performance. And for each free-stream Mach number tested, a drop of about 10 percent in pressure recovery and a large increase in distortion and in average turbulence occurred over the range of engine-face Mach numbers between 0.25 and 0.67. Three cowl lip positions, namely, baseline (no droop), 40° droop, and 70° droop, were tested separately with the inlet at static free stream ($M_0 = 0.0$) and over a range of engine-face Mach numbers. Performance

results (fig. 11(b)) indicate that drooping the cowl lip significantly improved the inlet performance.

Figure 12 shows the effect of angle of attack on the baseline inlet performance. The engine-face Mach number was set at the design value of 0.533 for all angle-of-attack data. At each free-stream Mach number, inlet performance decreased as the angle of attack increased, as shown in figure 12(a). The rate at which performance fell off because of the increase in angle of attack was low at low free-stream Mach numbers and became greater at the higher free-stream Mach numbers. Below an angle of attack of 50°, the performance was better for a free-stream Mach number of 0.18 than for free-stream Mach numbers of 0.06 and 0.12, respectively. However, above the angle of attack of 50°, the trends of the performance curves inverted.

Flow characteristics associated with angle-of-attack positions at 0°, 45°, and 90° for a free-stream Mach number of 0.12 are presented in figures 12(b) to (e). The cowl lip static-pressure distributions in figure 12(b) indicate that increasing the angle of attack from 0° to 90° moved the stagnation point aft on the cowl lip external surface from $X/l = 0.525$ to $X/l = 0.6$. This shifting of the stagnation point induced a higher flow acceleration around the cowl lip leading edge as evidenced by a drop in static pressure on the cowl lip internal surface. Just downstream of the inlet throat, the rake total-pressure distributions (fig. 12(c)) indicate that cowl lip flow separation occurred at angles of attack of 45° and 90°. This separation is shown by the wall static pressure being equal to or greater than the local total pressure. At an angle of attack of 0°, the flow was attached. The separation in figure 12(c) is not evident in figure 12(d), which shows total pressures for the engine-face rake at a circumferential position ϕ of 0°. These profiles do indicate a low total-pressure recovery near the cowl side. In the vicinity of the cowl, the profiles are obviously influenced by the upstream flow separation as shown in figure 12(c). Figure 12(e) shows total-pressure recovery contours at the engine face. Again the engine-face low-pressure region on the cowl side was the result of the low-pressure flow entering the diffuser, as shown in figure 12(c). Increasing the angle of attack caused the lower pressure region to spread toward the sidewalls, inducing a greater total-pressure loss and a higher pressure distortion.

Drooping the cowl lip to better align the lip with the approaching flow is one method to help reduce the cowl lip separation at high angles of attack. Figure 13 presents the effect of angle of attack on inlet performance for a 40° drooped cowl lip at the design engine-face Mach number of 0.533. The recovery curve (fig. 13(a)) for each free-stream Mach number exhibits similar characteristics to those associated with the baseline configuration shown in figure 12(a), but the fall-off rate is much less. The three performance curves crossed at an angle of attack of about 80°, which is 30° higher than the crossover observed with the baseline configuration. A comparison of figure 12(a) with 13(a) shows that drooping the cowl lip from 0° to 40° improved the recovery by approximately 6 percent at angles of attack below 80° and by approximately 8 percent at higher angles of attack. Distortion and average turbulence were reduced significantly by drooping the cowl lip.

The cowl lip surface static-pressure distributions shown in figure 13(b) display the shifting of the stagnation point corresponding to angles of attack of 0°, 45°, and 90°. Stagnation points on the 40° drooped cowl lip (fig. 13(b)) corresponding to the 45° and 90° angles of attack are further upstream than those on the baseline cowl lip shown in figure 12(b). This upstream movement of the stagnation points resulting from drooping the cowl lip eliminated the separation at the cowl rake as shown in figure 13(c). The engine-face total-pressure recovery contours shown in figure 13(d) indicate a very small pressure loss at an angle of attack of 0°. A comparison with the baseline pressure recovery at an angle of attack of 90° (fig. 12(e-3)) indicates that drooping the cowl lip by 40° improved the inlet recovery from 0.852 (baseline) to 0.949 as shown in figure 13(d-3).

The effect of angle of attack on inlet performance with a 70° drooped cowl lip is shown in figure 14 for the design engine-face Mach number of 0.533. A comparison of inlet recovery from figure 14(a) with the baseline performance shown in figure 12(a) indicates that a nominal 6 percent increase in recovery was achieved for angles of attack below 45° and a 10 percent increase was achieved for larger angles of attack. For angles of attack below 45°, the 70° drooped cowl lip produced an improvement in inlet recovery (fig. 14(a)) comparable to that for the 40° drooped cowl lip (fig. 13(a)). For higher angles of attack, the 70° drooped cowl lip outperformed the latter.

The flow characteristics associated with the 70° drooped cowl lip are presented in figures 14(b) and (c). Static-pressure distributions (fig. 14(b)) indicate that the stagnation points on the cowl lip leading edge moved aft with increasing angle of attack. The total-pressure profiles in figure 14(c) indicate that at an angle of attack of 0° the flow was in good condition and that at an angle of attack of 45° a small flow separation occurred but that at an angle of attack of 90° the separation disappeared. A comparison of the cowl rake total-pressure recovery for the baseline cowl lip (fig. 12(c)) with the higher cowl rake total-pressure recoveries (fig. 14(c)) indicates that the 70° drooped cowl lip improved the inlet flow conditions over the angles of attack from 0° to 90°. A comparison with the cowl rake total-pressure recovery (fig. 13(c)) for the 40° drooped cowl lip indicates that a 70° drooped cowl lip (fig. 14(c)) provided no improvement to the inlet flow conditions at an angle of attack of 0° and only some improvement at an angle of attack of 90°. At an angle of attack of 45°, the cowl rake total-pressure recovery indicates that a 70° drooped cowl lip produced a small flow separation, whereas the 40° drooped cowl lip did not. In contrast to the short diffuser results, with the long diffuser (ref. 1), the inlet with a 70° drooped cowl lip induced no

flow separation with angles of attack from 0° to 90°. The reasons for this difference are not known at this time. The engine-face total-pressure contours at angles of attack of 45° and 90° (fig. 14(d)) indicate high levels of pressure recovery and moderate distortion levels. A comparison of the total-pressure contours in figures 12(e), 13(d), and 14(d) indicates that a large increase in recovery and decrease in distortion at high angles of attack were achieved by drooping the cowl lip. At an angle of attack of 90°, the pressure recovery increased from 0.852 to 0.973 with a decrease in distortion from 0.397 to 0.105 when the droop angle was increased from the baseline to 70°.

Effect of Diffuser Length

The inlet performance with the short subsonic diffuser was compared with the inlet performance with a long subsonic diffuser obtained from a previous research study (ref. 1). The comparison is shown in figure 15.

As shown in figures 11 to 14, variations in engine-face Mach number and in angle of attack have a profound effect on the inlet performance. Therefore, these variables were used to compare the effect of the short and long subsonic diffusers on the performance of the inlet. Figure 15(a) shows inlet performance for various engine-face Mach numbers at static ($M_0 = 0.0$) free-stream conditions. Figure 15(b) shows inlet performance for various angles of attack at a free-stream Mach number of 0.12 and a design engine-face Mach number of 0.533. Both figures show that, at low speeds, drooping the cowl lip had a much greater influence on the total-pressure recovery than did the length of the diffuser. The short diffuser with the baseline cowl lip induced a significantly higher distortion level than did the long diffuser. This difference was attributed to the shorter length available for flow mixing. With a 70° drooped cowl lip, the distortion associated with either diffuser fell to about the same level. The trends of turbulent levels resulting from using the short or long diffuser are similar.

Analytical Results

One problem that occurs in a short subsonic diffuser with a high divergent area distribution is flow separation. A general guideline to aid in the design of subsonic diffusers is presented in figure 16 (which is from ref. 5). The plot shows the region where flow separation can be expected to occur as a function of the diffuser-exit to entrance-area ratio and average diffuser wall angle θ_{avg}. The design guideline curves are for both axisymmetric conical and two-dimensional straight-wall diffusers. The short diffuser of this experimental program has a rectangle shape at the entrance and a circular shape at the exit. Figure 16 shows peripheral contours of four internal cross sections. The inlet flow would diffuse mainly on the diffuser ramp side, whose wall angle with respect to a horizontal line is taken to be the diffuser average wall angle. The location of the data point, as represented by a filled circle with a length-to-exit diameter dl/d of 1.25, indicates that this diffuser would have a flow separation. To help prevent this, a BLC blowing system using slots or discrete nozzles was incorporated into the design of the short diffuser.

Insight into the flow physics associated with the short subsonic diffuser can be gained through an analytical study of the diffuser using the Hess potential flow panel method code (ref. 2) in conjunction with the Herring two-dimensional boundary-layer analysis code (ref. 3). Figure 17 shows the inlet panel grid used for the analysis and the schematic diagram of the code computation. An outline of the side view of the panel grid is shown in figure 18. It depicts the model parameters and the blowing station incorporated to control the computed flow boundary layer. For the inlet, the parameters include actual inlet length and width, throat area, and cowl lip droop angle. For the diffuser, the parameters include actual diffuser length, exit diameter, and entrance to exit area ratio. The actual location for BLC blowing was used in the analysis. The panel grid was designed such that it would represent the actual model as closely as possible.

The results of the analytical study are presented in figure 18 for the diffuser entrance Mach number of 0.8. Figure 18(a) shows the diffuser surface skin friction coefficients for flow with no BLC. The curves indicate flow separation in the subsonic diffuser on the ramp side (skin friction coefficient, $C_f = 0$ at $X/l = 0.76$), but no separation on the cowl and sidewall. A comparison of the skin friction on the ramp surface with and without boundary-layer blowing is shown in figure 18(b). These results indicate that the use of BLC by blowing with a blowing pressure ratio of 2.0 and a reasonable level of blowing mass flow will eliminate separation. The results shown in figure 18 for no BLC blowing verify the indication of flow separation from the general guideline curve (fig. 16).

Diffuser Performance at Simulated High-Speed Conditions

Test results for a range of inlet high-speed throat Mach numbers that simulate high-speed conditions are presented in figures 19 to 27. The values of recovery presented for high-speed simulation conditions represent the subsonic diffuser only. They are not overall inlet recovery values. To obtain inlet recovery values, an adjustment is required to account for the loss in total pressure through the external oblique and terminal shock systems. For this inlet at a flight Mach number of 2.2 and angle of attack of 0°, the theoretical recovery from the free stream to the subsonic diffuser entrance would be 90 percent. This value should be used as a multiplication factor for the recovery levels from the figures to obtain approximate values of the inlet recovery at Mach 2.2.

Diffuser-simulated high-speed performance was obtained with the wind tunnel operating at Mach 0.12, the inlet ramp

position set for Mach 2.2, and its cowl lip drooped at 20°. The facility suction system was varied to test the diffuser over a range of inlet throat Mach numbers corresponding to inlet high-speed design operation. Figure 19 shows the baseline performance with no BLC in terms of diffuser pressure recovery, distortion, and average turbulence. With increasing throat Mach number, the recovery decreased while the distortion and average turbulence increased (fig. 19(a)).

Diffuser flow characteristics for a throat Mach number of 0.77 are shown in figure 19(b). Inlet throat rake total-pressure profiles are shown in figure 19(b-1). They indicate a very small growth of the boundary layer on the inlet cowl side and sidewall and a very small separation on the ramp side. The effect of this minute separation is negligible in relation to the overall total pressure at this station. Therefore, it is reasonable to assume that the throat average total pressure equals the tunnel free-stream total pressure because the front part of the inlet simulates a bellmouth. Consequently, for this high-speed simulation case, the diffuser total-pressure recovery P_{T2}/P_{T1} is the same as P_{T2}/P_{T0}, where the free-stream total pressure P_{T0} is replaced by the average total pressure at the inlet throat P_{T1}.

The mid-diffuser rake total-pressure profiles of figure 19(b-2) show a massive separation on the diffuser ramp side. On the cowl side the flow almost separated, and on the sidewall side the flow was attached. The diffuser wall centerline static-pressure distributions (fig. 19(b-3)) show that on the inlet cowl side the static pressure steadily increased through the diffuser. The near constant level of static pressure on the ramp from the inlet throat to the near diffuser exit indicates the extent of the separation region. The ramp separation continues downstream to the engine face as indicated by the rake pressure distributions for the three throat Mach numbers that are shown in figure 19(c). This figure also indicates that the flow was still attached on the hub at this circumferential location.

Engine-face rake total-pressure contours for three throat Mach numbers are shown in figure 19(d). At a throat Mach number of 0.65, the diffuser ramp separation resulted in a distortion of about 14 percent (fig. 19(d-1)). The separation effect became stronger at a throat Mach number of 0.77 (fig. 19(d-2)) and induced a sizeable pressure gradient across the engine face, with total-pressure loss mostly toward the ramp side. The lower pressures on the cowl side are the result of lower energy (near separation) flow indicated by mid-diffuser cowl rake in figure 19(b-2). As the separation became more pronounced because of a greater pressure gradient, the core flow progressively developed a secondary flow motion that promoted greater viscous and boundary-layer frictional losses. At a throat Mach number of 0.88 (fig. 19(d-3)) two small, low-pressure pockets appeared on the engine-face ramp side.

Diffuser baseline high-speed simulated performance data, as indicated by the discussion of figure 19, showed that the flow separation occurred as predicted. During the experimental program, this separation was controlled by blowing through slots and through discrete nozzles. Each blowing device was installed and tested separately with the diffuser. The installation of the slot blowing hardware produced a small rearward facing step on the diffuser surface, whereas the discrete nozzles protruded into the diffuser flow. A test was conducted with each blowing device installed, but with no blowing flow, to assess the effect of adding the blowing hardware. Figure 20 compares performance as a function of throat Mach number for the diffuser with and without blowing devices. Test results shown in this figure indicate that the installation of each device affected performance by less than 1 percent.

When tested, each type of BLC device was installed on all four walls of the diffuser. Because the flow separation was on the diffuser ramp side, testing was performed by blowing first on the ramp side, then on the ramp and cowl sides, and finally on all four sides. Figure 21 presents plots of slot and discrete nozzle blowing mass flow ratio as a function of blowing pressure ratio at a throat Mach number of 0.77. For the individual blowing alternatives (ramp, ramp plus cowl, and all four sidewalls) shown in the figure, the blowing mass flow ratio for the slots was about twice that for the discrete nozzles for the same blowing pressure ratio. The reason for this difference was that the sum of the jet-exit areas for slots was about twice the sum of the jet-exit areas for discrete nozzles as shown in figure 6.

Performance in terms of pressure recovery, distortion, and average turbulence resulting from BLC blowing for three values of throat Mach numbers (0.66, 0.77, and 0.88) are plotted versus blowing mass flow ratios in figures 22, 23, and 24, respectively. At a throat Mach number of 0.65 (fig. 22(a)), slot blowing on the diffuser ramp increased pressure recovery by about 2 percent over the no-blowing condition at a blowing mass flow ratio of 0.017. For about the same gain in pressure recovery, discrete nozzle blowing required a blowing mass flow ratio of 0.02. Distortion dropped to a minimum value, 5 percent lower than for the no-blowing condition, at a blowing mass flow ratio of 0.017 for the slot. A 2 to 3 percent reduction in distortion was obtained for the discrete nozzles at a blowing mass flow ratio of 0.017. For further increases in blowing mass flow ratio, slot blowing induced no further effect on distortion, but discrete nozzle blowing caused distortion to increase.

For the same throat Mach number of 0.65, ramp-and-cowl blowing (fig. 22(b)) increased pressure recovery by 4 percent over the no-blowing condition. This 4 percent gain corresponds to a blowing mass flow ratio of 0.04 for either slots or discrete nozzles. Despite the steady improvement of recovery with increasing values of blowing mass flow ratio, the largest reduction in distortion occurred at a blowing mass flow ratio of 0.04, beyond which the distortion level increased.

Blowing on four sidewalls, for the same throat Mach number of 0.65, improved the pressure recovery about 5 percent (fig. 22(c)); this improvement corresponds to a blowing

mass flow ratio of 0.06. A comparison of the diffuser total-pressure recovery curves in figure 22(b) with those in figure 22(c) indicates the same basic trend for a comparable blowing mass flow ratio. Therefore, the increase in recovery was basically due to the larger blowing mass flow attainable with the four-sidewall blowing. The maximum drop in distortion occurred at a blowing mass flow ratio of 0.06, which is 0.02 greater than the drop obtained by blowing on the ramp and cowl sides.

Figures 23(a) to (c) show diffuser performances for blowing on the ramp side, on the ramp and cowl sides, and on all four sides at a throat Mach number of 0.77. For each alternative, with the same blowing mass flow ratio, the effect of slot blowing on diffuser performance was similar to that of discrete nozzle blowing. The trend in recovery improvement resulting from blowing on the ramp and cowl sides is similar to that resulting from blowing on all four sides, but it is better than the trend obtained by blowing on the ramp side only. For a blowing mass flow ratio of 0.043, a gain in recovery of 4.5 percent (fig. 23(b)) was obtained from blowing on the ramp and cowl sides. And for a blowing mass flow ratio of 0.063, a gain in recovery of 5.5 percent (fig. 23(c)) was obtained from blowing on all four sides. This additional 1 percent gain in recovery resulting from an additional 2 percent increase in the blowing mass flow ratio was also observed in the diffuser recovery improvement attainable when blowing was used with a throat Mach number of 0.65 (figs. 22(b) and (c)). With a throat Mach number of 0.77, distortion continuously declined as blowing mass flow increased for all three blowing alternatives—in contrast to the distortion trends resulting from blowing at a throat Mach number of 0.65. A reason for this could be that the diffuser separation associated with a throat Mach number of 0.77 was more severe than that associated with a throat Mach number of 0.65. Therefore, the blowing effect at a throat Mach number of 0.77 only reduced the level of separation; it did not reach the level at which blowing-induced distortion would take effect as it did for a throat Mach number of 0.65.

Diffuser performance resulting from blowing at a throat Mach number of 0.88 is presented in figures 24(a) to (c) for blowing on the ramp, ramp and cowl, and all four sidewalls. Improvement in recovery and reduction in distortion and average turbulence are similar to those obtained for the throat Mach numbers of 0.65 and 0.77. A comparison of figures 22, 23, and 24 shows that the gain in pressure recovery and the reduction in distortion for the same blowing mass flow ratios followed similar trends. However, for all three inlet throat Mach numbers, diffuser ramp-only blowing induced a noticeable difference between the average turbulence resulting from blowing through slots and discrete nozzles. By blowing on the ramp, slot blowing induced higher average turbulence than discrete nozzle blowing, and the difference became larger as the throat Mach number increased. However, this difference diminished when blowing was done on the ramp and cowl and on all four side walls.

Figure 25 shows the effects of slot blowing on diffuser flow characteristics for a throat Mach number 0.77. Figure 25(a) shows the effect of slot blowing on the diffuser ramp side with a blowing mass flow ratio of 0.02 and a blowing pressure ratio of 2.4. A comparison of the ramp mid-diffuser rake total-pressure profile in figure 25(a-1) with that in figure 19(b-2) shows that ramp-only blowing was able to eliminate diffuser ramp separation. However, it indicates that ramp-only blowing induced flow separation on the diffuser cowl side but did not have any adverse effect on the flow condition on the diffuser sidewall. A comparison of surface static-pressure distributions in figure 25(a-2) with those in figure 19(b-3) indicates that diffuser ramp blowing improved the flow diffusion process on the ramp and sidewall. Static-pressure distributions on the cowl surface remained about the same. Figure 25(b) shows the effect of slot blowing on the diffuser ramp and cowl sides for a blowing mass flow ratio of 0.044 and a blowing pressure ratio of 0.34. Comparison of figure 25(a) with (b) shows that ramp-and-cowl blowing produced a more favorable effect than blowing on the ramp side alone. Flow separation on the cowl surface is not evident in figure 25(b-1). Blowing on all four sides (fig. 25(c)) had an effect similar to blowing on the ramp and cowl sides, but the sidewall appears to have been overblown.

Referring to figures 25(a) to (c), note that blowing on the diffuser ramp alone, on the ramp and cowl, and on all four sides produced about the same ramp rake pressure recovery profiles. However, diffuser ramp-only blowing employed a blowing pressure ratio of 0.24, whereas either ramp-and-cowl or all-four-sides blowing employed a blowing pressure ratio of 3.4. To provide greater details of the flow characteristics on the diffuser ramp side, figure 26 presents the mid-diffuser ramp rake recovery profiles resulting from individual blowing alternatives for a throat Mach number of 0.77. Figure 26(a) shows diffuser-ramp pressure recovery profiles for the baseline (no BLC) and for slot blowing with blowing pressure ratios of 1.0, 1.8, 2.4, and 3.4.

So that flow separation on the diffuser ramp could be eliminated with slot blowing, a blowing pressure ratio of 2.4 was required for ramp-only blowing (fig. 26(a-1)). However, diffuser ramp-only blowing caused the diffuser flow to separate on the cowl side as indicated in figure 25(a-1). A pressure ratio of 3.4 for either ramp-and-cowl (fig. 26(a-2)) or all-four-sides blowing (fig. 26(a-3)) was required to eliminate ramp flow separation. Ramp-and-cowl blowing, as well as all-four-sides blowing, was able to control flow separation on both the ramp and cowl sides as shown in figure 25(b-1).

Mid-diffuser rake pressure recovery profiles resulting from discrete nozzle blowing are shown in figure 26(b). A comparison of figure 26(a) with (b) reveals similar mid-diffuser

ramp rake recovery profiles. The difference between the two is that discrete nozzle blowing required about twice the blowing pressure ratio that was required for slot blowing.

Figure 27 shows engine-face rake total-pressure contours resulting from slot and discrete nozzle blowing on the diffuser ramp, ramp and cowl, and all four sides for a throat Mach number of 0.77. In all cases (figs. 27(a) to (f)), increasing the blowing mass flow improved diffuser performance. Blowing on all four sides produced a more uniform flow at the engine face than blowing on the ramp and on the ramp and cowl sides. For ramp-only blowing, a comparison of figure 27(a) with (d) shows that, for about the same blowing mass flow ratio, slot blowing produced about 0.5 percent better pressure recovery and 2.0 percent lower distortion than discrete nozzle blowing. For ramp-and-cowl blowing, a comparison of figure 27(b) with (e) indicates that slot blowing and discrete nozzle blowing induced similar engine-face pressure contour maps. A comparison of figure 27(c) with (f) also shows similar effects resulting from blowing on all four sides through slot and discrete nozzles. Blowing on all four sides, through either slots or discrete nozzles, provided a slightly better performance than that obtained by blowing on the ramp and cowl sides, but the former required significantly larger blowing mass flow than the latter.

Penalties Associated With Boundary Layer Control Blowing

The data presented for the high-speed simulated conditions show that flow separation induced by a short diffuser can be eliminated by BLC blowing. However, there are penalties associated with the BLC blowing method which reduce the benefit gained. A weight penalty would be associated with hardware required for ducting the blowing air from the engine and also with assuring a highly reliable system. Some thrust penalty also would need to be assessed because the blowing system uses a high-pressure air supply that would likely be bled off of the engine. With a particular blowing device, slots or discrete nozzles, the amount of blowing mass flow depends directly on the level of the blowing pressure. For the short diffuser, a blowing mass flow ratio of 4.0 percent, by either slots or discrete nozzles, was needed to obtain a reasonable improvement in diffuser performance. For this amount of blowing mass flow ratio, a blowing pressure ratio of 3.0 was required for the slots and a blowing pressure ratio of 6.0 was required for the discrete nozzles (fig. 21).

Summary of Results

A two-dimensional supersonic inlet with a very short subsonic diffuser (d/dl = 1.25) was tested in the NASA Lewis Research Center's 9– by 15–Foot Low-Speed Wind Tunnel. The test objective can be subdivided in two phases: (1) determining the effect of the short diffuser on the inlet's low-speed performance and (2) determining the short diffuser's performance in a simulated high-speed configuration that incorporates slots and discrete nozzles for BLC blowing. The test results can be summarized as follows:

Phase 1

1. The performance of the baseline inlet with a short diffuser continuously dropped as the angle of attack or engine-face Mach number was increased. This drop in performance was attributed to the inlet cowl lip separation at a high angle of attack or at a high engine-face Mach number.

2. At the design engine-face Mach number of 0.533, a cowl lip droop of 40° or 70° substantially improved the inlet performance with the short diffuser.

3. For the baseline configuration, a comparison of the performance of the inlet with the short diffuser with that of the inlet with the long diffuser shows that the difference in diffuser length did not significantly affect the inlet total-pressure recovery. However, the inlet distortion associated with the short diffuser was significantly higher than the inlet distortion associated with the long diffuser at both high angles of attack and high engine-face Mach numbers.

4. The use of a 70° drooped cowl lip reduced the difference in inlet distortions associated with the short and long diffusers to comparable levels.

Phase 2

1. The short diffuser induced flow separation on the ramp side as was predicted by the Hess potential flow panel method with the Herring flow boundary-layer analysis. The separation became more severe as the inlet throat Mach number increased, with a resulting decrease in the diffuser performance.

2. BLC blowing through either slots or discrete nozzles effectively eliminated flow separation, improving the diffuser performance. For a particular blowing mass flow ratio, slot blowing was as effective as discrete nozzle blowing provided that the blowing was done on the same diffuser sidewalls: ramp side only, ramp and cowl sides, or all four sides. Improvement in diffuser performance was observed to depend primarily on the magnitude of the blowing mass flow ratio.

3. For this short diffuser, blowing on the diffuser ramp side alone induced flow separation on the diffuser cowl side. Blowing on the ramp and cowl sides was capable of eliminating the diffuser flow separation. Blowing on all four sides also eliminated flow separation and slightly improved the diffuser performance, but a significantly larger amount of blowing mass flow was required.

4. At an inlet throat Mach of 0.65, the diffuser pressure recovery continuously increased with increased blowing mass-flow ratio while the distortion dropped to a minimum value and then increased. This increase in the diffuser pressure distortion may have resulted from the blowing itself (a blowing mass or pressure that was too high). At an inlet throat Mach number of 0.88, the diffuser pressure recovery continuously increased and the pressure distortion continuously dropped as the blowing mass flow was increased.

Lewis Research Center
National Aeronautics and Space Administration
Cleveland, Ohio, August 14, 1992

References

1. Mark, J.L.; Mcgarry, M.A.; and Reagan, P.V.: Research on a Two-Dimensional Inlet for a Supersonic V/STOL Propulsion System. NASA CR–174945, 1989.
2. Hess, L.J.; and Friedman, M.D.: Calculation of Compressible Flow in and About Three-Dimensional Inlets With and Without Auxiliary Inlets by a Higher-Order Panel Method. NASA CR–168009, 1982.
3. Herring, H.J.: PLA – A Calculation Method for Two-Dimensional Boundary Layers With Crossflow and Heat Transfer. NASA Contract NAS3–21810, 1981.
4. Yuska, J.A.; Diedrich, J.H.; and Clough, N.: Lewis 9– by 15–Foot V/STOL Wind Tunnel. NASA TM X–2305, 1971.
5. Kline, S.J.; Abbot, D.E.; and Fox, R.W.: Optimum Design of Straight-Walled Diffusers. J. Basic Eng., vol. 81, no. 3, Sept. 1959, pp. 321–331.

TABLE I.—COWL INSTRUMENTATION

(a) Lip static pressures

Axial location, X, cm	Vertical location, Y, cm	Transverse location, Z, cm
Internal surface		
57.90	34.01	0.0
58.55	33.76	
59.76	33.60	
60.96	33.90	
62.33	34.01	
63.45	34.26	
65.33	34.40	
67.61	34.52	
70.00	34.64	
72.20	34.64	▼
External surface		
25.59	34.65	0.0
59.31	35.53	
60.10	35.33	
61.24	35.81	
62.28	36.20	
63.40	36.58	
64.92	37.00	
66.60	37.41	
68.22	37.74	
69.85	38.02	▼

(b) Total-pressure rake

Axial location, X, cm	Vertical location, Y, cm	Transverse location, Z, cm
81.02	34.44	0.0
81.05	33.14	
81.11	33.68	
81.17	33.22	
81.25	32.45	
81.40	31.44	
81.50	30.45	
81.61	29.44	
81.73	28.44	
81.75	27.43	▼

TABLE II. – MODEL INSTRUMENTATION LOCATION FOR SIMULATED HIGH-SPEED TEST

(a) Inlet static pressures

Axial location, X, cm	Vertical location, Y, cm	Transverse location, Z, cm
Ramp		
31.75	3.33	0.0
41.30	4.34	
51.40	5.40	
58.98	6.99	
66.56	7.01	
77.42	19.50	
81.94	17.38	
86.84	15.08	
90.30	13.46	
95.94	10.82	
98.78	9.49	
101.60	8.18	
104.84	6.98	
107.63	6.98	
110.81	6.98	
Cowl		
82.92	34.92	0.0
86.21	35.31	
89.07	35.66	
92.10	36.02	
95.13	36.37	
98.16	36.73	
102.42	37.24	
105.16	37.46	
108.20	37.46	
111.20	37.46	
Both side walls		
83.00	22.21	±12.31
85.75		
88.65		
91.90		
95.00		
98.00		
102.24		
104.83		±12.51
107.88		±13.40
110.93		±14.27

(b) Inlet throat total-pressure rake

Axial location, X, cm	Vertical location, Y, cm	Transverse location, Z, cm
Ramp		
77.93	12.46	0.0
	12.95	
	13.48	
	14.12	
	14.75	
	16.02	
Cowl		
76.45	31.55	0.0
	31.04	
	30.53	
	29.90	
	29.26	
	28.00	
Both side walls		
75.10	24.17	±12.05
		±11.54
		±11.04
		±10.40
		±9.77
		±8.50

(c) Inlet aft total-pressure rake

Axial location, X, cm	Vertical location, Y, cm	Transverse location, Z, cm
Ramp		
98.30	10.00	0.0
98.40	10.26	
98.63	10.70	
98.83	11.10	
98.14	11.80	
99.57	12.72	
100.00	13.63	
100.43	14.55	
100.86	15.46	
101.29	15.54	
Cowl		
97.79	36.47	0.0
97.85	36.17	
97.97	35.70	
98.15	35.23	
98.41	34.47	
98.79	33.48	
99.30	32.46	
99.92	31.47	
100.66	30.45	
101.52	29.46	
Both side walls		
97.62	22.21	±12.05
		±11.77
		±11.31
		±10.84
		±10.07
		±9.06
		±8.05
		±7.04
		±6.03
		±5.02

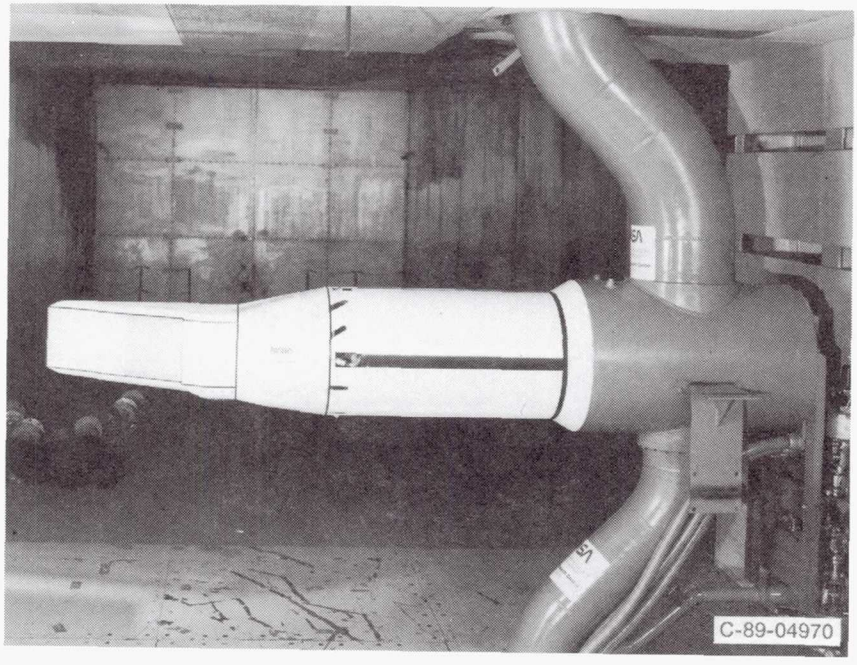

Figure 1.—Low-speed configuration of two-dimensional inlet with short diffuser.

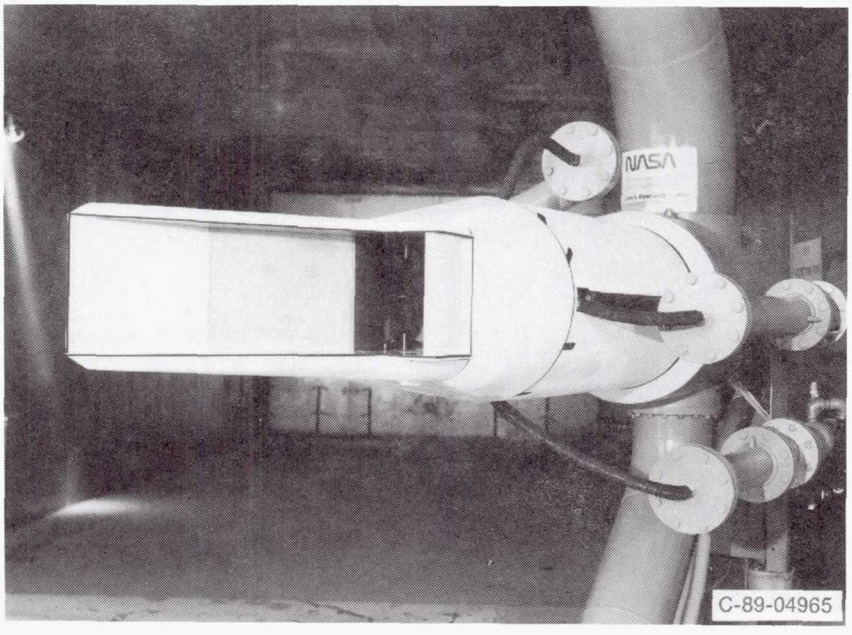

Figure 2.—Simulated high-speed configuration of two-dimensional inlet with short diffuser equipped with boundary layer control (BLC) blowing system.

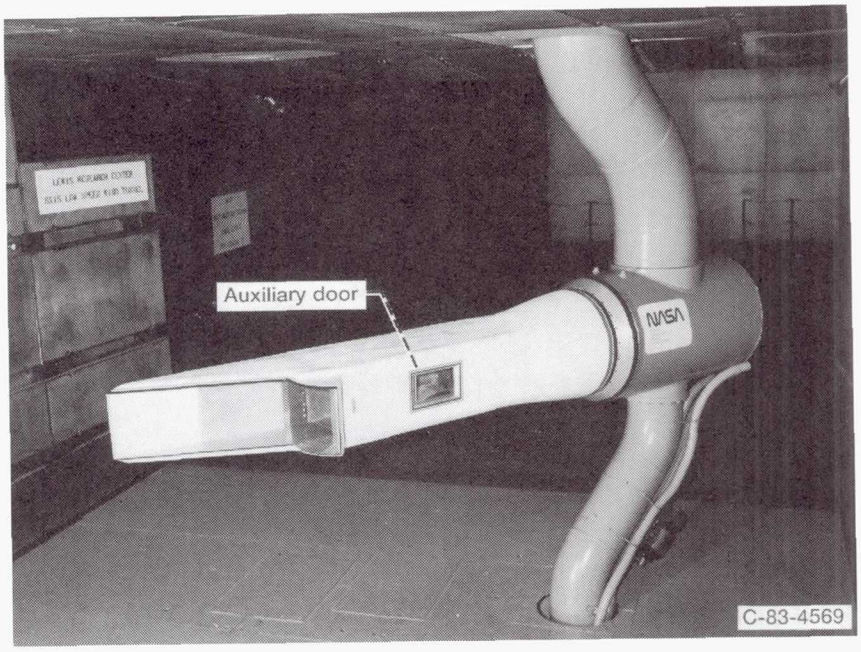

Figure 3.—Two-dimensional inlet with drooped cowl lip, auxiliary door, and long, conventional diffuser (axial-length to exit-diameter ratio, dl/d = 4.5).

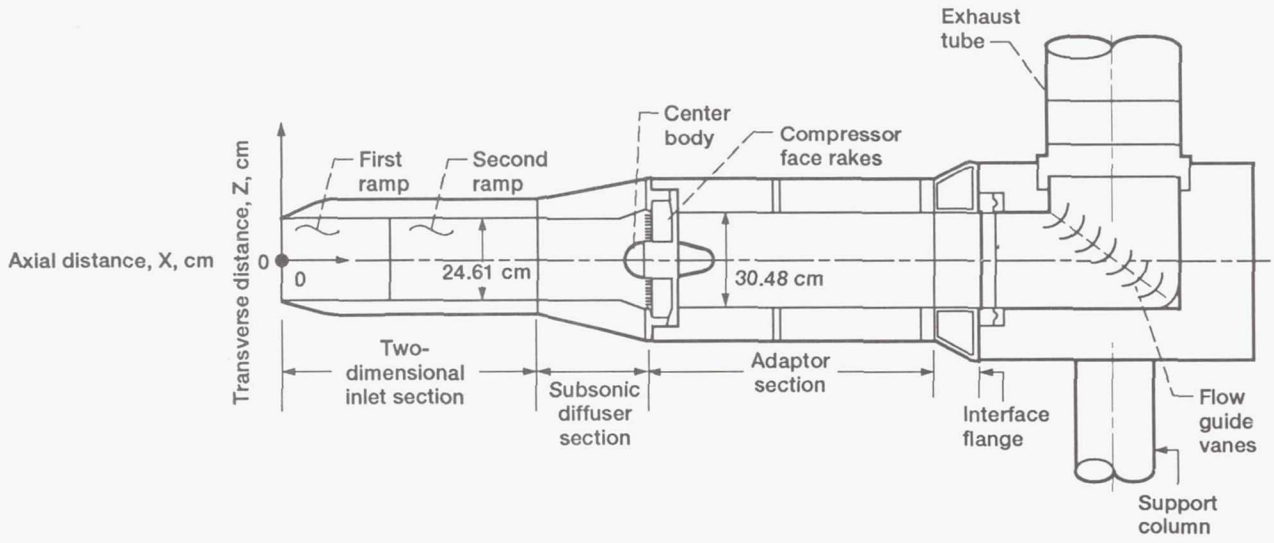

(a) Schematic model installation in the test section.

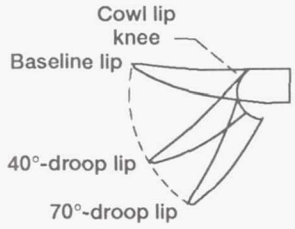

(b) Cowl lip at baseline and drooped at 40° and 70°.

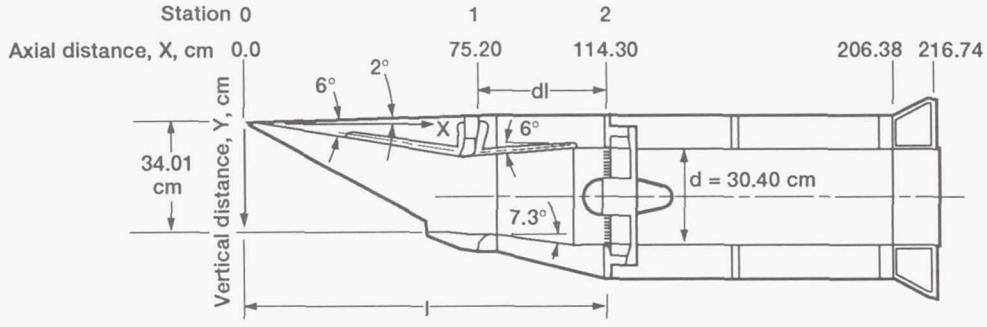

(c) Inlet model configuration for low-speed data.

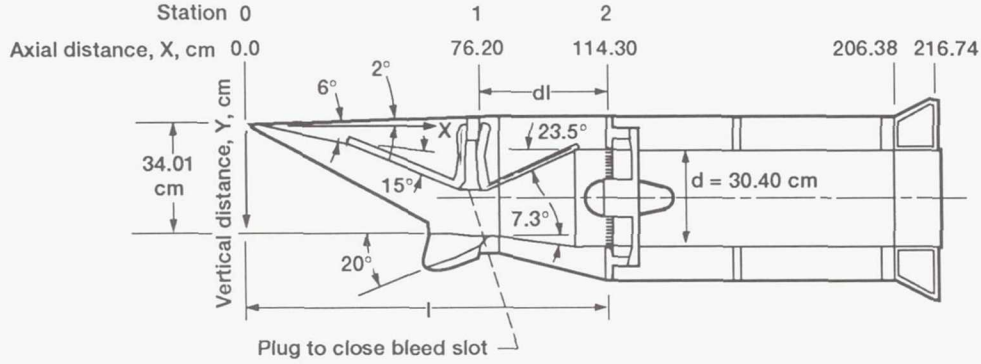

(d) Model configuration for high-speed simulation data.

Figure 4.—Schematic descriptions of model installation and model configurations for low-speed and high-speed simulation data.

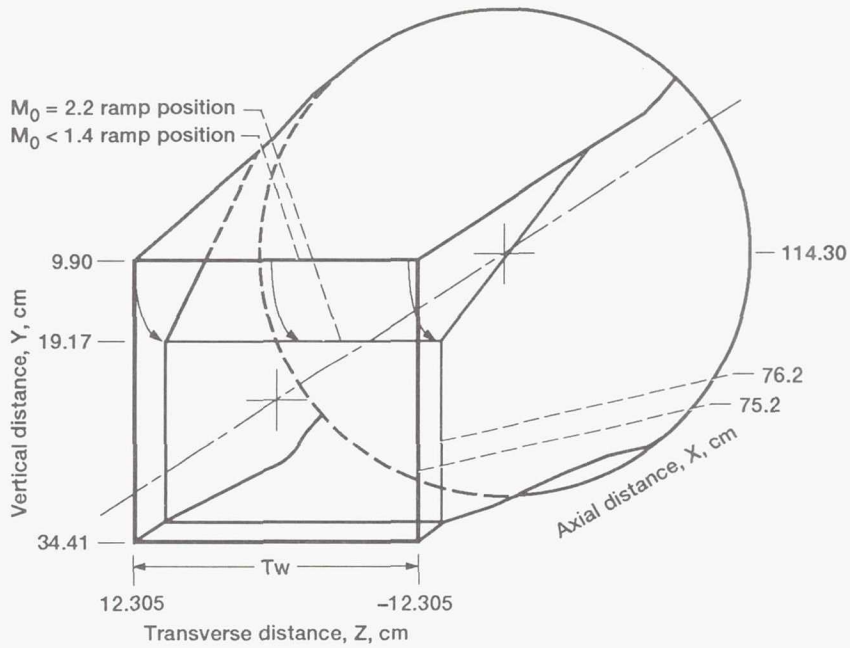

(a) Schematic of short diffuser configuration. X, Y, and Z are referenced to figure 4.

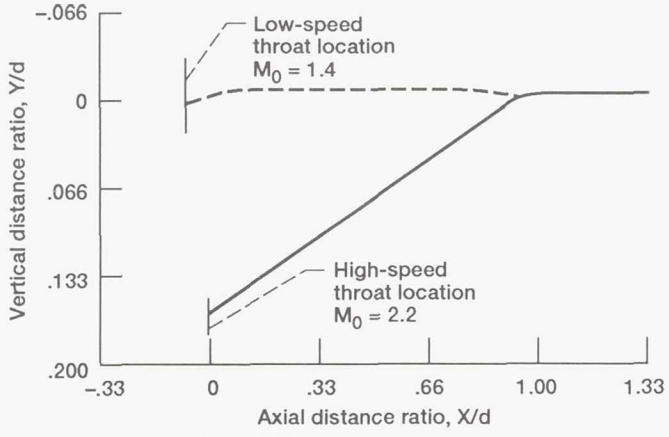

(b) Short diffuser centerline distribution.

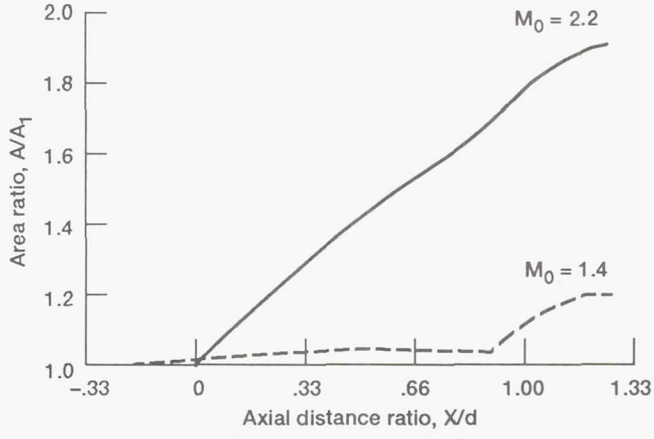

(c) Short diffuser area distribution.

Figure 5.—Short diffuser geometry variation.

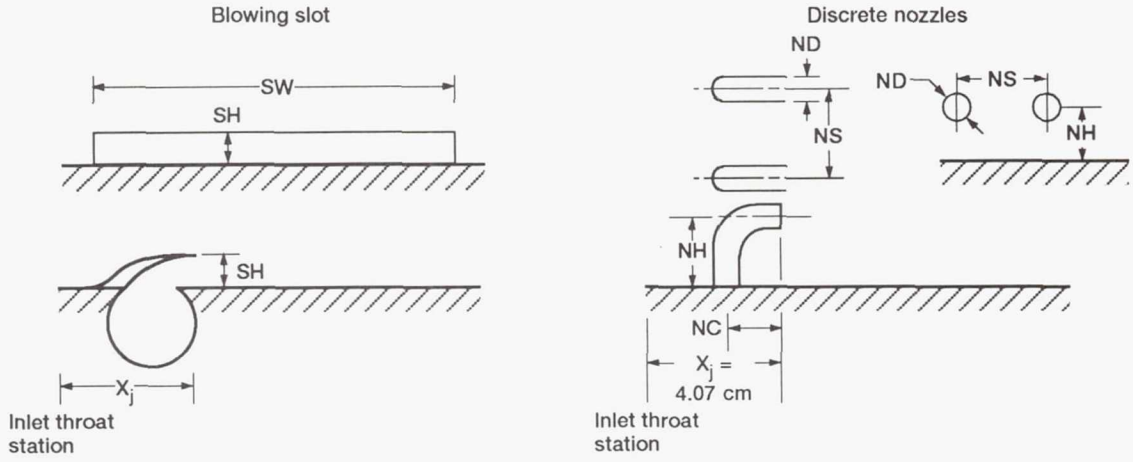

Location	Slot width, SW, cm	Slot height, SH, cm
Ramp	20.066	0.152
Cowl	18.826	.102
Sidewall	13.970	.046

Location	Number of nozzles	Nozzle diameter, ND, cm	Spacing between jet nozzles, NS, cm
Ramp	13	0.396	1.588
Cowl	31	.178	.610
Sidewall	27	.178	.533

Location	Distance between nozzle base and jet exit, NC, cm	Nozzle height, NH, cm	Equivalent slot height, SH, cm
Ramp	0.711	0.955	0.077
Cowl	.478	.478	.041
Sidewall	.533	.533	.047

Figure 6.—Design parameters of blowing slot and discrete nozzles.

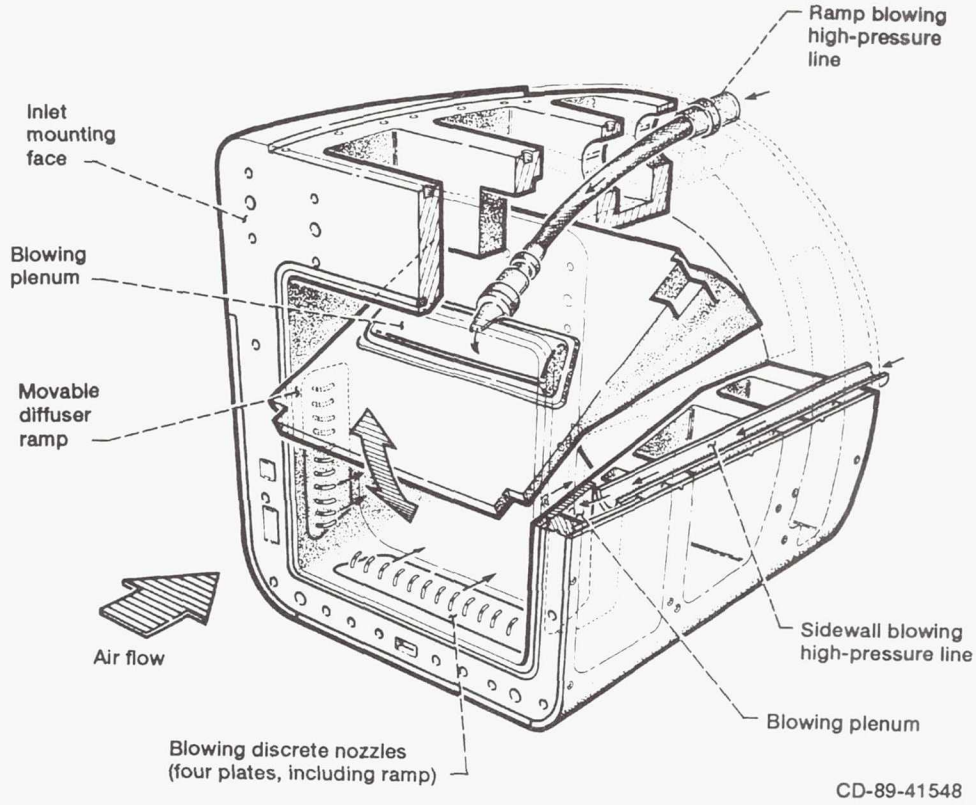

(a) Subsonic diffuser variable geometry and blowing system.

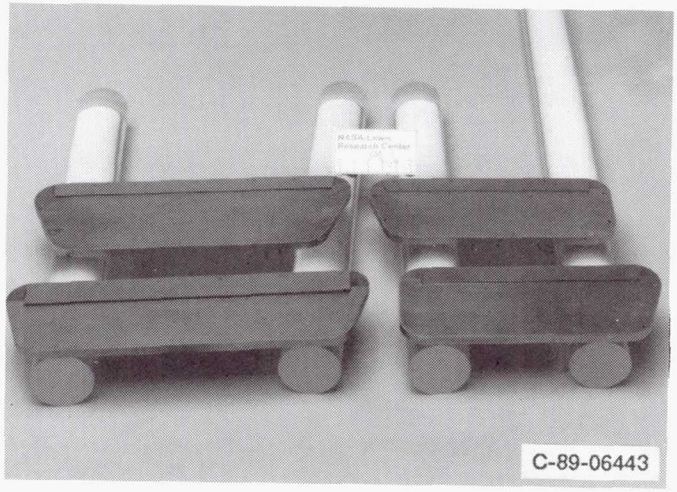

Blowing slot

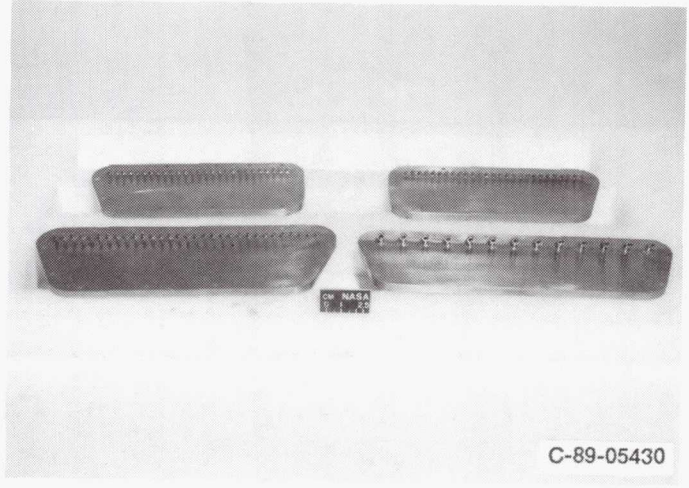

Discrete nozzles

(b) Blowing devices.

Figure 7.—Details of blowing system installed in short diffuser.

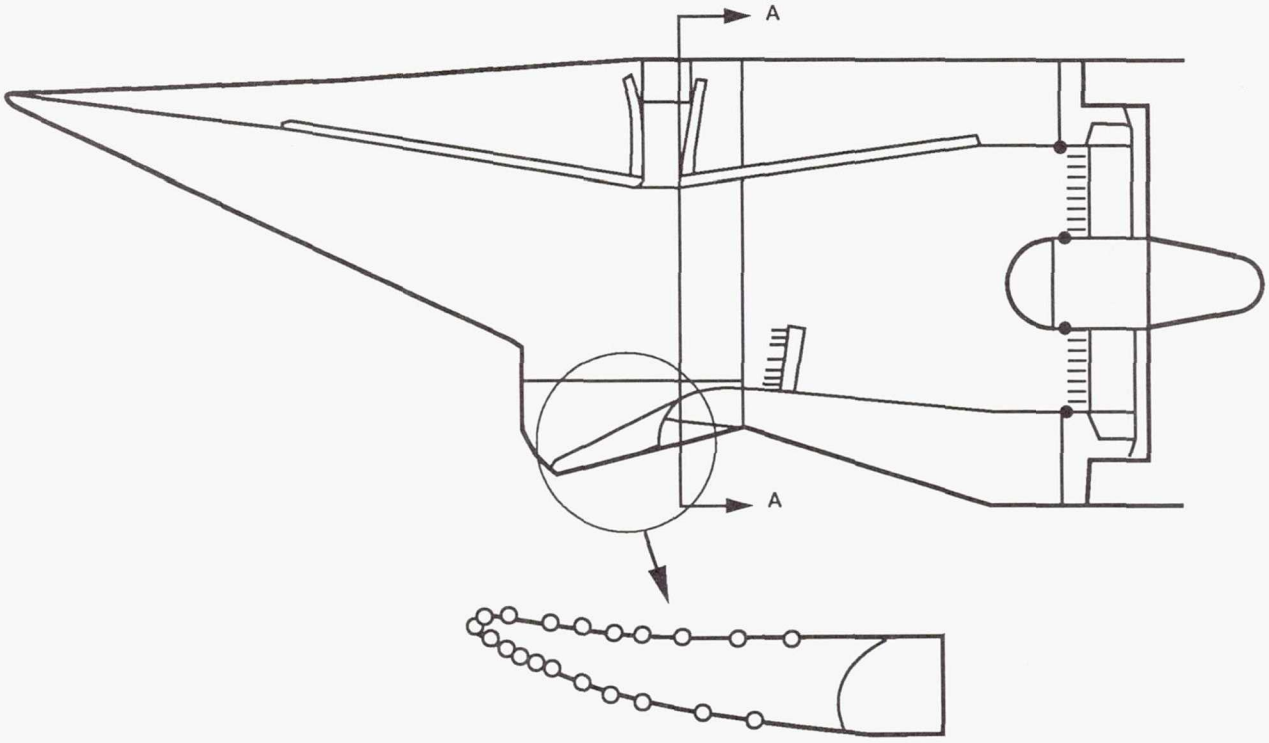

Cowl lip static-pressure tap locations

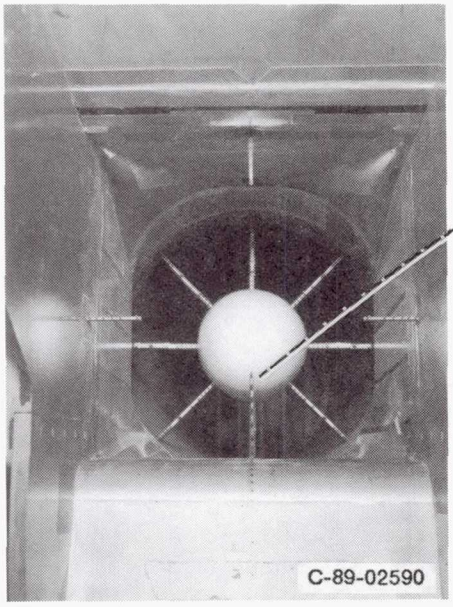

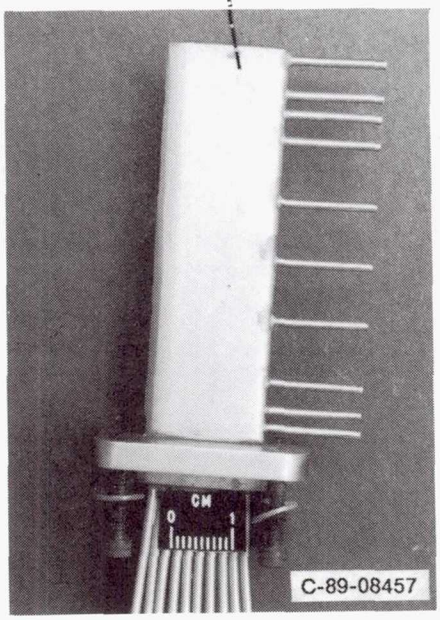

Inlet cowl total-pressure rake

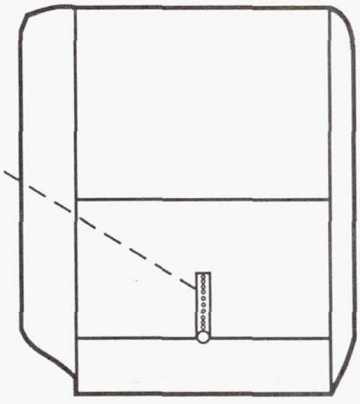

Section A-A

Figure 8.—Inlet low-speed static- and total-pressure instrumentation.

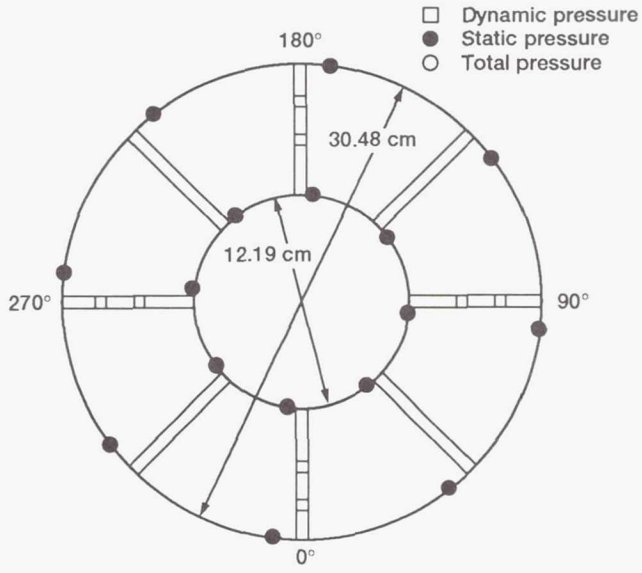

(a) Engine-face rake arrangement.

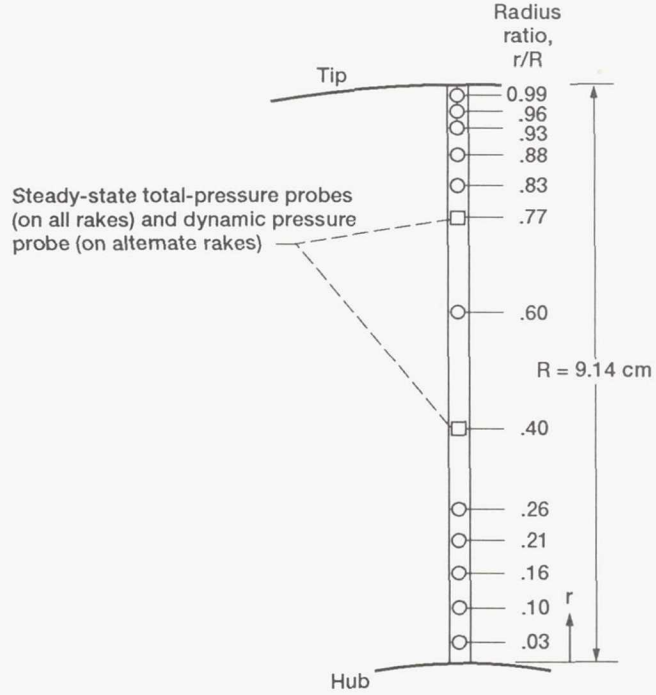

(b) Typical engine-face rake.

Figure 9.—Engine-face instrumentation.

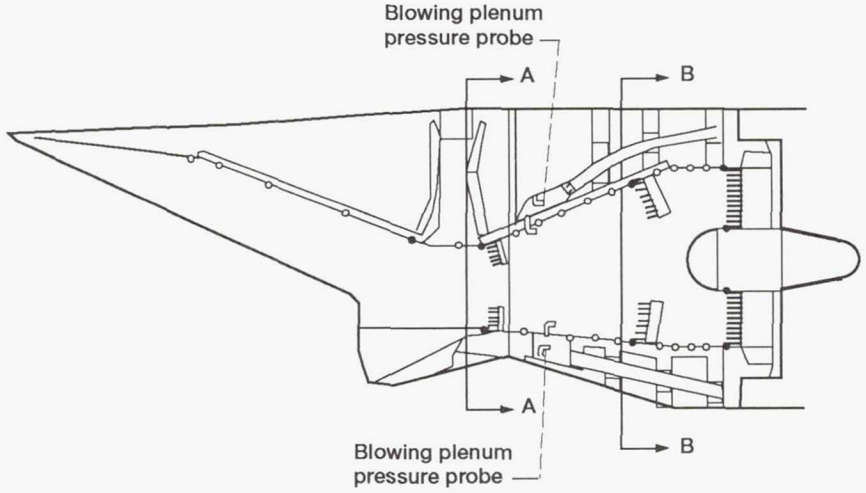

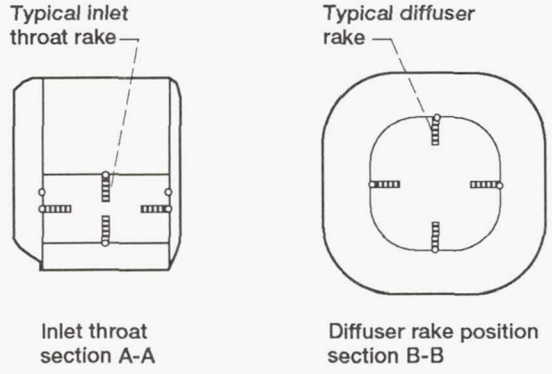

(a) Inlet static and total pressures.

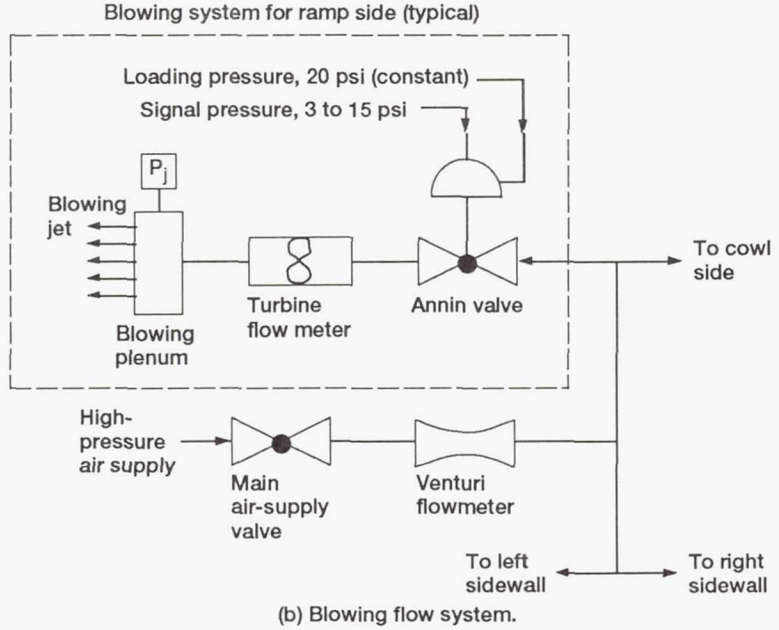

(b) Blowing flow system.

Figure 10.—Instrumentation for high-speed simulation.

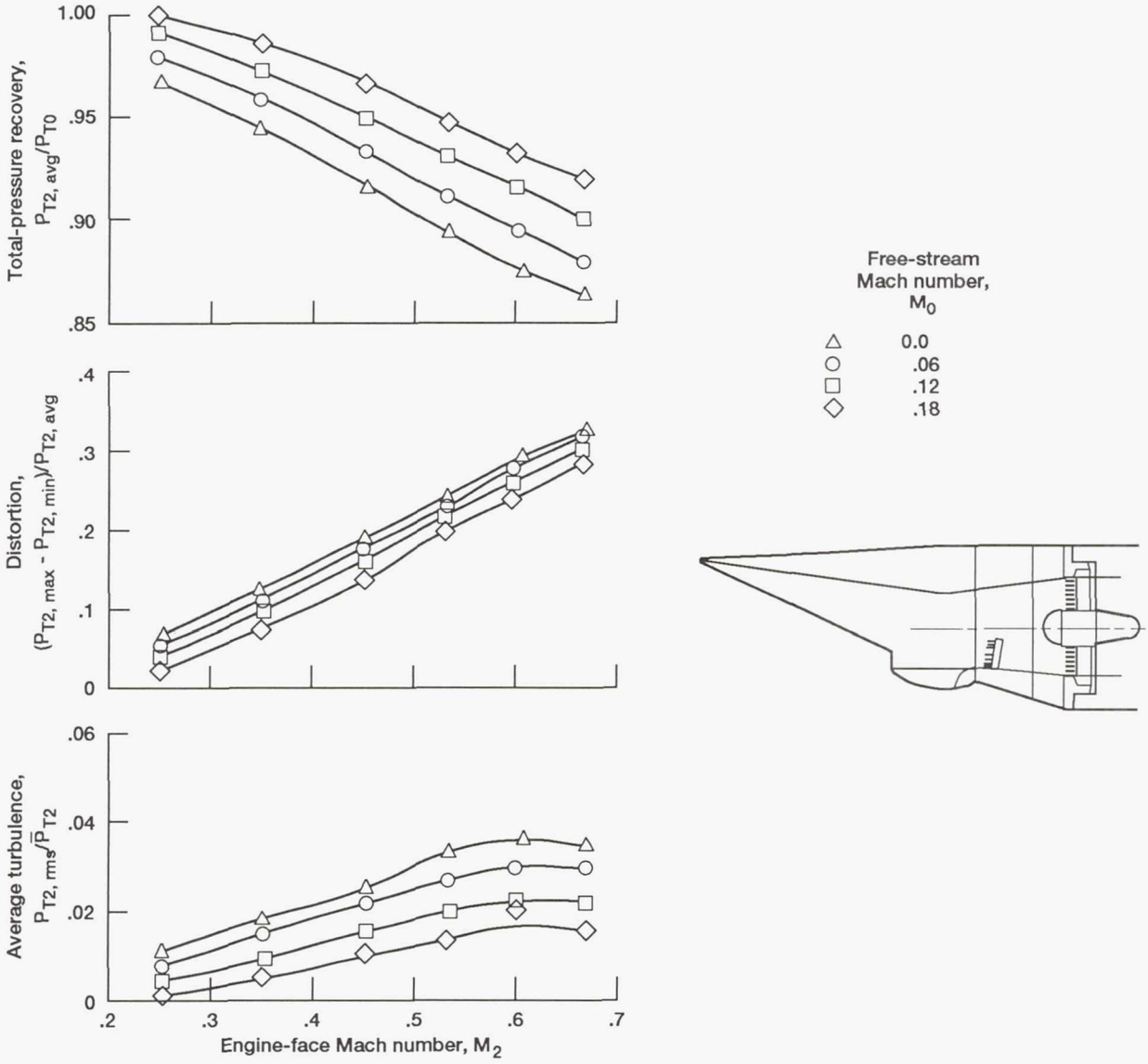

(a) Baseline inlet performance for several free-stream Mach numbers.

Figure 11.—Effect of engine-face Mach number on inlet performance. Angle of attack, $\alpha = 0°$; sideslip angle, $\beta = 0°$.

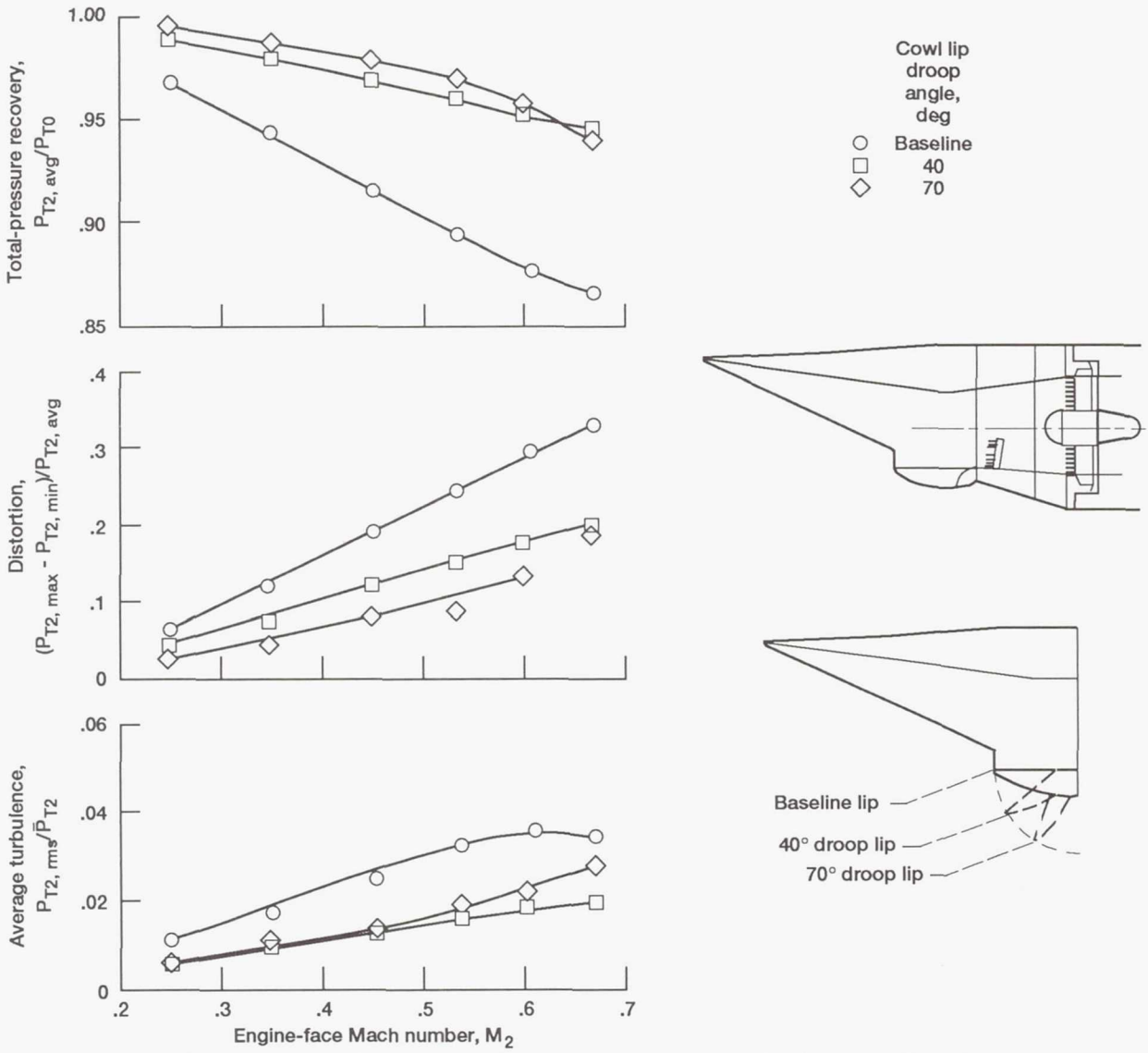

(b) Effect of droop lip angle on inlet performance. Free-stream Mach number, $M_0 = 0.0$.

Figure 11.—Concluded.

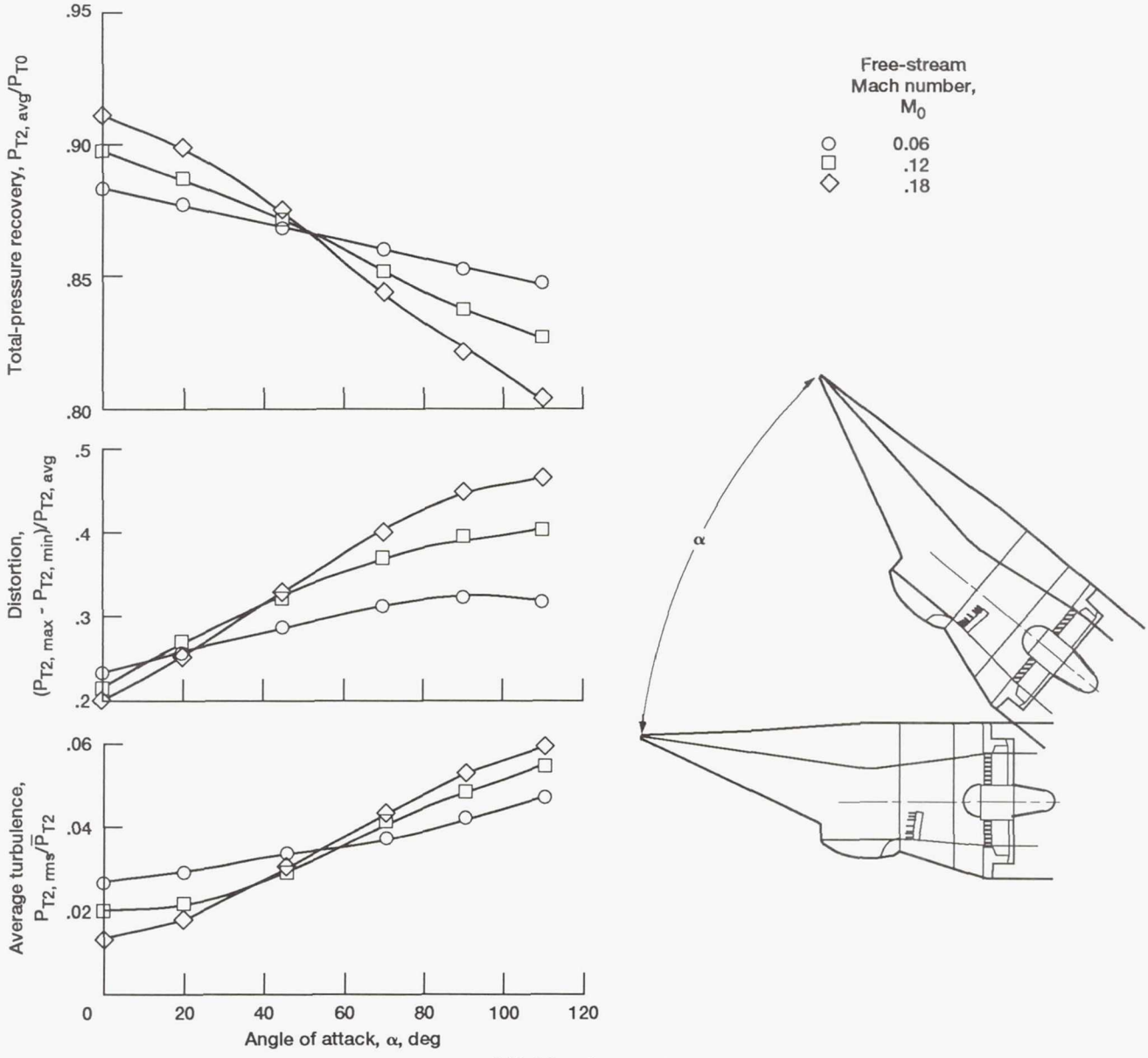

(a) Inlet performance.

Figure 12.—Effect of angle of attack, α, on inlet baseline performance. Design engine-face Mach number, M_2 = 0.533; sideslip angle, β = 0°.

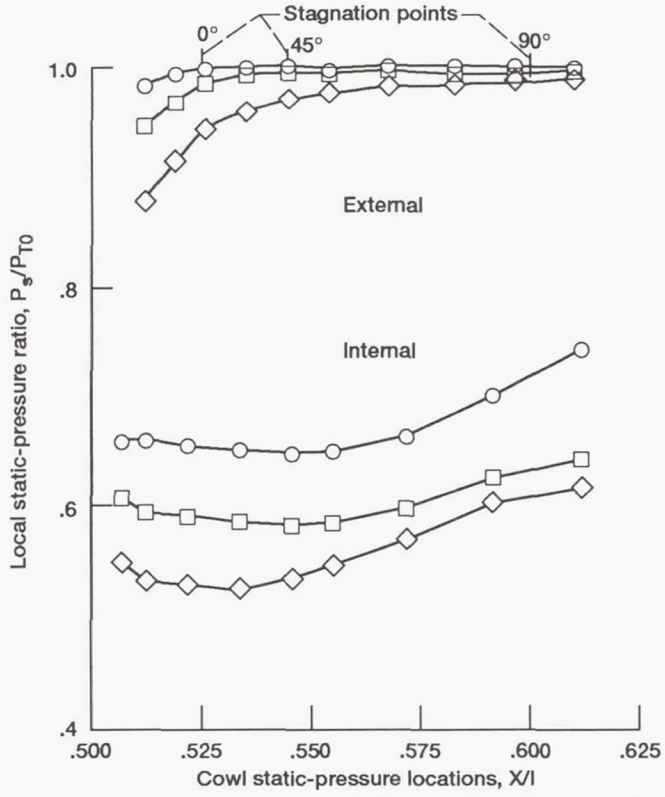

(b) Cowl static-pressure distribution. Free-stream Mach number, $M_0 = 0.12$.

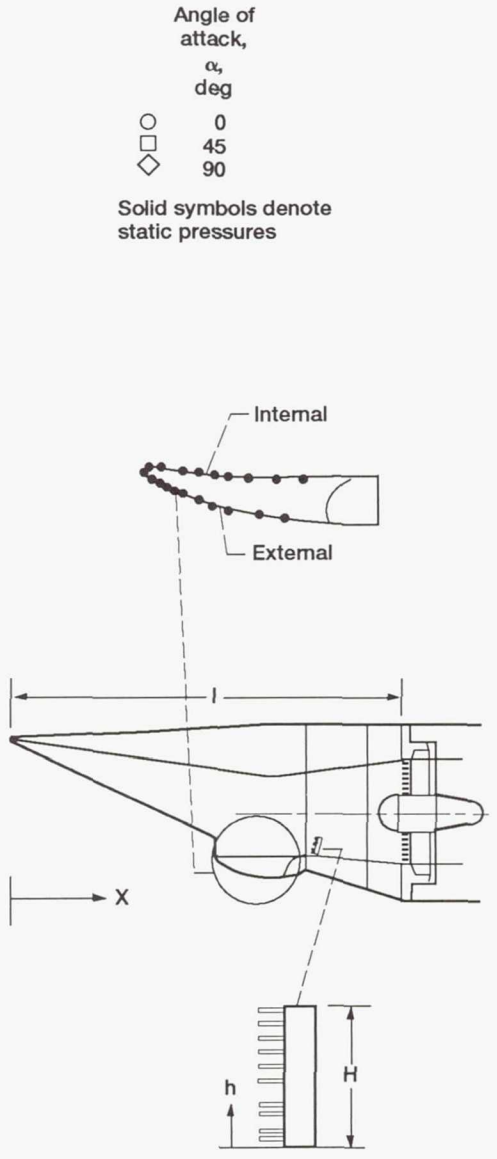

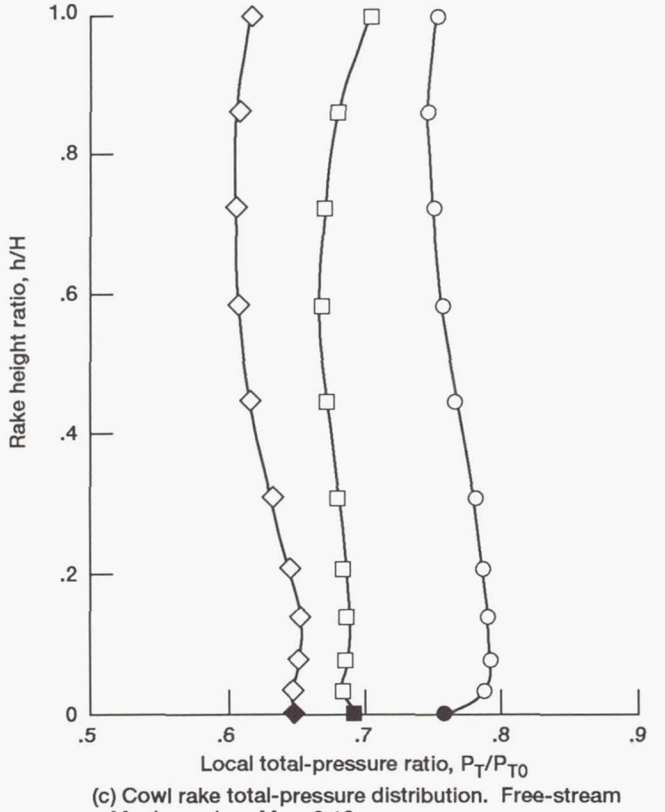

(c) Cowl rake total-pressure distribution. Free-stream Mach number, $M_0 = 0.12$.

Figure 12.—Continued.

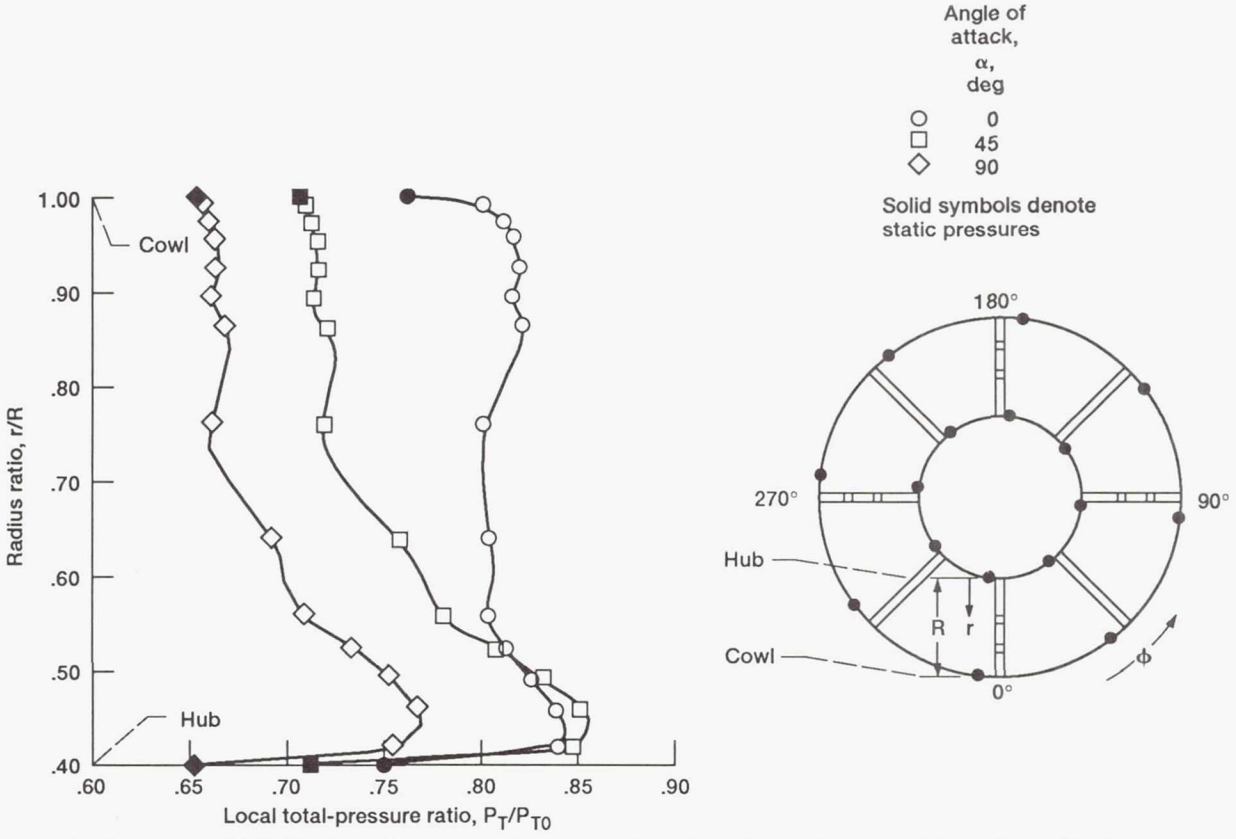

(d) Total-pressure distribution for bottom engine face rake. Circumferential position, $\phi = 0°$; free-stream Mach number, $M_0 = 0.12$.

Figure 12.—Continued.

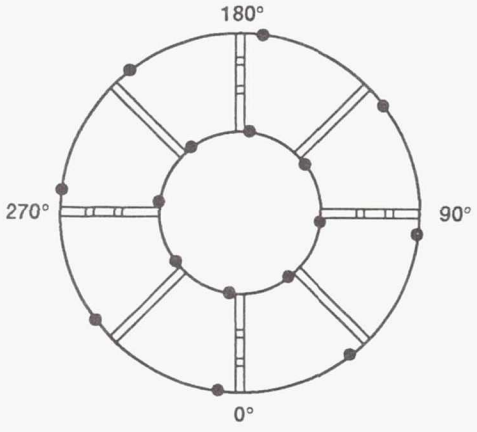

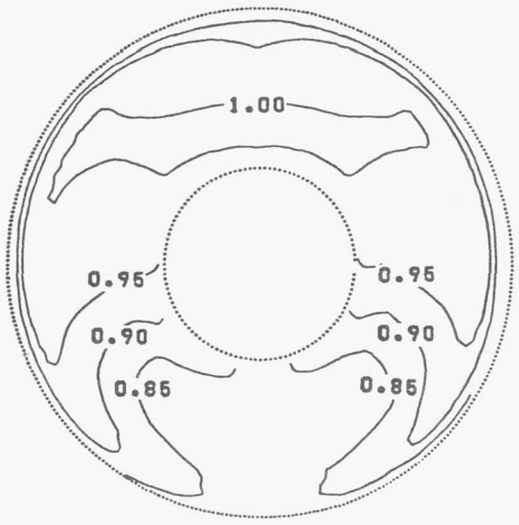

(e-1) Angle of attack, $\alpha = 0°$. Total-pressure recovery, $P_{T2, avg}/P_{T0} = 0.932$; distortion, $(P_{T2, max} - P_{T2, min})/P_{T2, avg} = 0.215$.

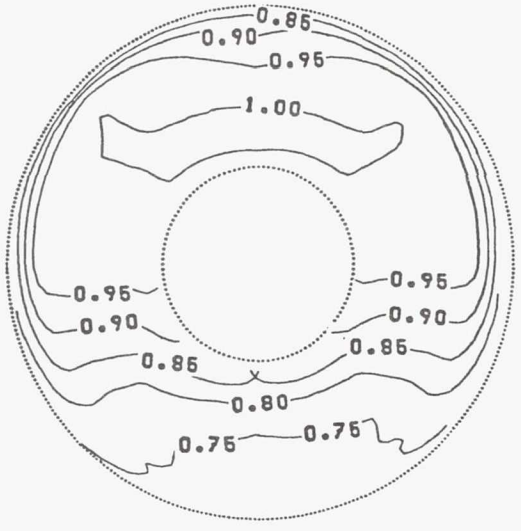

(e-2) Angle of attack, $\alpha = 45°$. Total-pressure recovery, $P_{T2, avg}/P_{T0} = 0.896$; distortion, $(P_{T2, max} - P_{T2, min})/P_{T2, avg} = 0.319$.

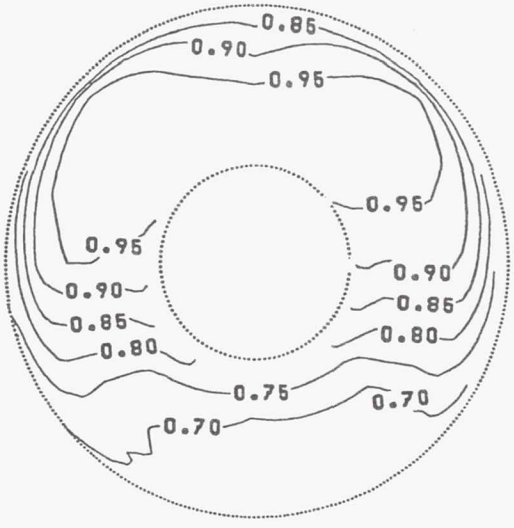

(e-3) Angle of attack, $\alpha = 90°$. Total-pressure recovery, $P_{T2, avg}/P_{T0} = 0.852$; distortion, $(P_{T2, max} - P_{T2, min})/P_{T2, avg} = 0.397$.

(e) Engine-face total-pressure recovery contours. Free-stream Mach number, $M_0 = 0.12$. (Numbers represent pressure ratios.)

Figure 12.—Concluded.

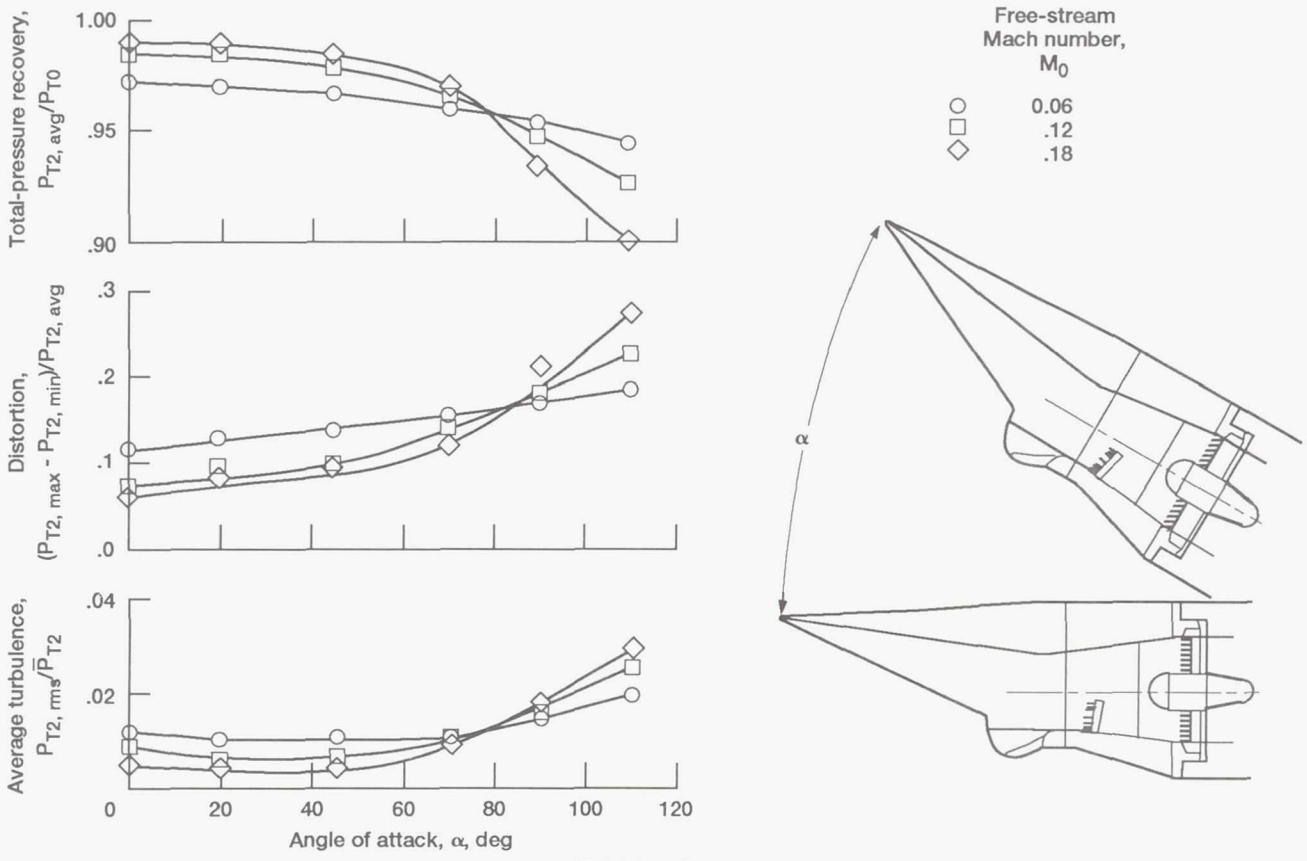

(a) Inlet performance.

Figure 13.—Effect of angle of attack on inlet performance with a 40°-droop cowl lip. Design engine-face Mach number, $M_2 = 0.533$; sideslip angle, $\beta = 0°$.

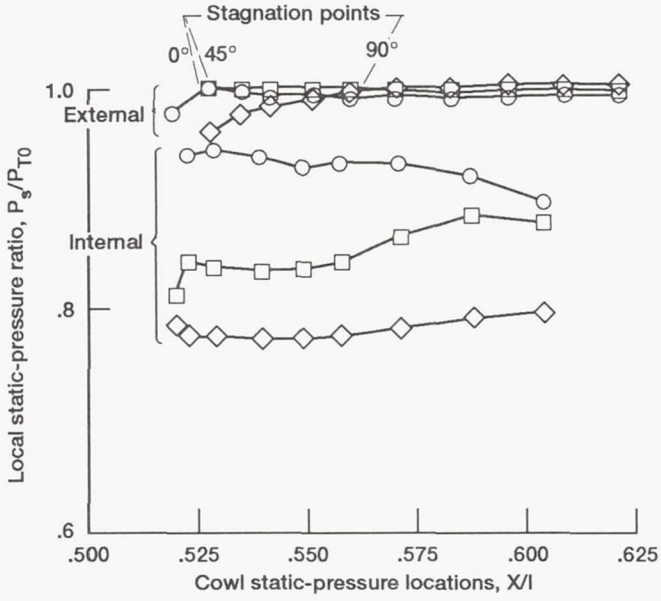

(b) Cowl surface static-pressure distribution. Free-stream Mach number, $M_0 = 0.12$.

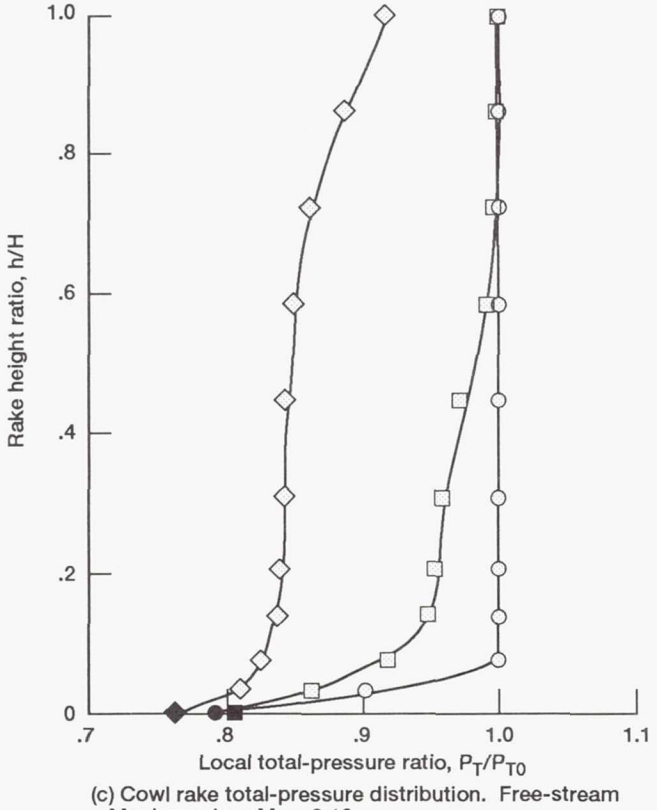

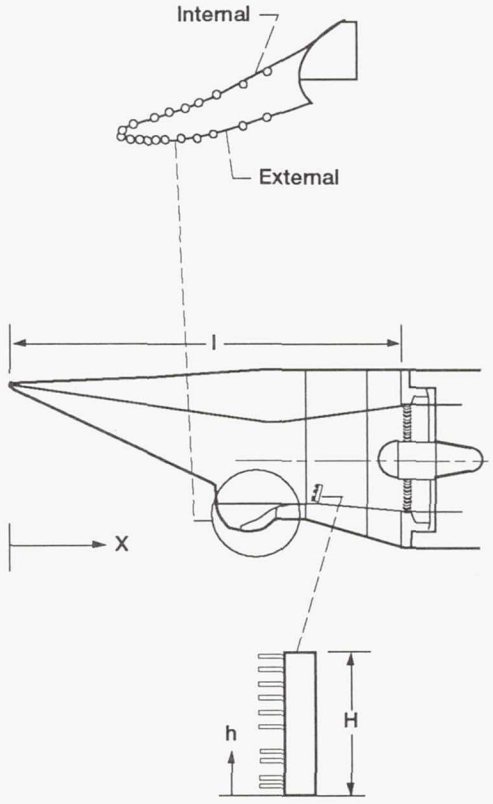

(c) Cowl rake total-pressure distribution. Free-stream Mach number, $M_0 = 0.12$.

Figure 13.—Continued.

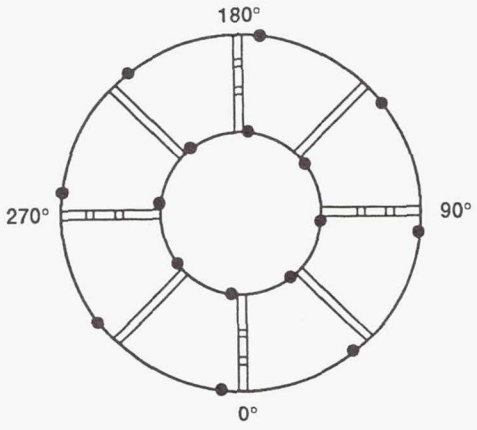

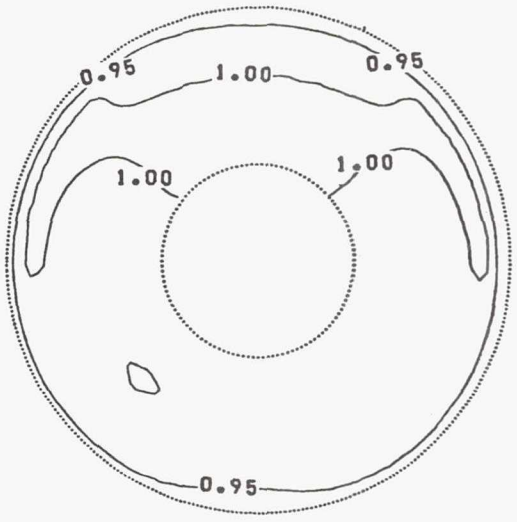

(d-1) Angle of attack, $\alpha = 0°$. Total-pressure recovery, $P_{T2, avg}/P_{T0} = 0.984$; distortion, $(P_{T2, max} - P_{T2, min})/P_{T2, avg} = 0.073$.

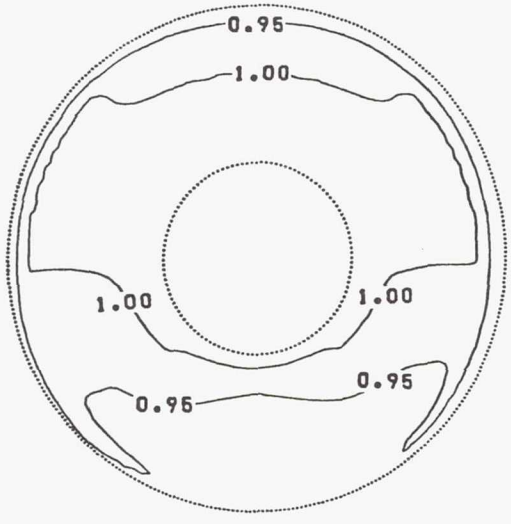

(d-2) Angle of attack, $\alpha = 45°$. Total-pressure recovery, $P_{T2, avg}/P_{T0} = 0.979$; distortion, $(P_{T2, max} - P_{T2, min})/P_{T2, avg} = 0.103$.

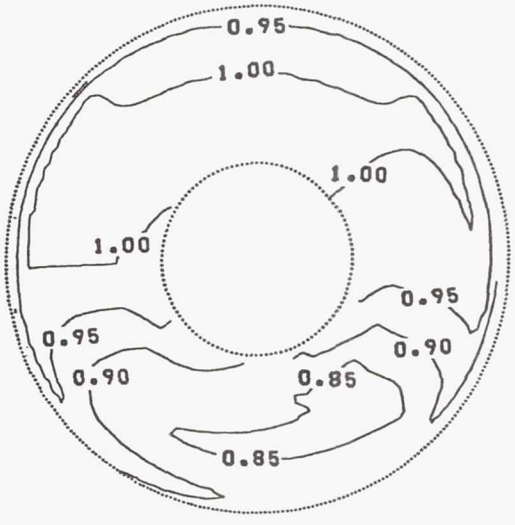

(d-3) Angle of attack, $\alpha = 90°$. Total-pressure recovery, $P_{T2, avg}/P_{T0} = 0.949$; distortion, $(P_{T2, max} - P_{T2, min})/P_{T2, avg} = 0.181$.

(d) Engine-face total-pressure recovery contours. Free-stream Mach number, $M_0 = 0.12$. (Numbers represent pressure ratios.)

Figure 13.—Concluded.

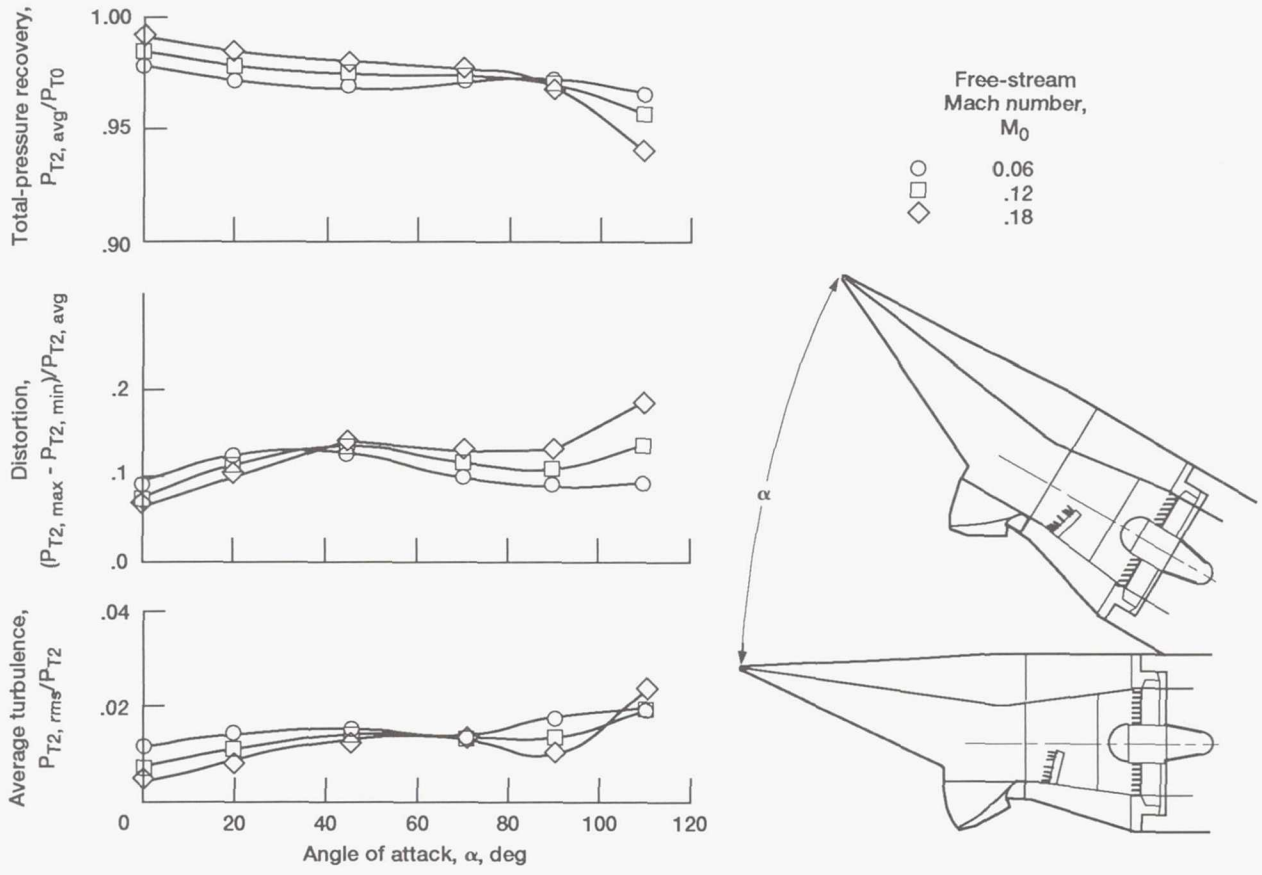

(a) Inlet performance.

Figure 14.—Effect of angle of attack, α, on inlet performance with a 70°-droop cowl lip. Design engine-face Mach number, $M_2 = 0.533$; sideslip angle, $\beta = 0°$.

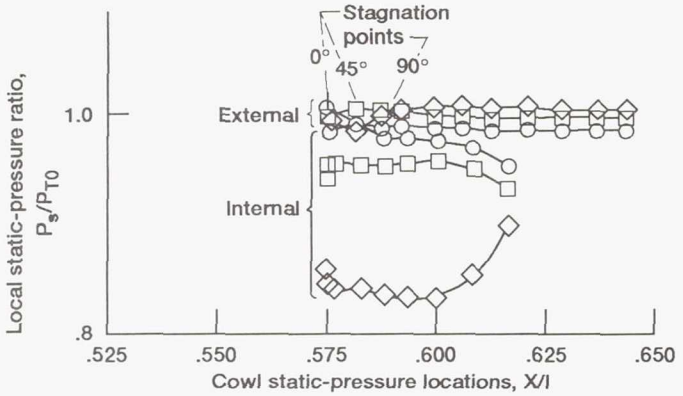

(b) Cowl static-pressure distribution. Free-stream Mach number, $M_0 = 0.12$.

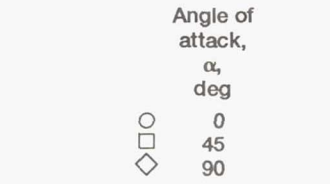

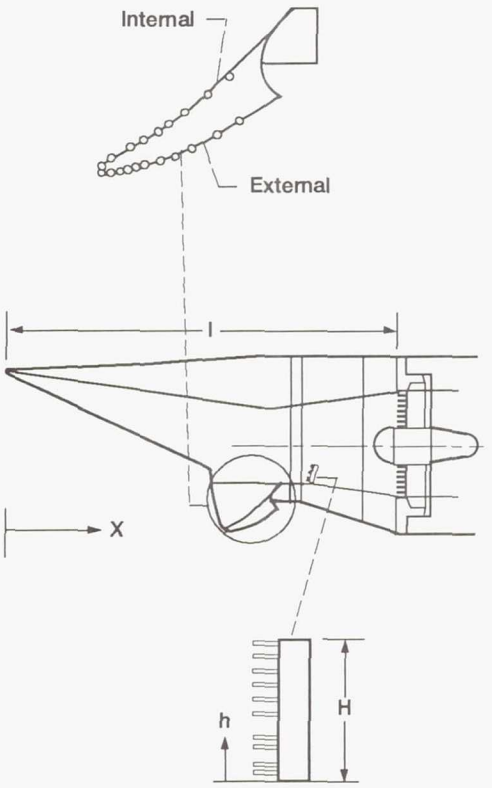

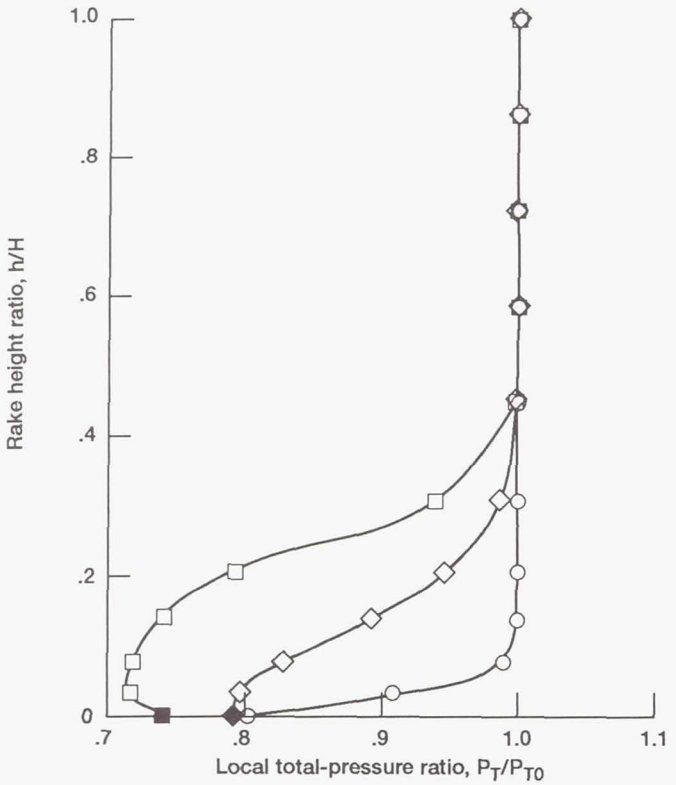

(c) Cowl rake total-pressure distribution. Free-stream Mach number, $M_0 = 0.12$.

Figure 14.—Continued.

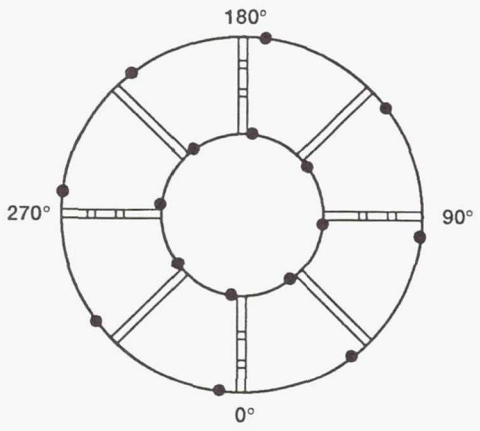

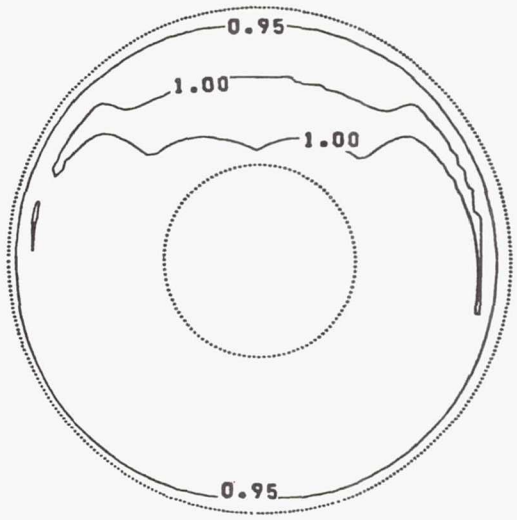

(d-1) Angle of attack, $\alpha = 0°$. Total-pressure recovery, $P_{T2, avg}/P_{T0} = 0.986$ distortion, $(P_{T2, max} - P_{T2, min})/P_{T2, avg} = 0.069$.

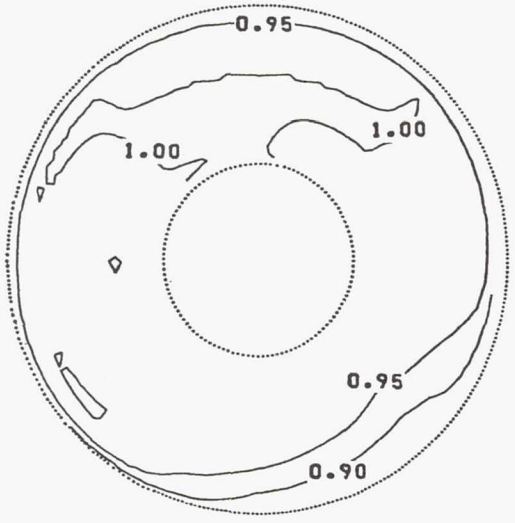

(d-2) Angle of attack, $\alpha = 45°$. Total-pressure recovery, $P_{T2, avg}/P_{T0} = 0.976$; distortion, $(P_{T2, max} - P_{T2, min})/P_{T2, avg} = 0.135$.

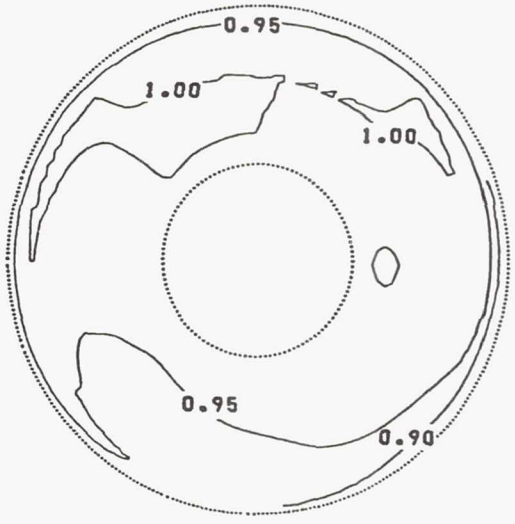

(d-3) Angle of attack, $\alpha = 90°$. Total-pressure recovery, $P_{T2, avg}/P_{T0} = 0.973$; distortion, $(P_{T2, max} - P_{T2, min})/P_{T2, avg} = 0.105$.

(d) Engine-face total-pressure recovery contours. Free-stream Mach number, $M_0 = 0.12$. (Numbers represent pressure ratios.)

Figure 14.—Concluded.

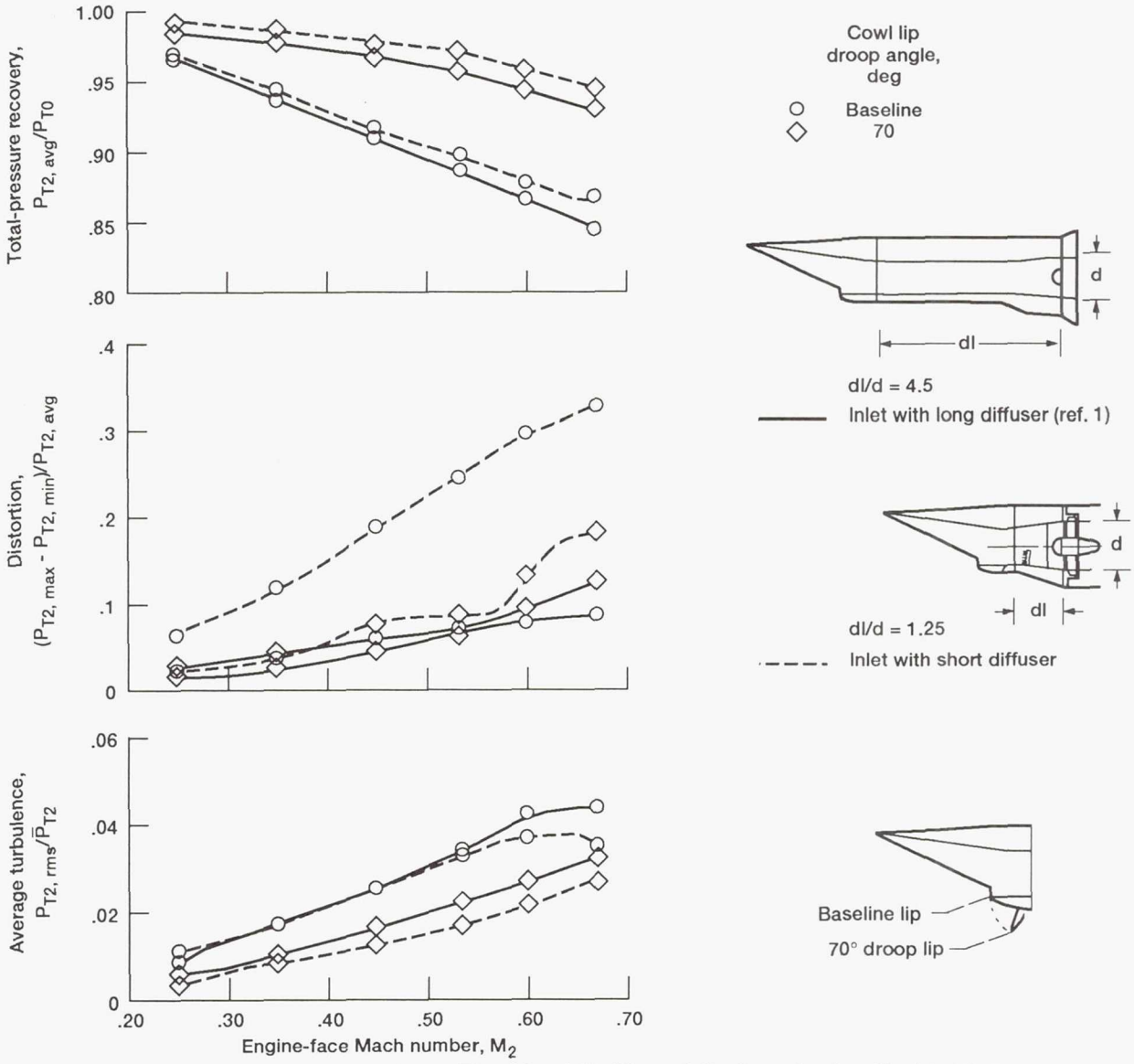

(a) Inlet performance at static condition (M_0 = 0.0) with a variation in engine-face Mach number.

Figure 15.—Comparison of inlet performance for the short diffuser versus the long diffuser. Sideslip angle, β = 0°.

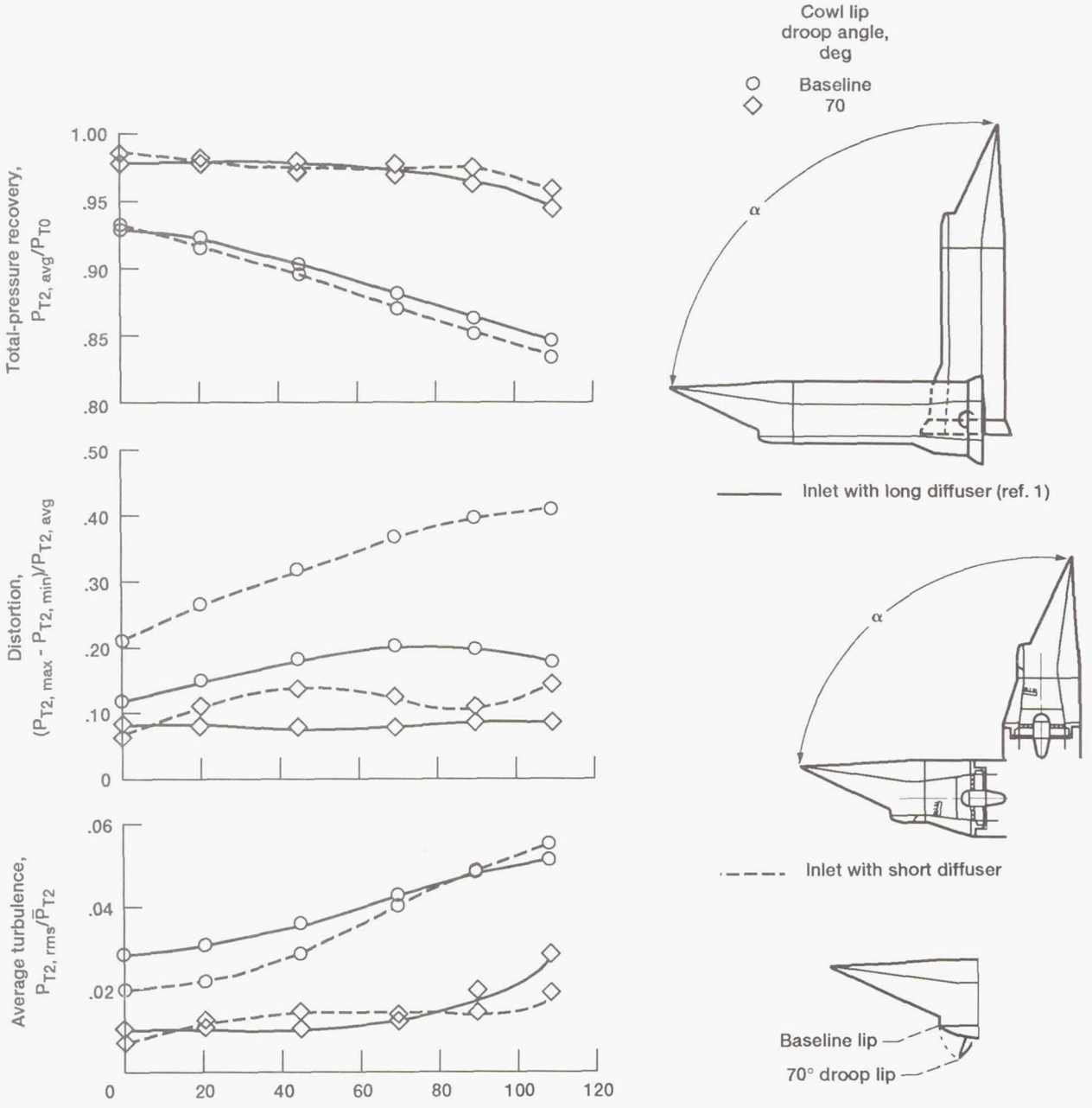

(b) Inlet performance at free-stream Mach number of 0.12 for various angles of attack, α. Engine-face Mach number, $M_2 = 0.533$.

Figure 15.—Concluded.

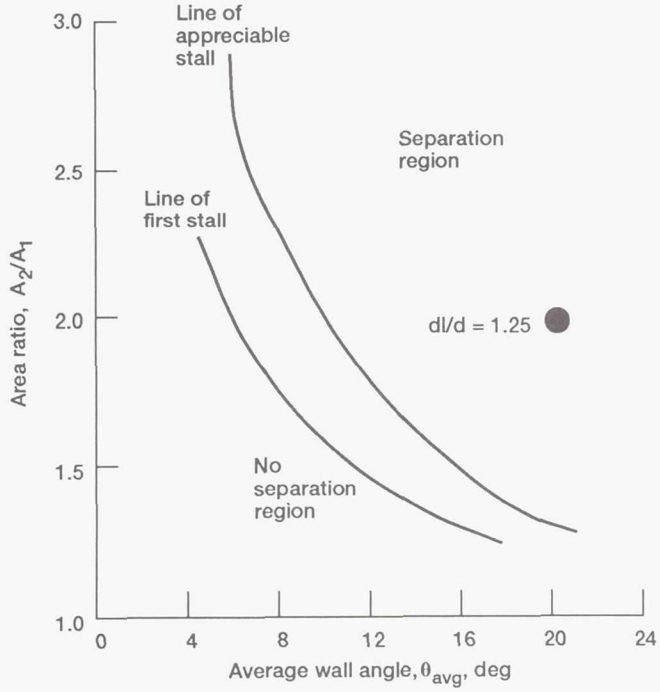

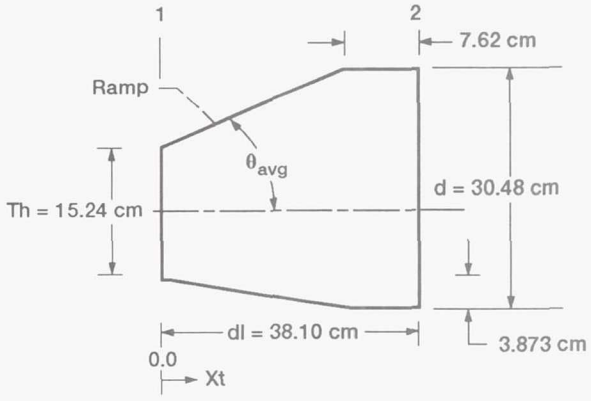

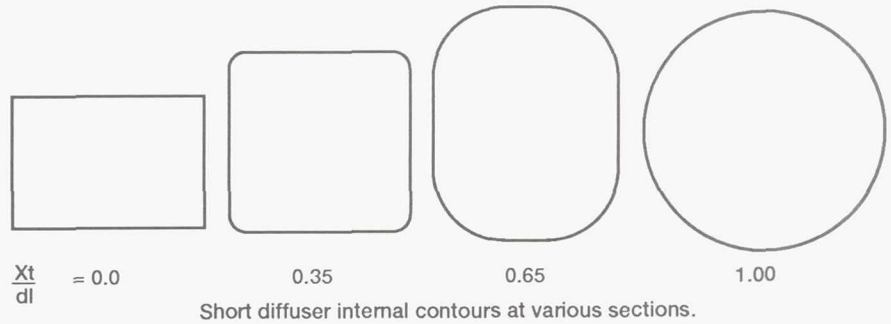

Short diffuser internal contours at various sections.

Figure 16.—Prediction of flow separation for the short diffuser.

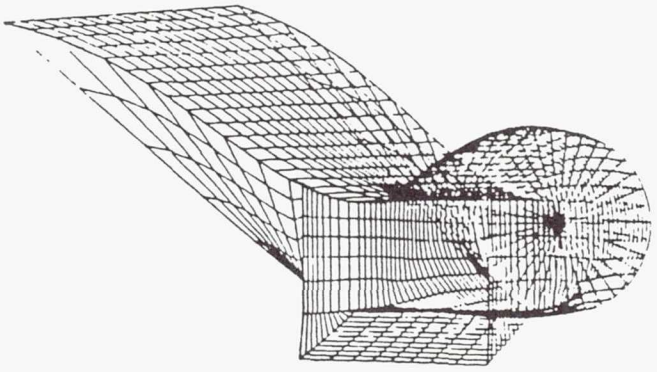

(a) Panel grid.

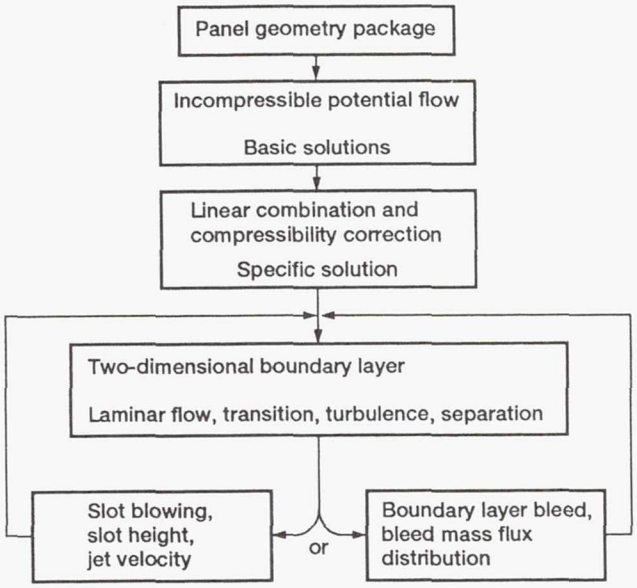

(b) Schematic diagram of Hess potential flow and Herring boundary layer analysis computer codes.

Figure 17.—Panel geometry and algorithm for code computation.

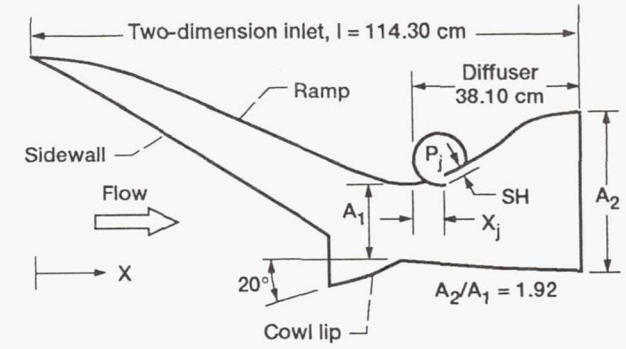

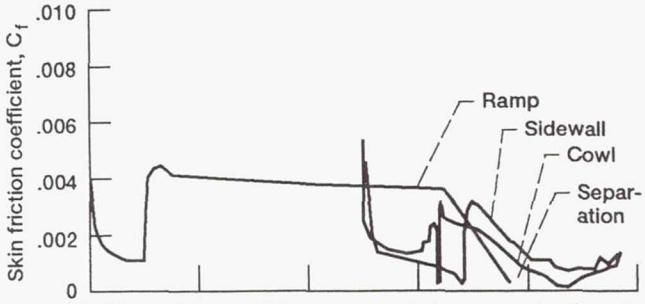

(a) Skin friction coefficient from analytical analysis without boundary layer control. Inlet throat station Mach number, M_1 = 0.8.

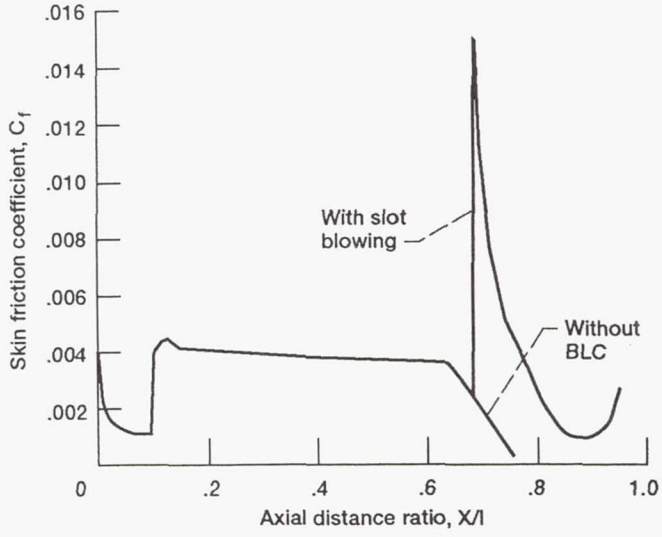

(b) Comparison of ramp skin friction coefficient from analytical analysis with and without slot blowing. For slot blowing, slot height, SH ≈ 0.076 cm; distance from inlet throat to blowing jet exit, X_j = 4.3 cm; blowing-jet to free-stream pressure ratio, P_j/P_{T0} = 2.0.

Figure 18.—Analytical prediction of skin friction coefficient for the short diffuser with and without boundary layer control (BLC) blowing.

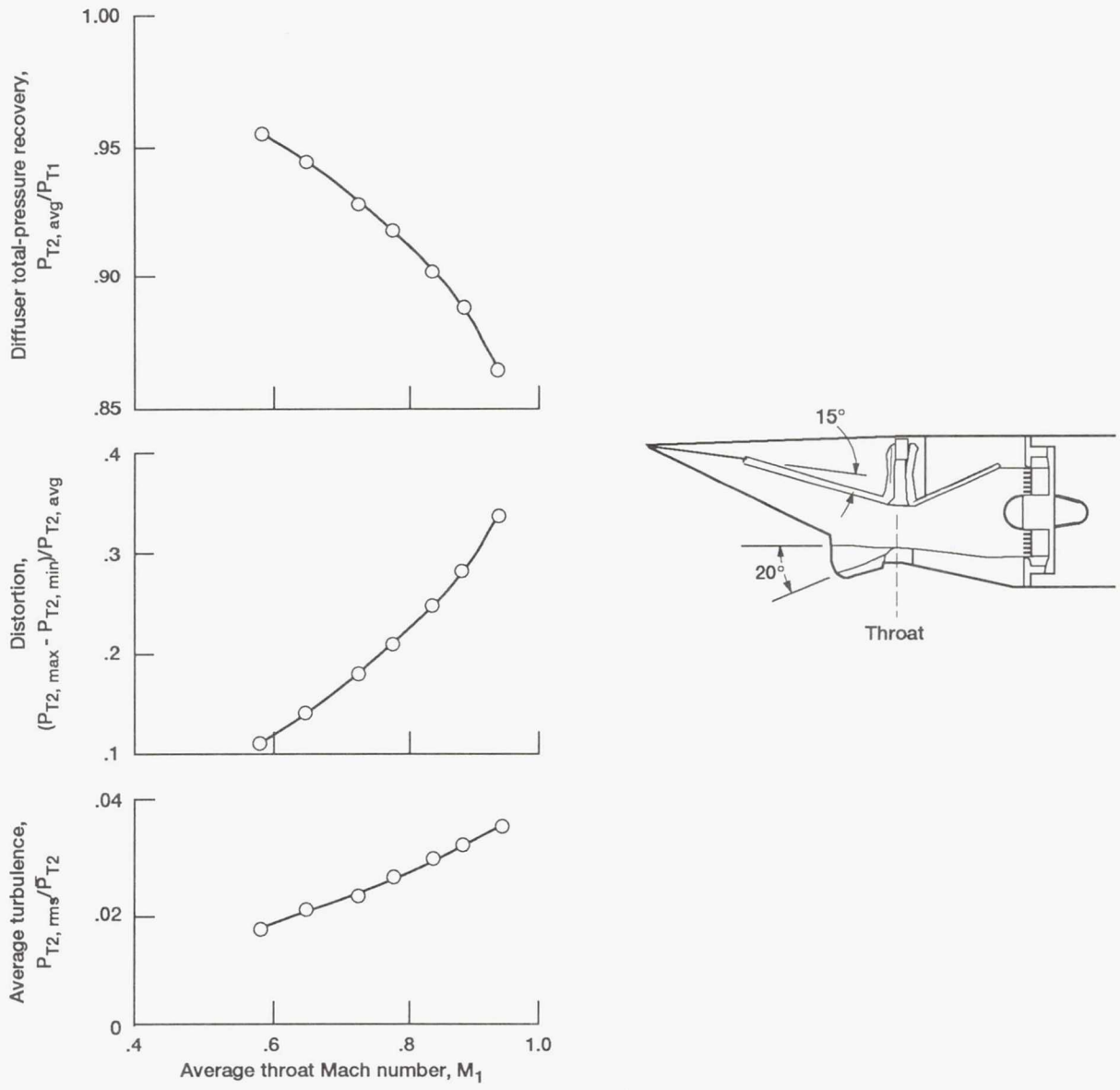

(a) Diffuser baseline performance.

Figure 19.—Diffuser baseline performance (no BLC) and pressure distributions for the diffuser configuration at Mach 2.2 ramp position. Free-stream Mach number, $M_0 = 0.12$; angle of attack, $\alpha = 0°$.

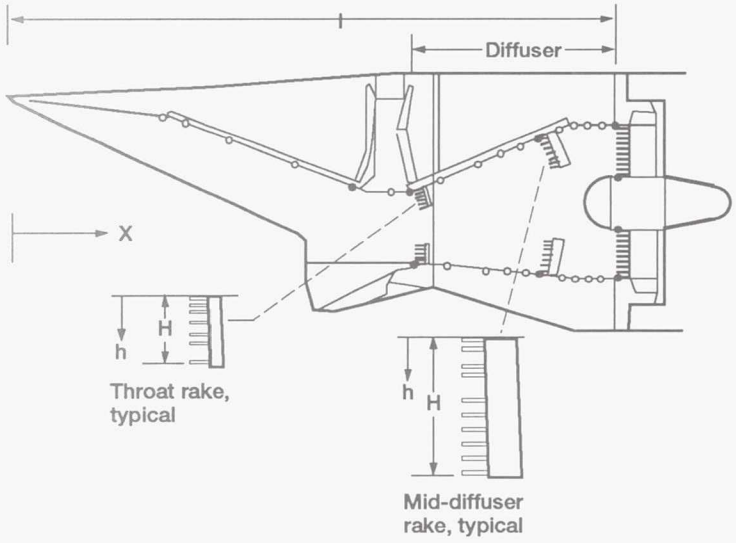

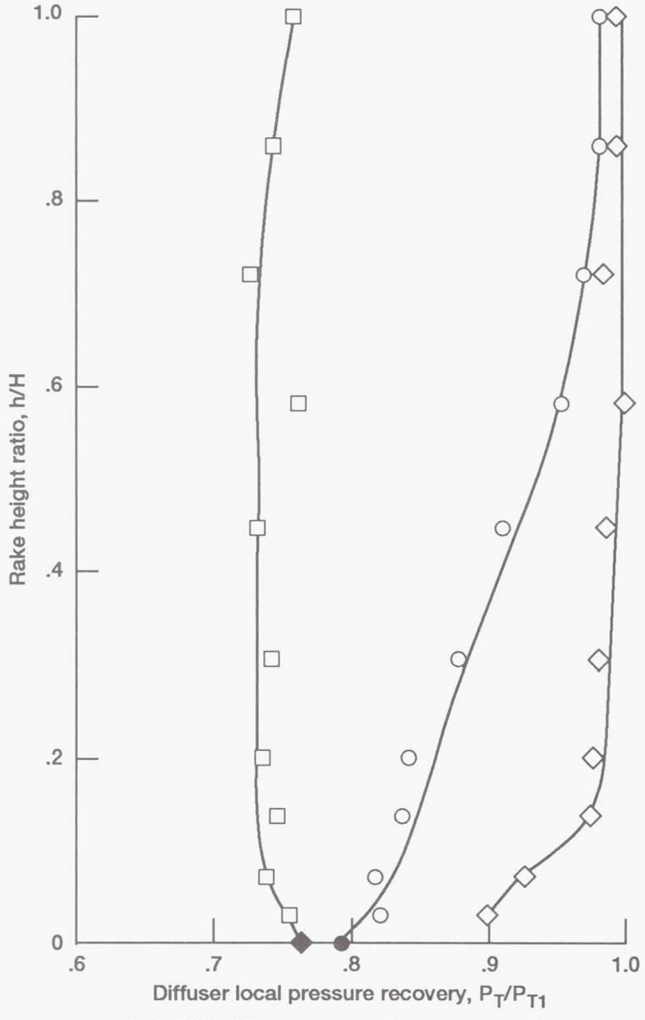

(b-2) Mid-diffuser rake total-pressure profiles.

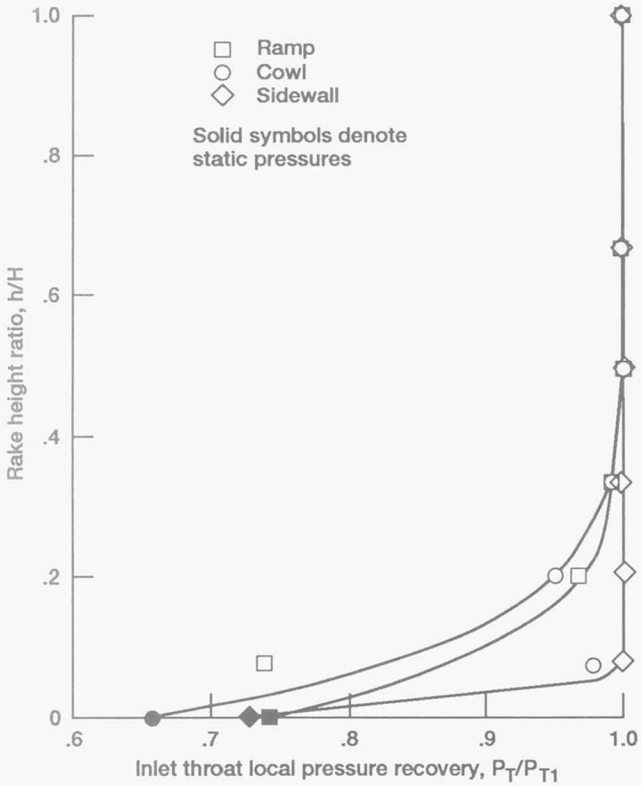

(b-1) Throat rake total-pressure profiles.

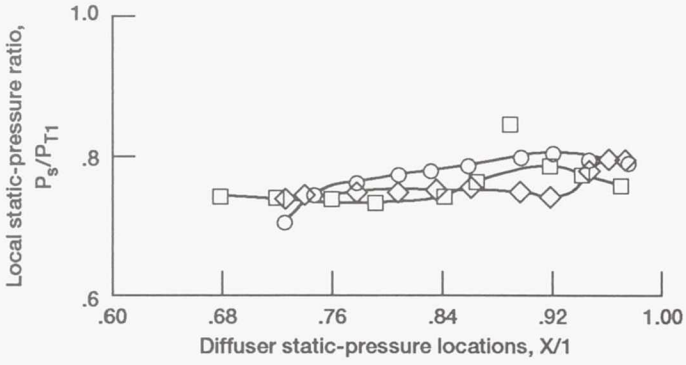

(b-3) Diffuser static-pressure distribution.

(b) Baseline diffuser total- and static-pressure distributions. Average throat Mach number, $M_1 = 0.77$.

Figure 19.—Continued.

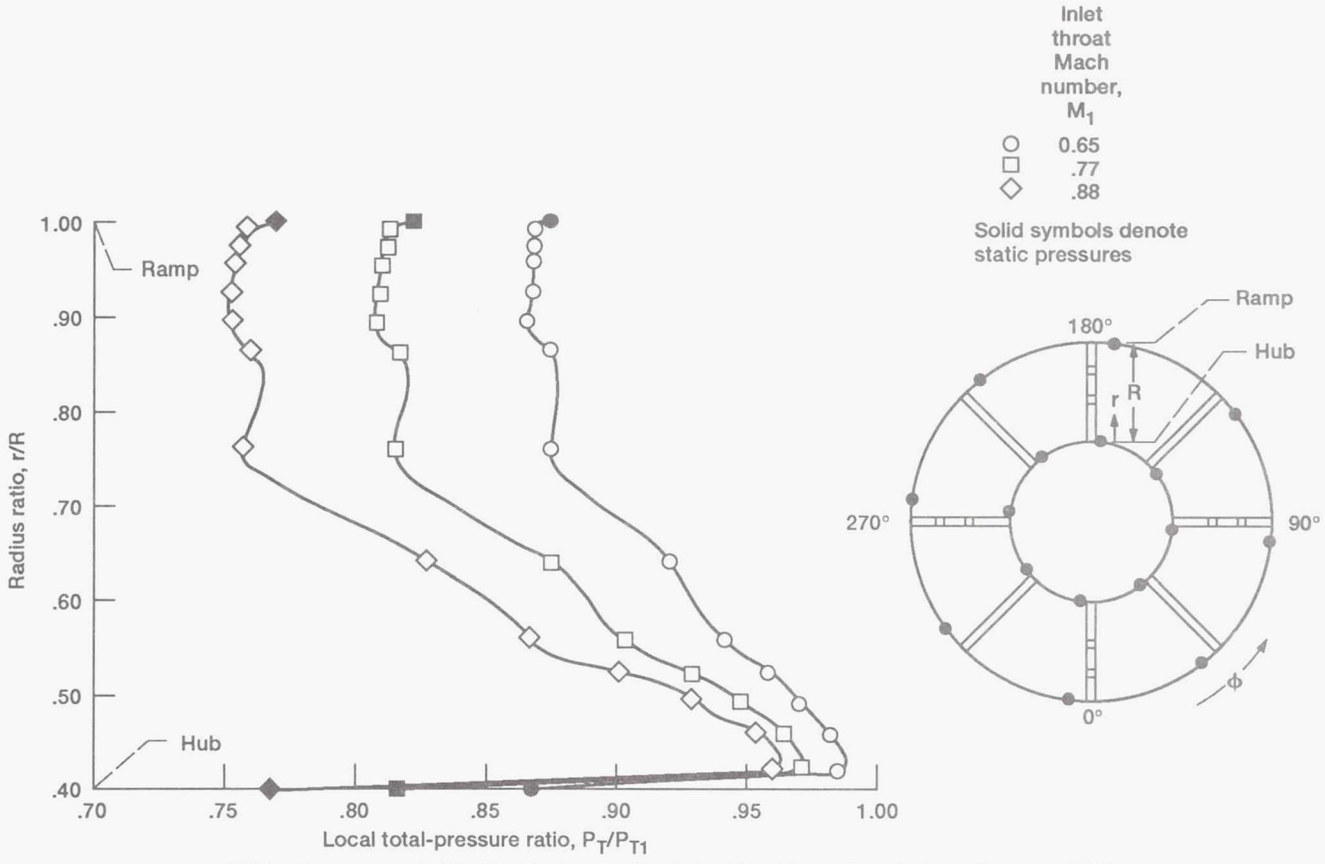

(c) Total-pressure distribution for top engine-face rake. Circumferential position, $\phi = 180°$.

Figure 19.—Continued.

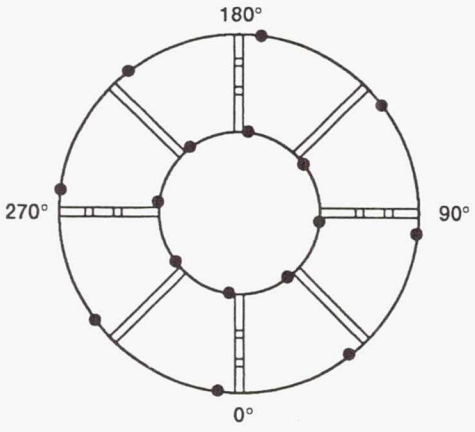

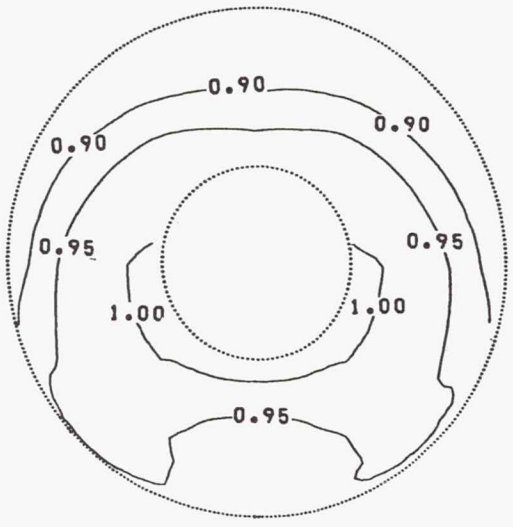

(d-1) Average throat Mach number, M_1 = 0.65; diffuser total-pressure recovery, $P_{T2,\,avg}/P_{T1}$ = 0.945; distortion, $(P_{T2,\,max} - P_{T2,\,min})/P_{T2,\,avg}$ = 0.142.

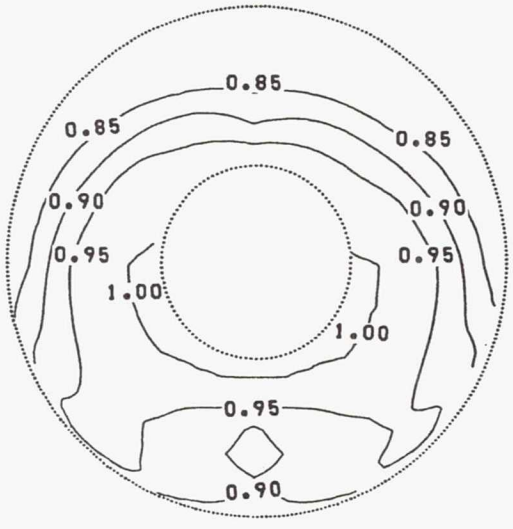

(d-2) Average throat Mach number, M_1 = 0.77; diffuser total-pressure recovery, $P_{T2,\,avg}/P_{T1}$ = 0.919; distortion, $(P_{T2,\,max} - P_{T2,\,min})/P_{T2,\,avg}$ = 0.211.

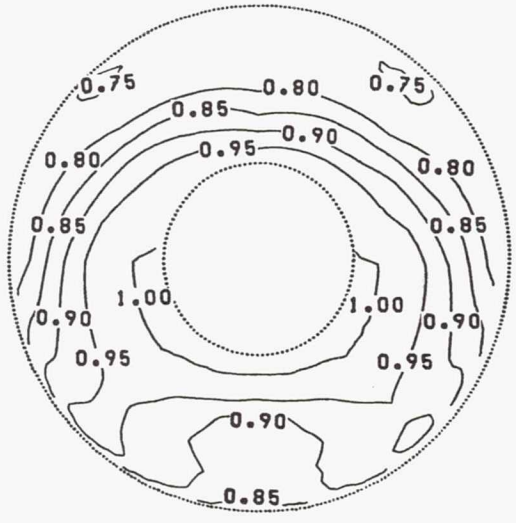

(d-3) Average throat Mach number, M_1 = 0.88; diffuser total-pressure recovery, $P_{T2,\,avg}/P_{T1}$ = 0.889; distortion, $(P_{T2,\,max} - P_{T2,\,min})/P_{T2,\,avg}$ = 0.285.

(d) Effect of average throat Mach number on diffuser baseline total-pressure recovery and distortion. (Numbers represent pressure ratios.)

Figure 19.—Concluded.

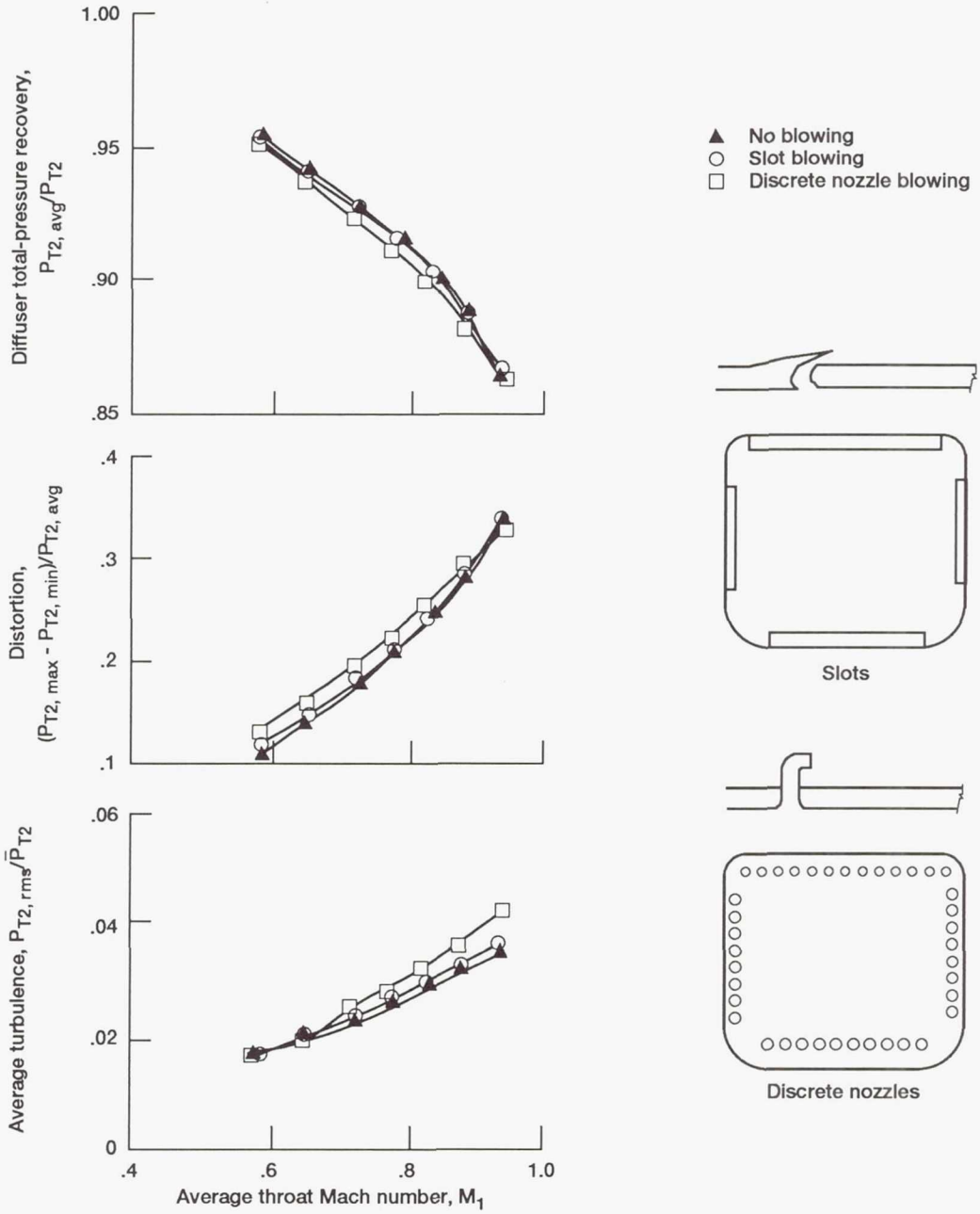

Figure 20.—Comparison of slots and discrete nozzles with diffuser baseline performance at Mach 2.2 ramp position. Free-stream Mach number, $M_0 = 0.12$; angle of attack, $\alpha = 0.0$.

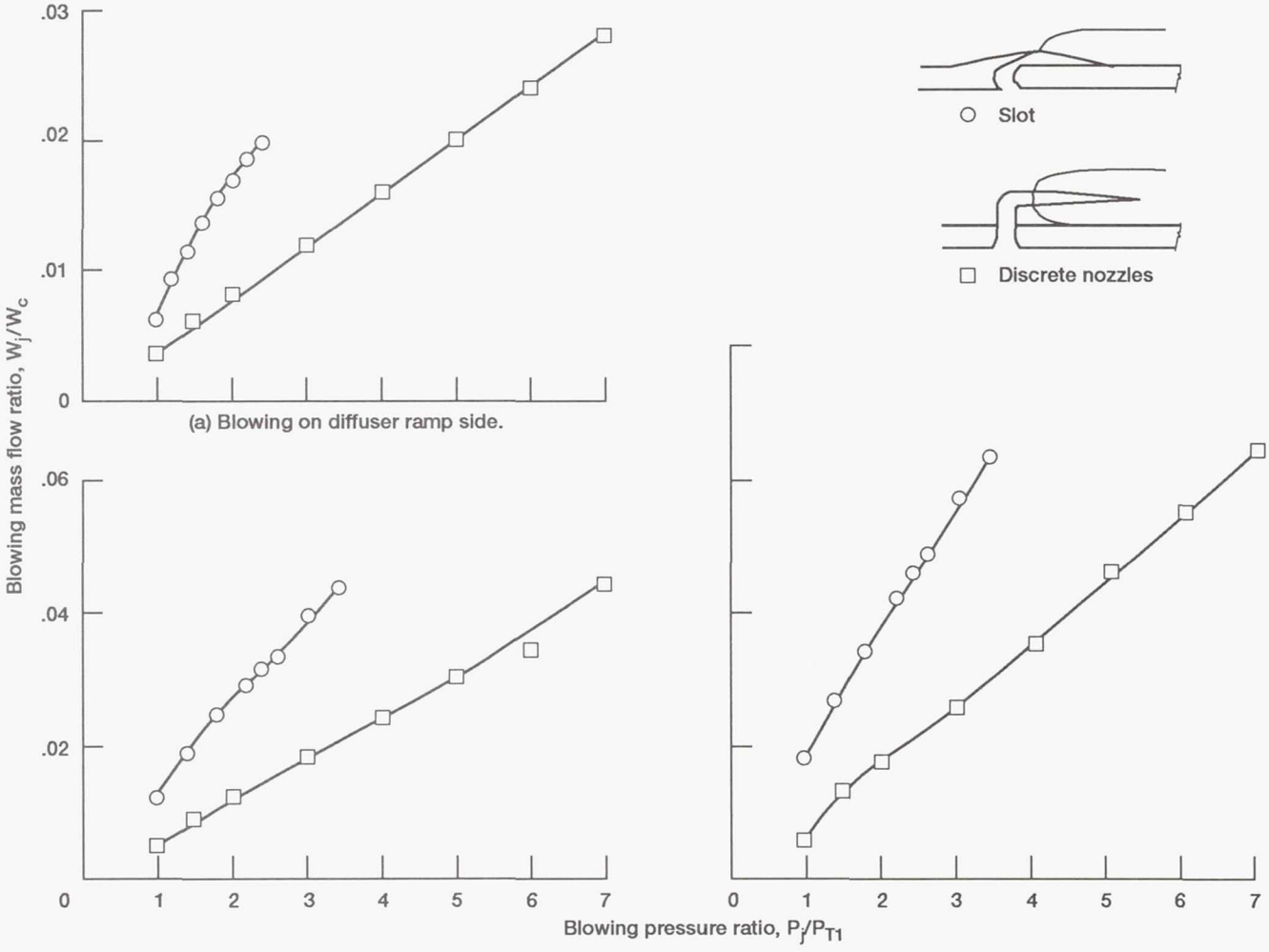

Figure 21.—Blowing mass flow ratio versus blowing pressure ratio for slots and discrete nozzles. Average throat Mach number, $M_1 = 0.77$.

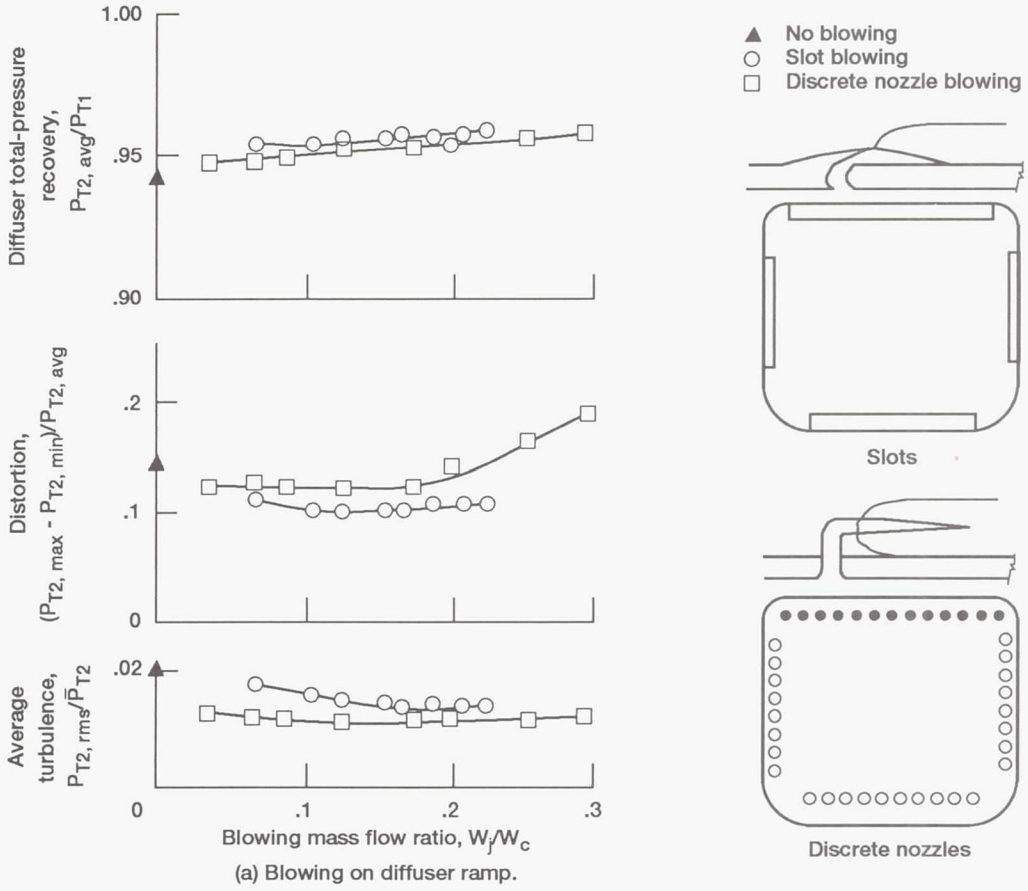

(a) Blowing on diffuser ramp.

Figure 22.—Effect of blowing on diffuser performance for throat Mach number, M_1, of 0.65 and a Mach 2.2 ramp position. Free-stream Mach number, $M_0 = 0.12$; angle of attack, $\alpha = 0°$.

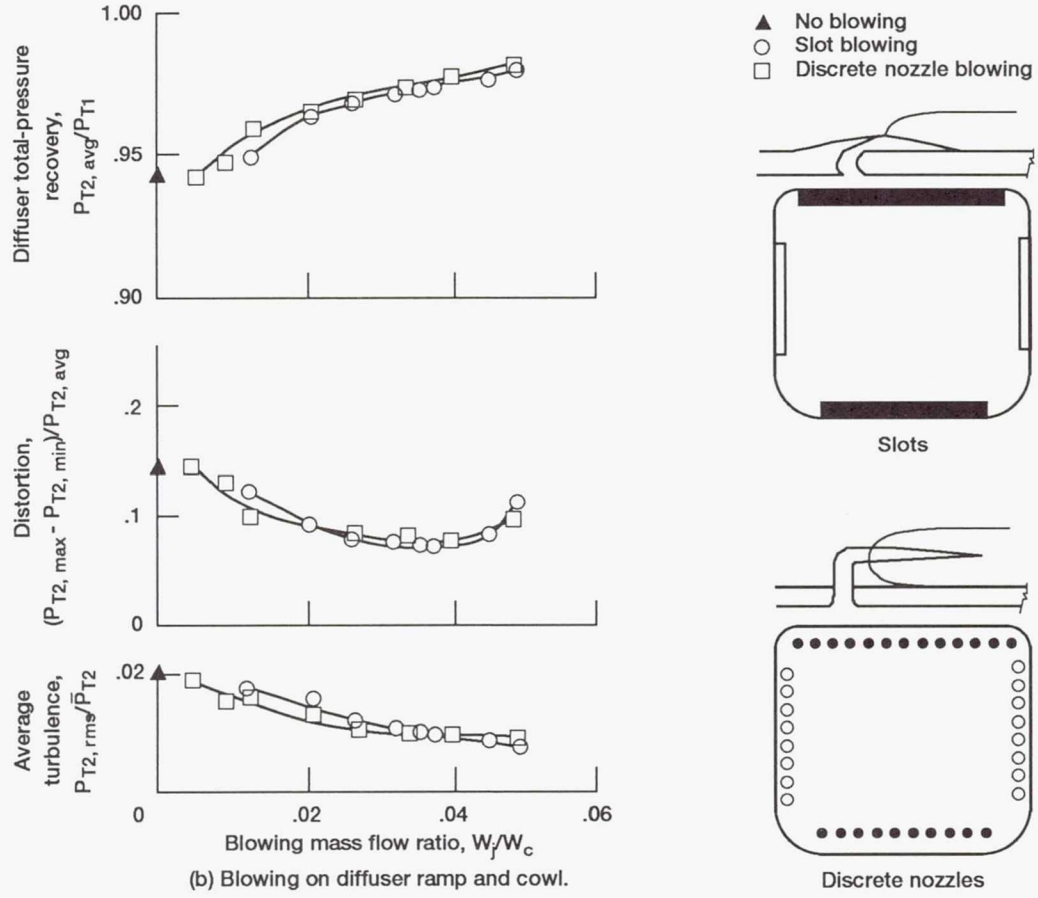

(b) Blowing on diffuser ramp and cowl.

Figure 22.—Continued.

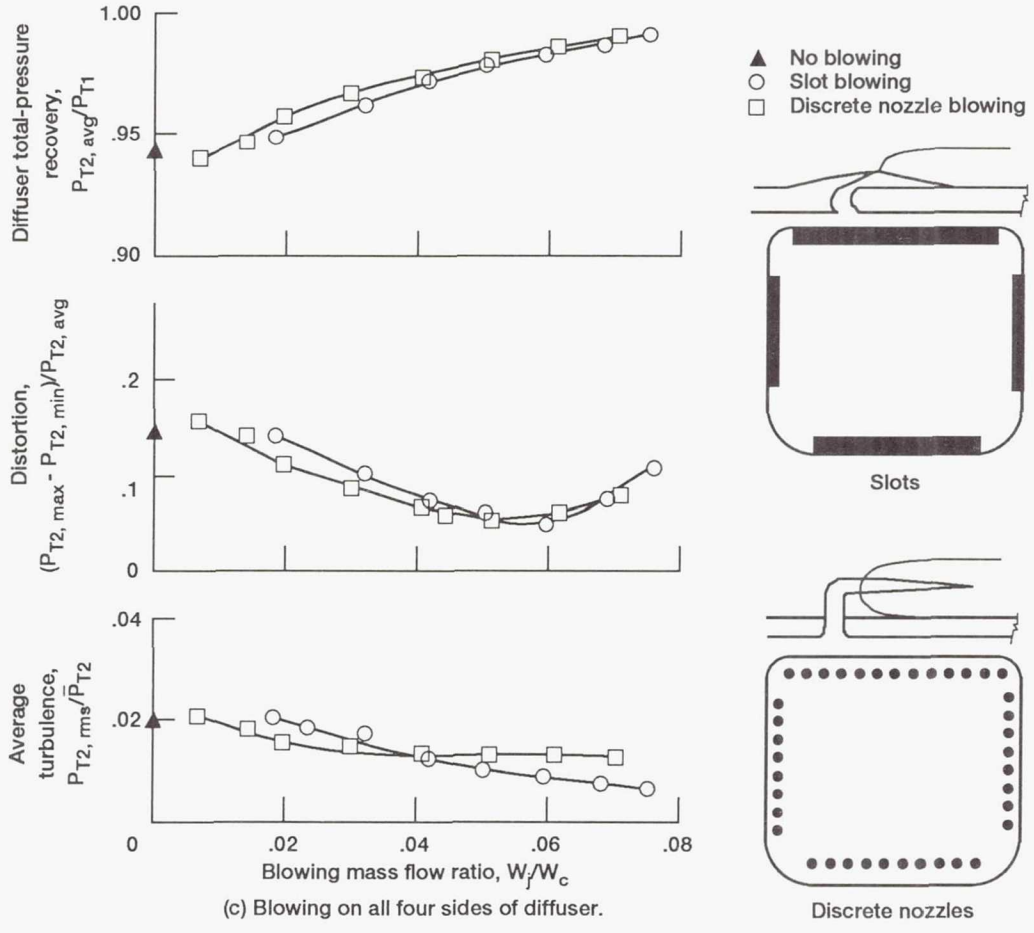

(c) Blowing on all four sides of diffuser.

Figure 22.—Concluded.

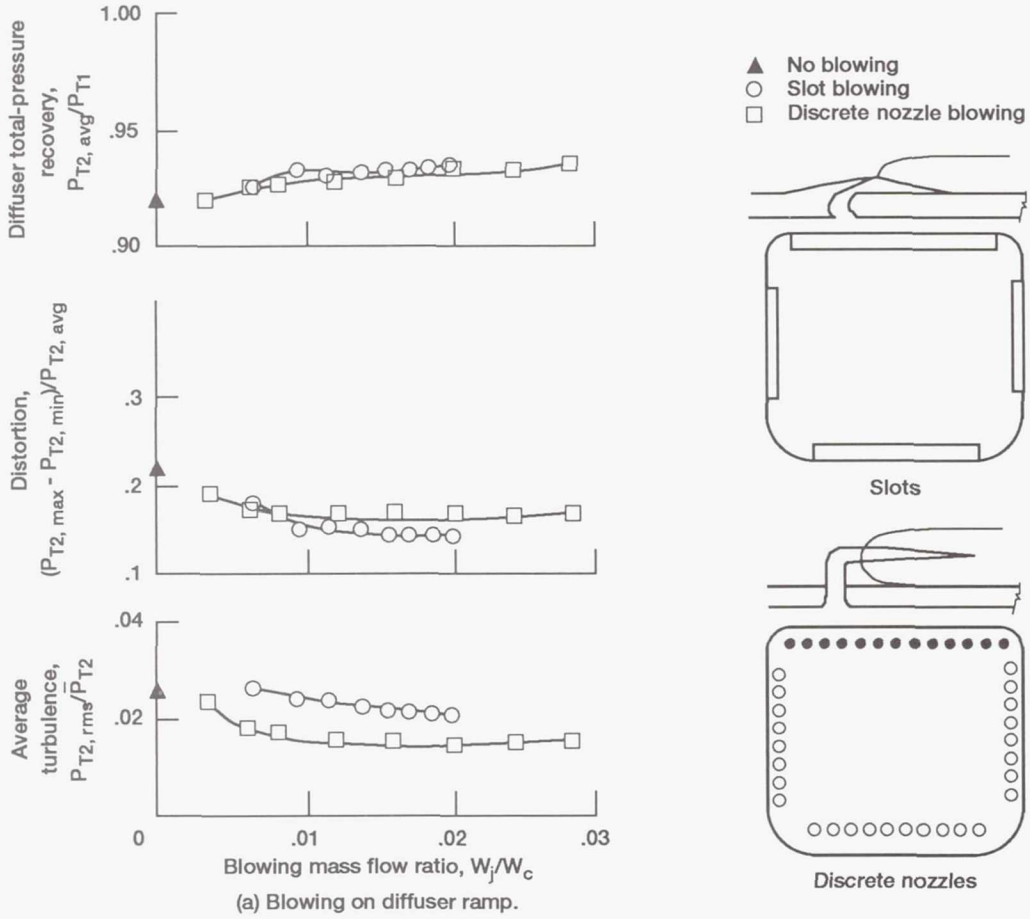

(a) Blowing on diffuser ramp.

Figure 23.—Effect of blowing on diffuser performance for throat Mach number, M_1, of 0.77 and a Mach 2.2 ramp position. Free-stream Mach number, $M_0 = 0.12$; angle of attack, $\alpha = 0°$.

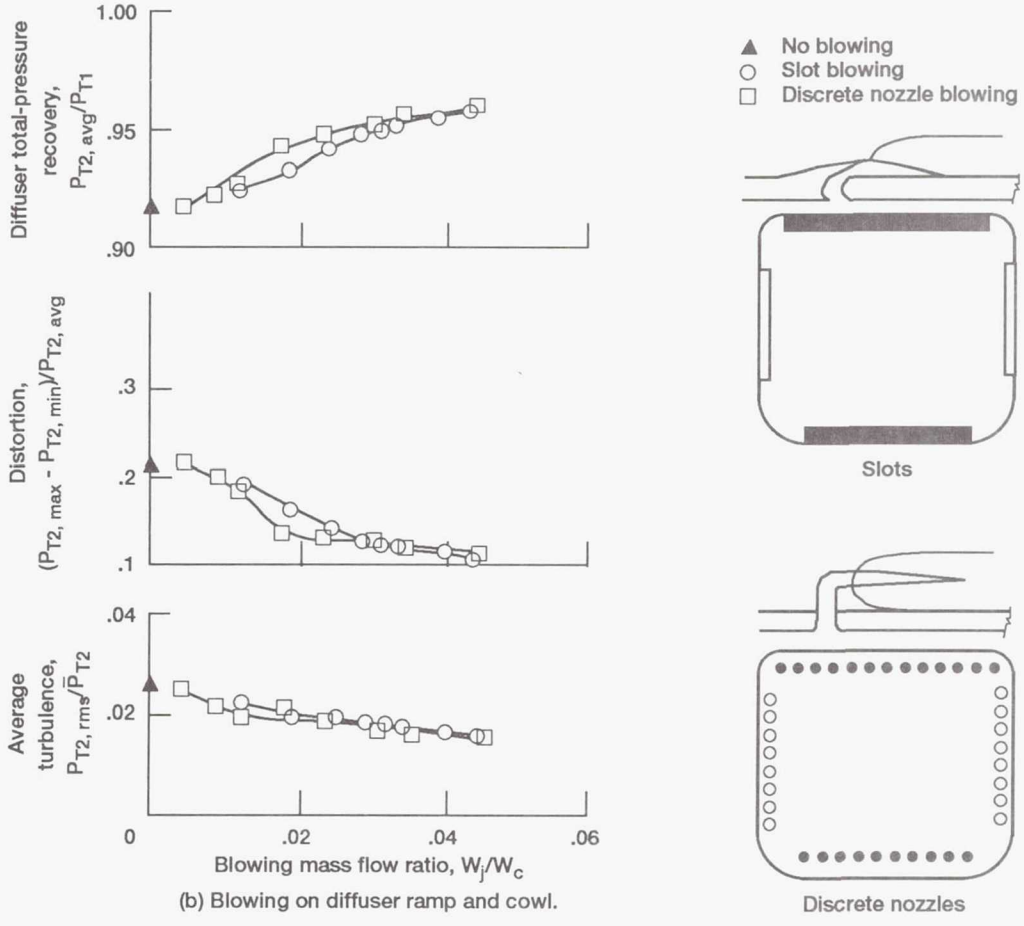

(b) Blowing on diffuser ramp and cowl.

Figure 23.—Continued.

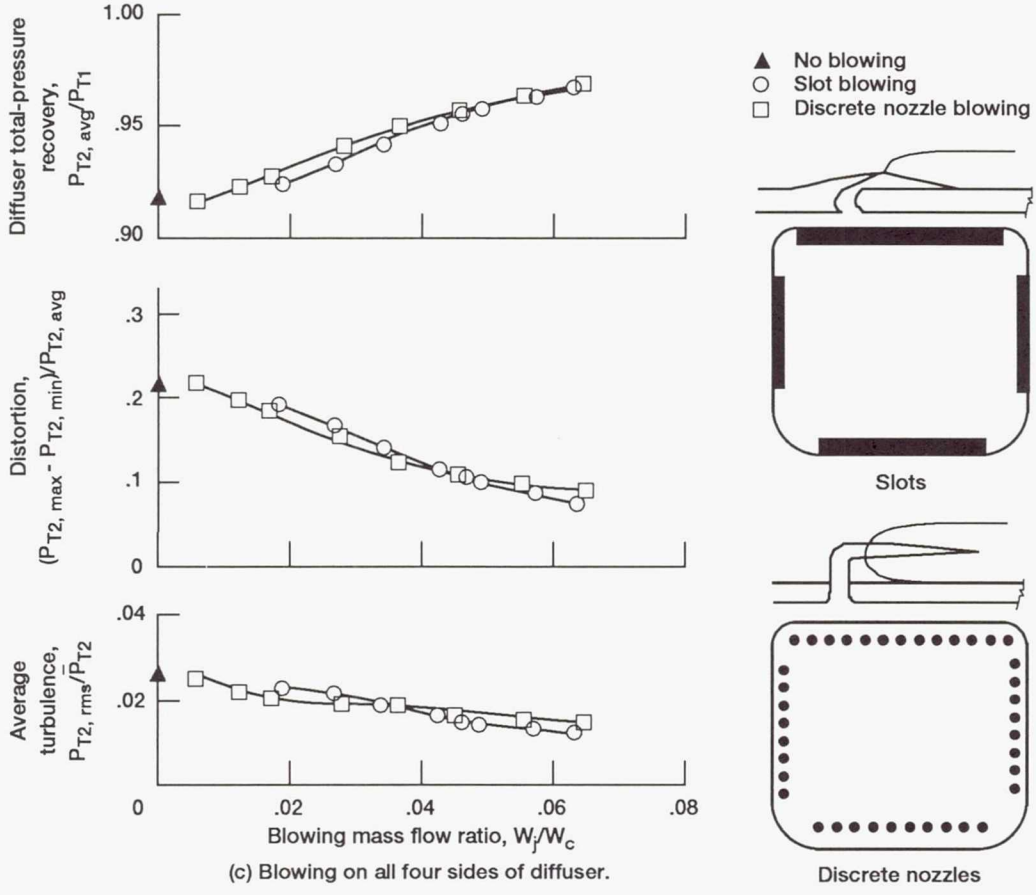

(c) Blowing on all four sides of diffuser.

Figure 23.—Concluded.

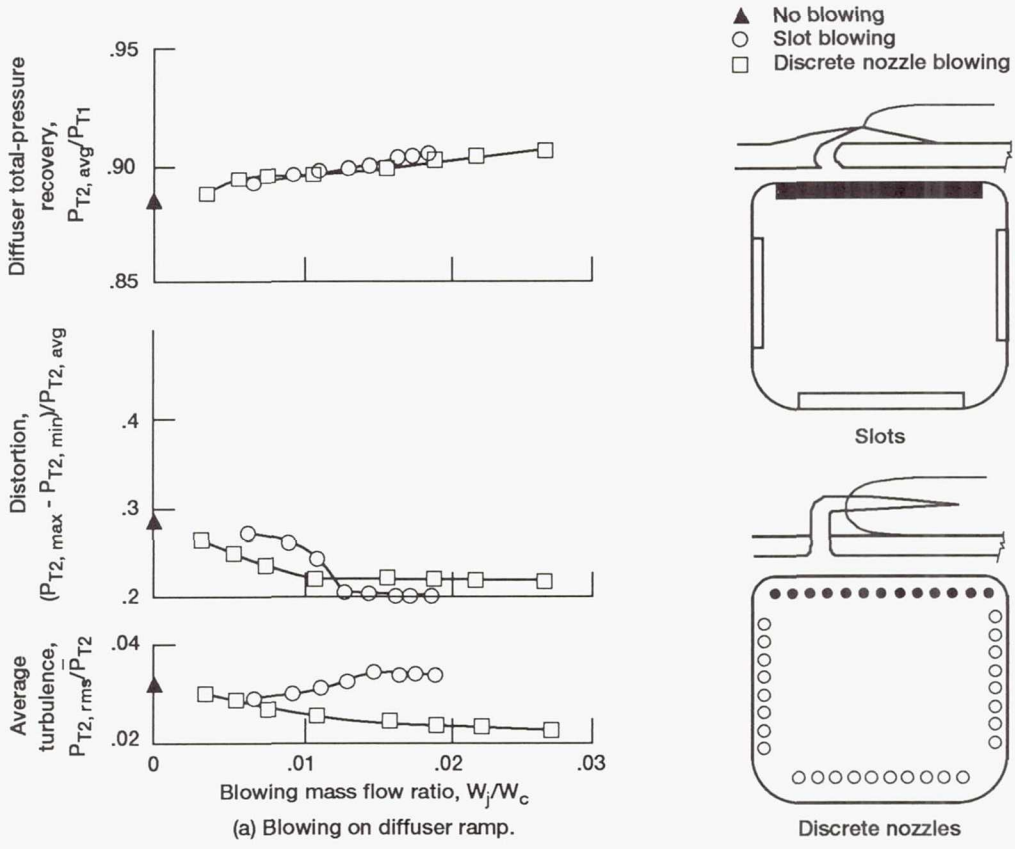

Figure 24.—Effect of blowing on diffuser performance for throat Mach number, M_1, of 0.88 and a Mach 2.2 ramp position. Free-stream Mach number, $M_0 = 0.12$; angle of attack, $\alpha = 0°$.

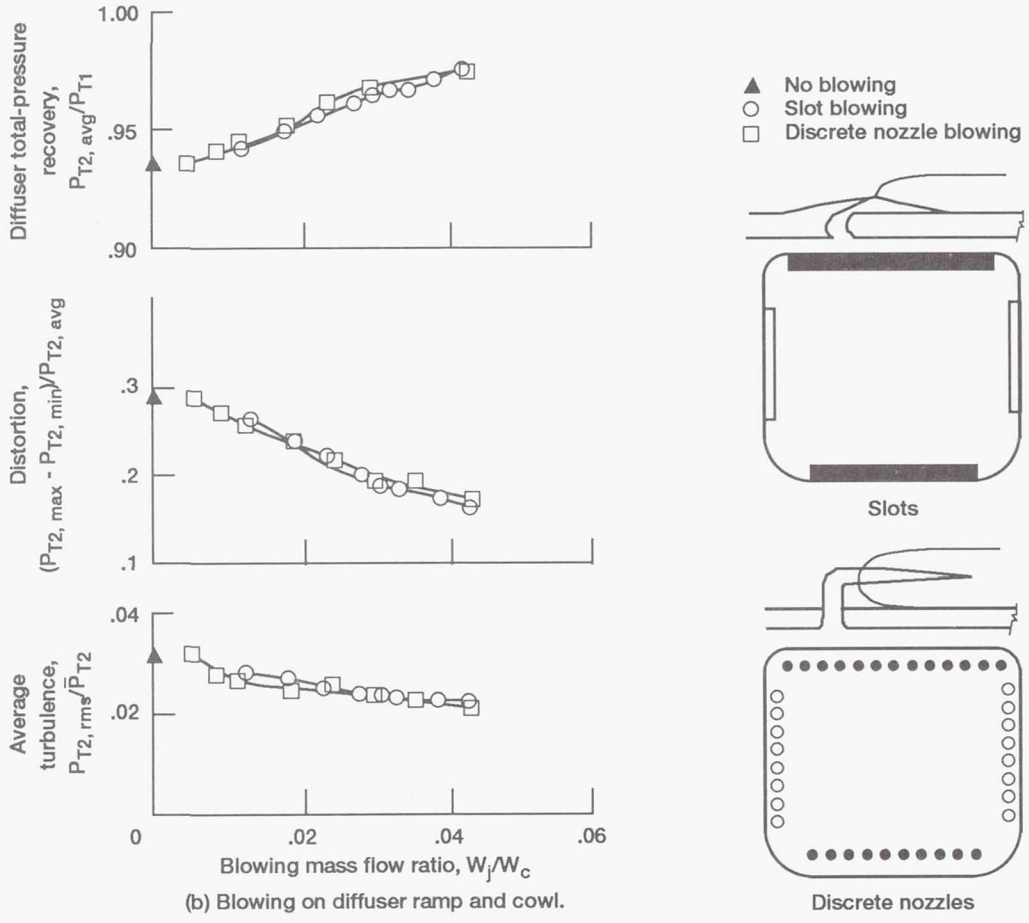

(b) Blowing on diffuser ramp and cowl.

Figure 24.—Continued.

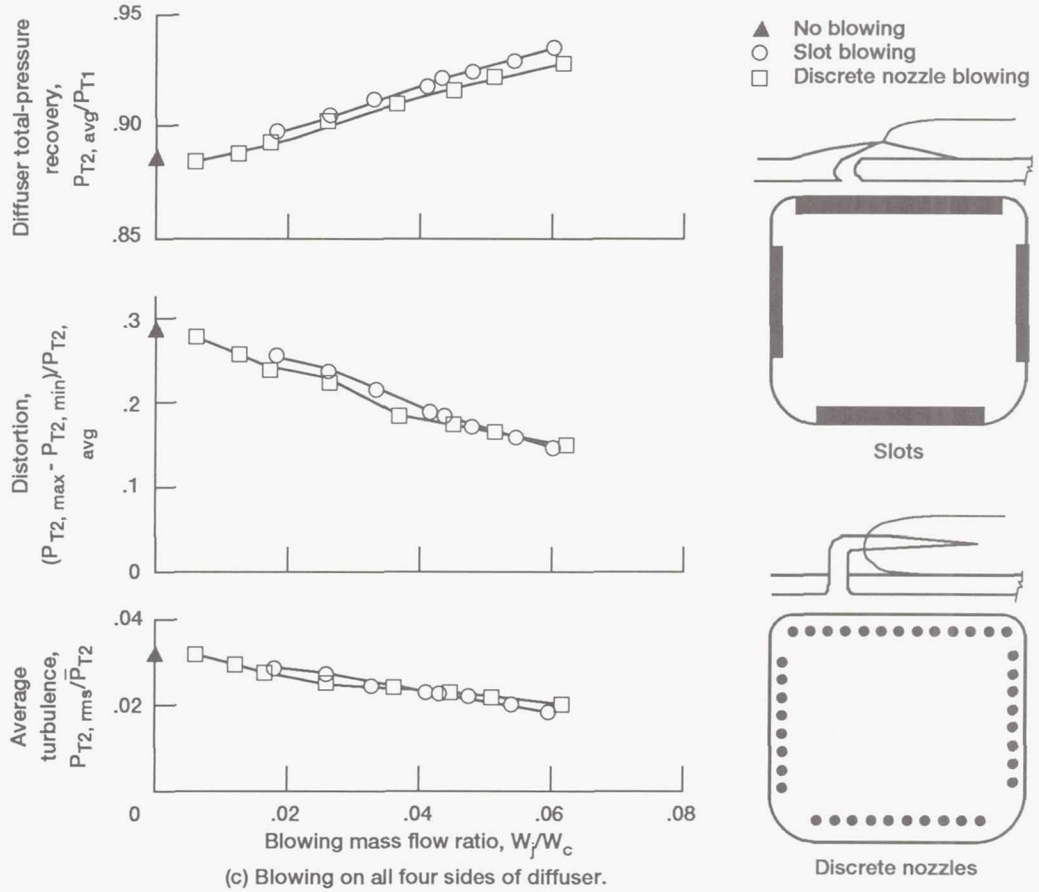

(c) Blowing on all four sides of diffuser.

Figure 24.—Concluded.

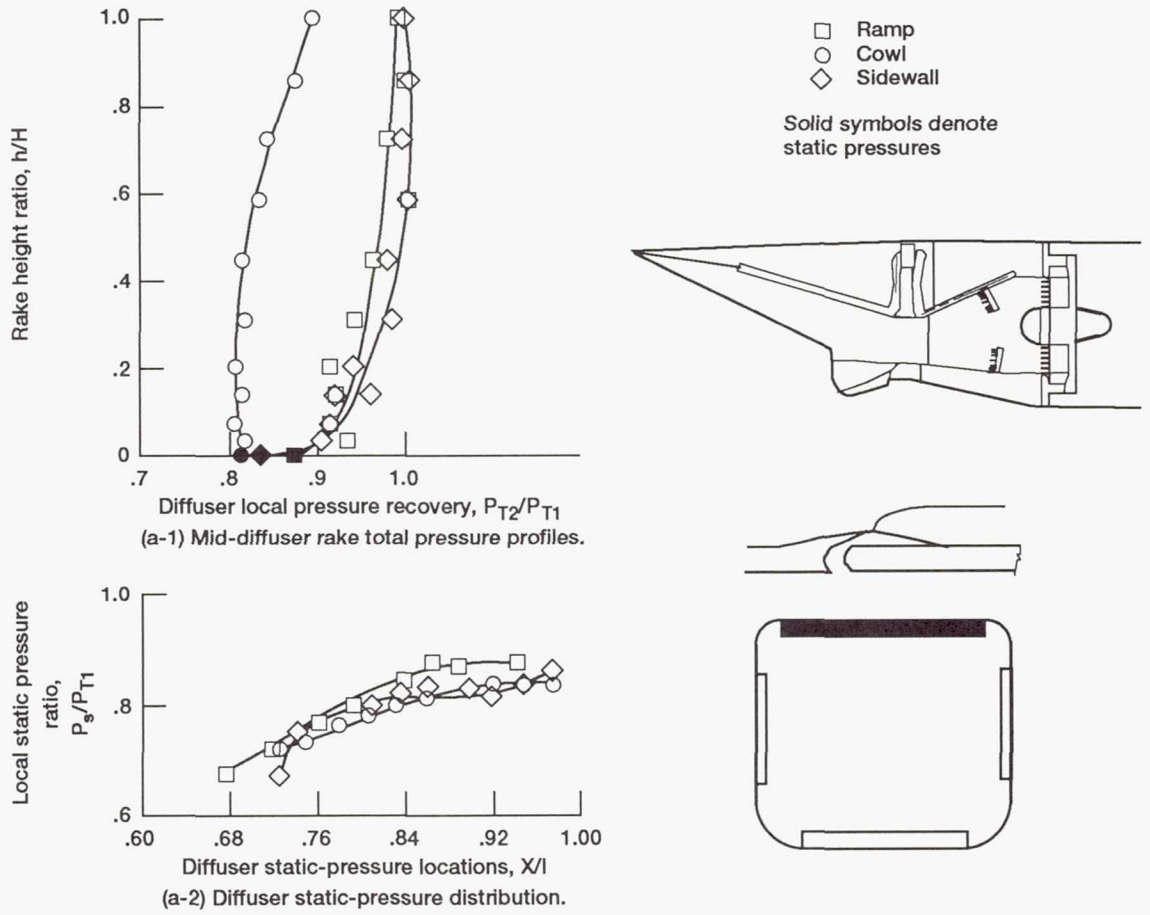

(a) Slot blowing on diffuser ramp only. Blowing mass flow ratio, $W_j/W_c = 0.020$; blowing pressure ratio, $P_j/P_{T1} = 2.4$.

Figure 25.—Effect of slot blowing on diffuser total rake and static-pressure distributions. Free-stream Mach number, $M_0 = 0.12$; average throat Mach number, $M_1 = 0.77$.

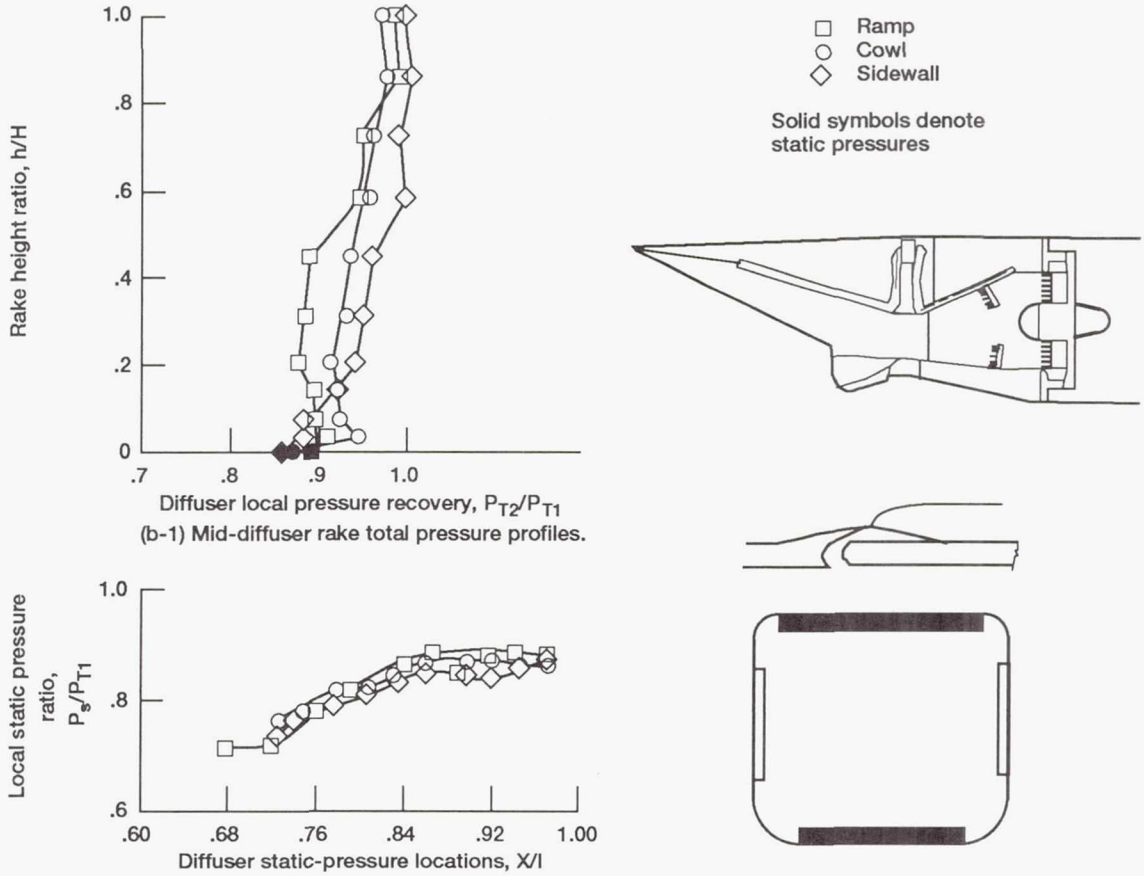

(b-1) Mid-diffuser rake total pressure profiles.

(b-2) Diffuser static-pressure distribution.

(b) Slot blowing on diffuser ramp and cowl. Blowing mass flow ratio, $W_j/W_c = 0.044$; blowing pressure ratio, $P_j/P_{T1} = 3.4$.

Figure 25.—Continued.

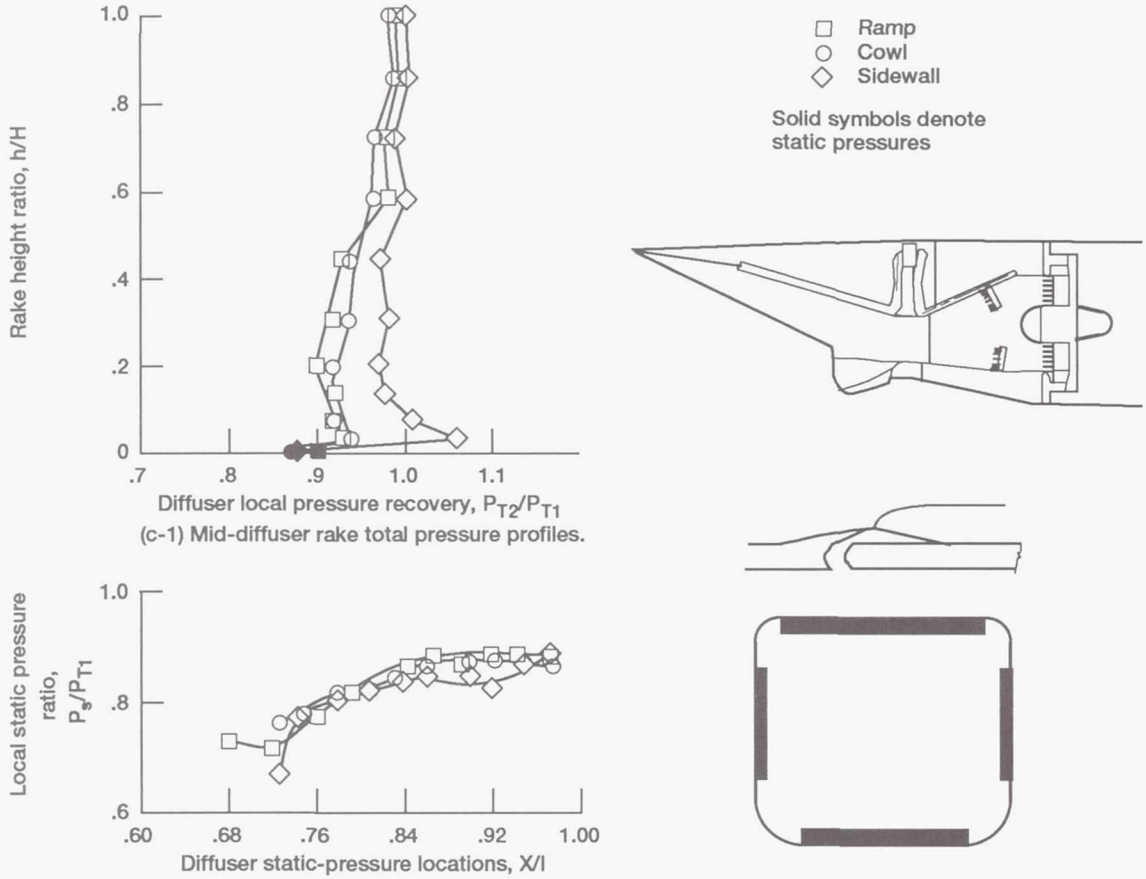

(c-1) Mid-diffuser rake total pressure profiles.

(c-2) Diffuser static-pressure distribution.

(c) Slot blowing on all four walls of diffuser. Blowing mass flow ratio, $W_j/W_c = 0.064$; blowing pressure ratio, $P_j/P_{T1} = 3.4$.

Figure 25.—Concluded.

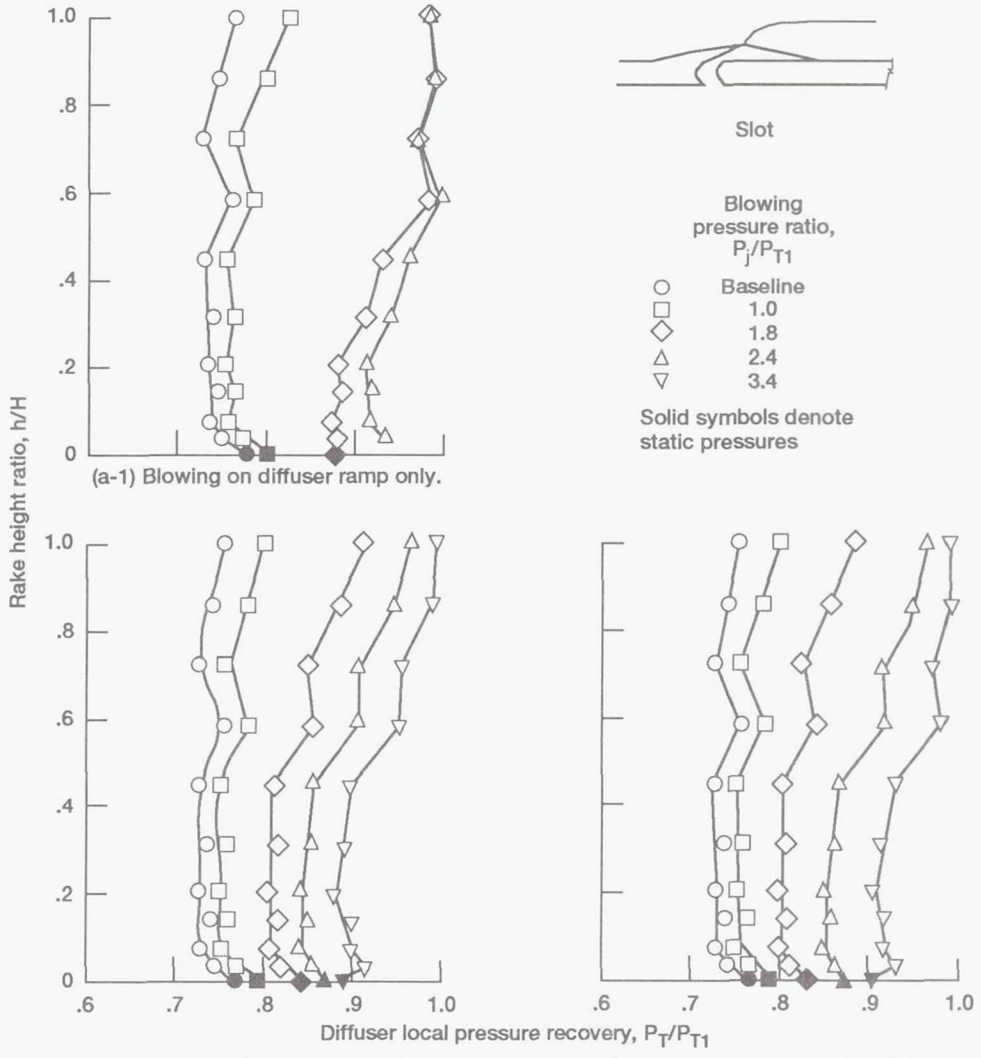

Figure 26.—Effect of blowing pressure ratio on the mid-diffuser ramp rake total-pressure recovery for a throat Mach number of 0.77. Free-stream Mach number, $M_0 = 0.12$.

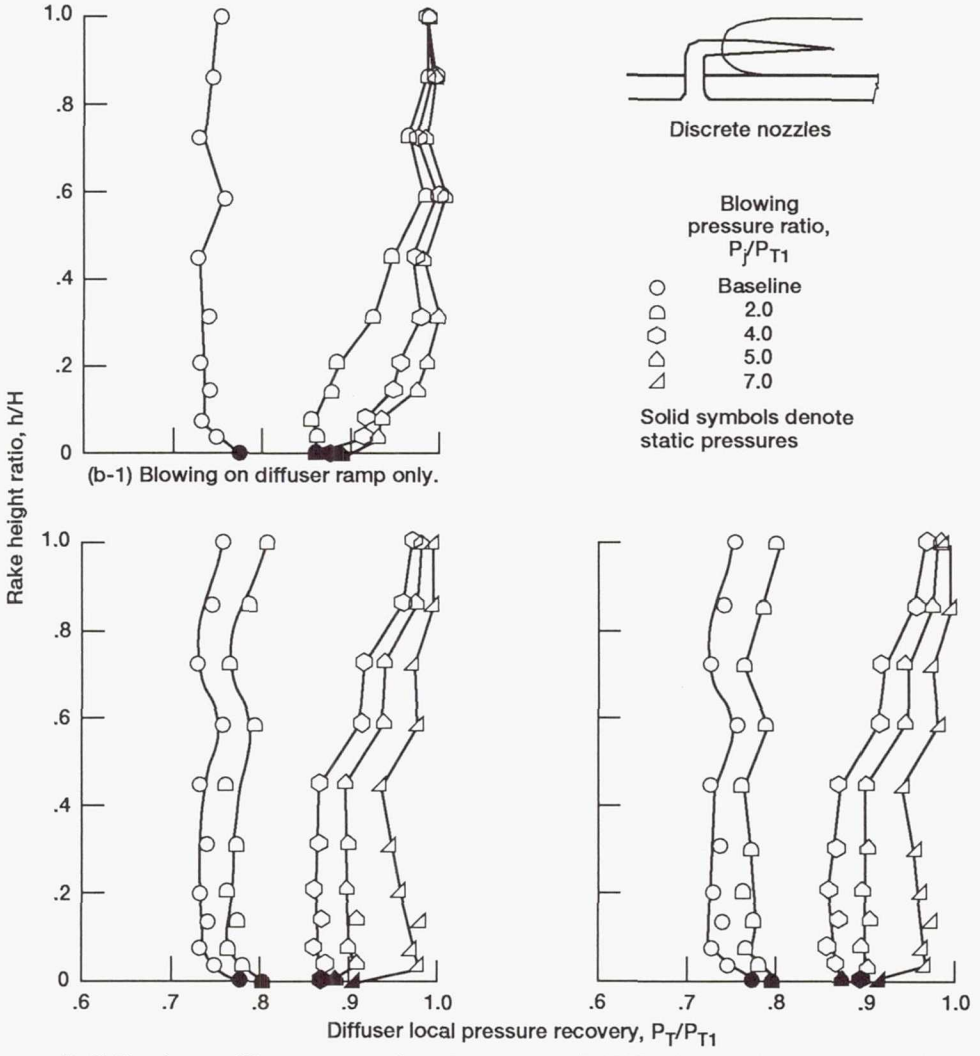

(b) Discrete nozzle blowing on various diffuser side walls.

Figure 26.—Concluded.

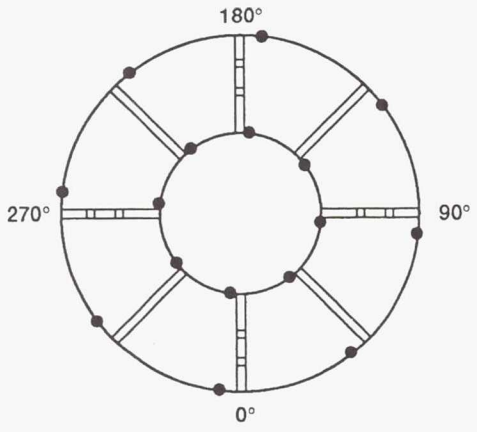

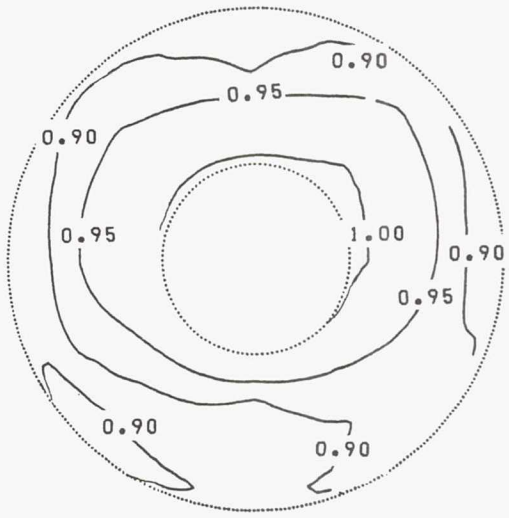

(a-1) Blowing mass flow ratio, W_j/W_c = 0.0094; diffuser pressure recovery, $P_{T2,\,avg}/P_{T1}$ = 0.933; distortion, $(P_{T2,\,max} - P_{T2,\,min})/P_{T2,\,avg}$ = 0.152.

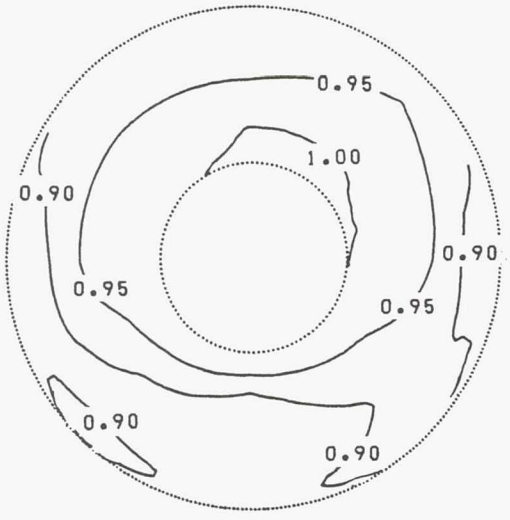

(a-2) Blowing mass flow ratio, W_j/W_c = 0.0156; diffuser pressure recovery, $P_{T2,\,avg}/P_{T1}$ = 0.934; distortion, $(P_{T2,\,max} - P_{T2,\,min})/P_{T2,\,avg}$ = 0.146.

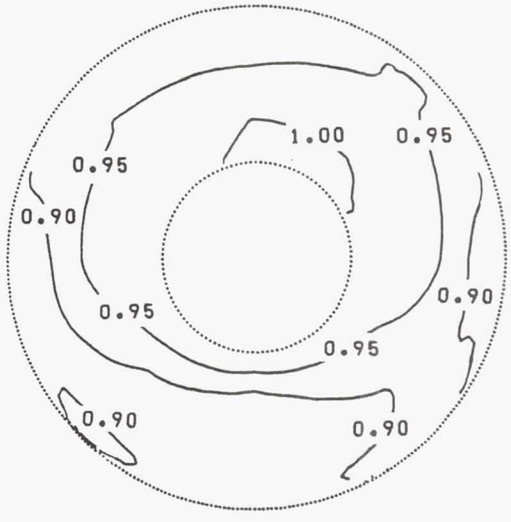

(a-3) Blowing mass flow ratio, W_j/W_c = 0.0199; diffuser pressure recovery, $P_{T2,\,avg}/P_{T1}$ = 0.936; distortion, $(P_{T2,\,max} - P_{T2,\,min})/P_{T2,\,avg}$ = 0.147.

(a) Slot blowing on diffuser ramp side.

Figure 27.—Engine-face rake total-pressure recovery contours for various blowing mass ratios and for a throat Mach number of 0.77. Mach 2.2 ramp position; free-stream Mach number, M_0 = 0.12; angle of attack, α = 0°. (Numbers denote pressure ratios.)

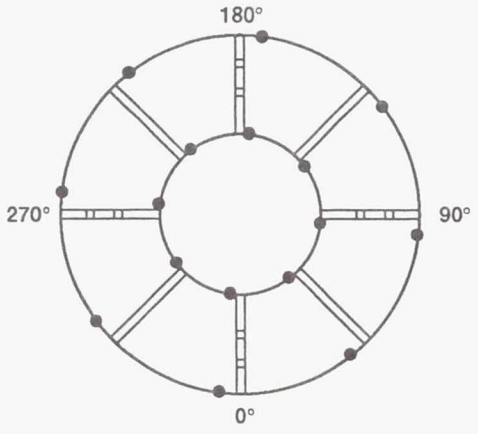

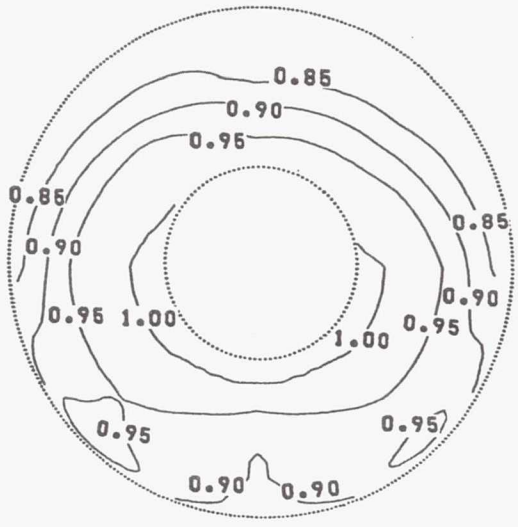

(b-1) Blowing mass flow ratio, $W_j/W_c = 0.012$; diffuser pressure recovery, $P_{T2, avg}/P_{T1} = 0.924$; distortion, $(P_{T2, max} - P_{T2, min})/P_{T2, avg} = 0.195$.

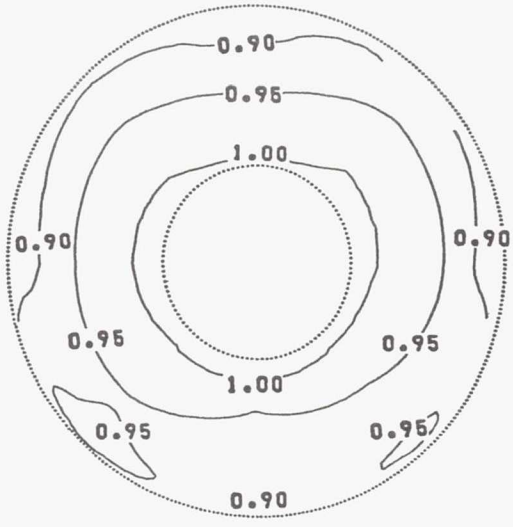

(b-2) Blowing mass flow ratio, $W_j/W_c = 0.032$; diffuser pressure recovery, $P_{T2, avg}/P_{T1} = 0.951$; distortion, $(P_{T2, max} - P_{T2, min})/P_{T2, avg} = 0.126$.

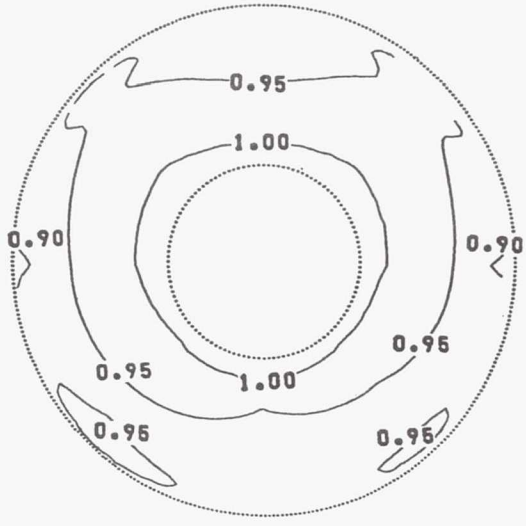

(b-3) Blowing mass flow ratio, $W_j/W_c = 0.044$; diffuser pressure recovery, $P_{T2, avg}/P_{T1} = 0.960$; distortion, $(P_{T2, max} - P_{T2, min})/P_{T2, avg} = 0.110$.

(b) Slot blowing on diffuser ramp and cowl.

Figure 27.—Continued.

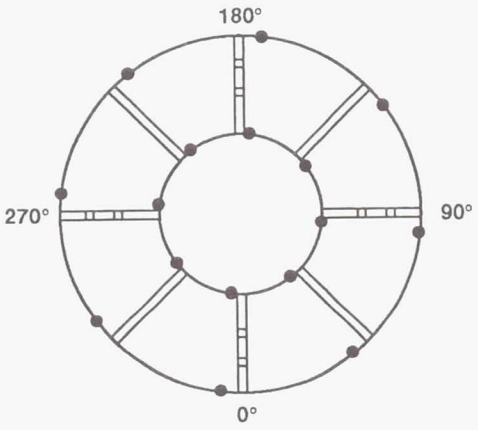

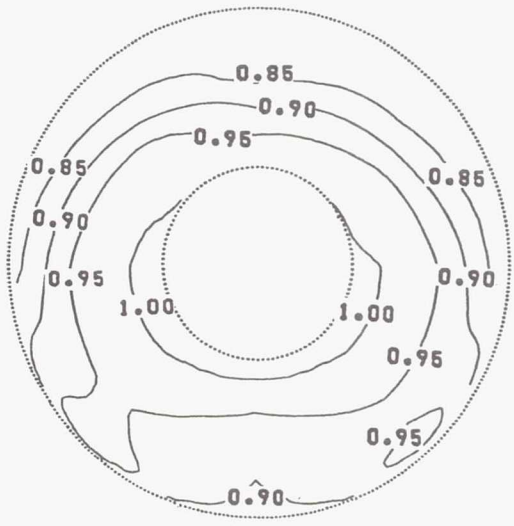

(c-1) Blowing mass flow ratio, W_j/W_c = 0.019; diffuser pressure recovery, $P_{T2,\,avg}/P_{T1}$ = 0.926; distortion, $(P_{T2,\,max} - P_{T2,\,min})/P_{T2,\,avg}$ = 0.194.

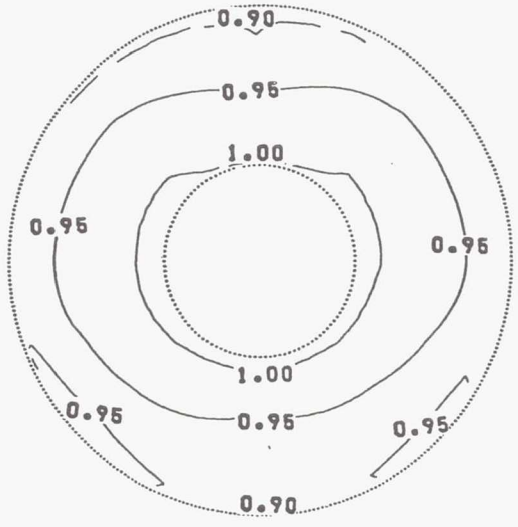

(c-2) Blowing mass flow ratio, W_j/W_c = 0.046; diffuser pressure recovery, $P_{T2,\,avg}/P_{T1}$ = 0.957; distortion, $(P_{T2,\,max} - P_{T2,\,min})/P_{T2,\,avg}$ = 0.107.

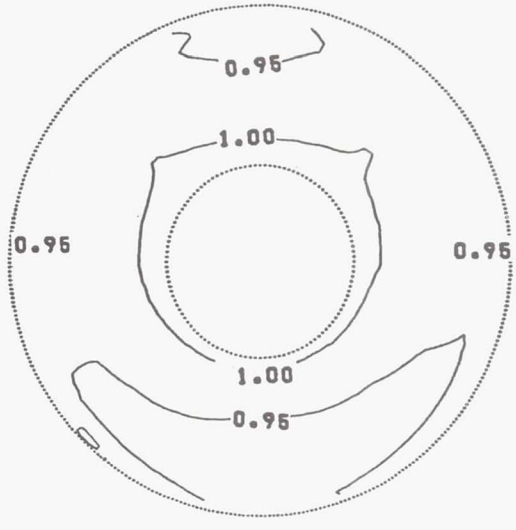

(c-3) Blowing mass flow ratio, W_j/W_c = 0.064; diffuser pressure recovery, $P_{T2,\,avg}/P_{T1}$ = 0.970; distortion, $(P_{T2,\,max} - P_{T2,\,min})/P_{T2,\,avg}$ = 0.075.

(c) Slot blowing on all four walls of diffuser.

Figure 27.—Continued.

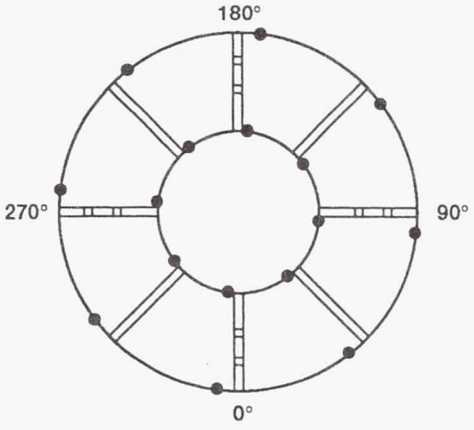

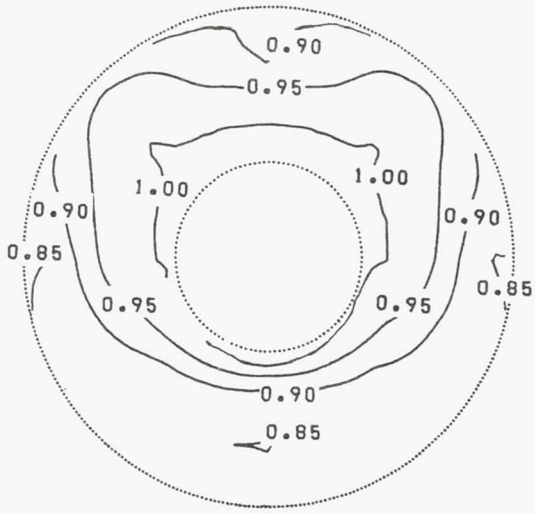

(d-1) Blowing mass flow ratio, W_j/W_c = 0.0080; diffuser pressure recovery, $P_{T2,\,avg}/P_{T1}$ = 0.926; distortion, $(P_{T2,\,max} - P_{T2,\,min})/P_{T2,\,avg}$ = 0.166.

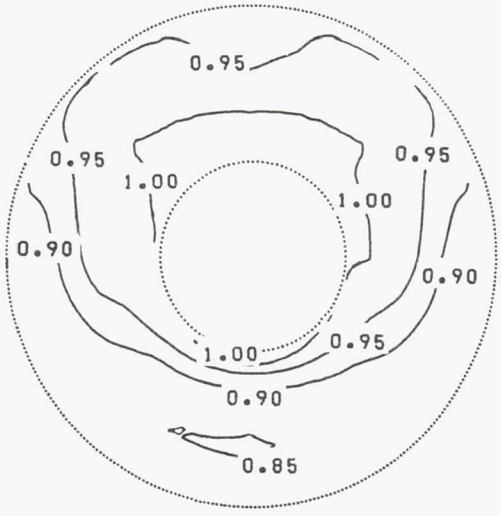

(d-2) Blowing mass flow ratio, W_j/W_c = 0.0160; diffuser pressure recovery, $P_{T2,\,avg}/P_{T1}$ = 0.929; distortion, $(P_{T2,\,max} - P_{T2,\,min})/P_{T2,\,avg}$ = 0.168.

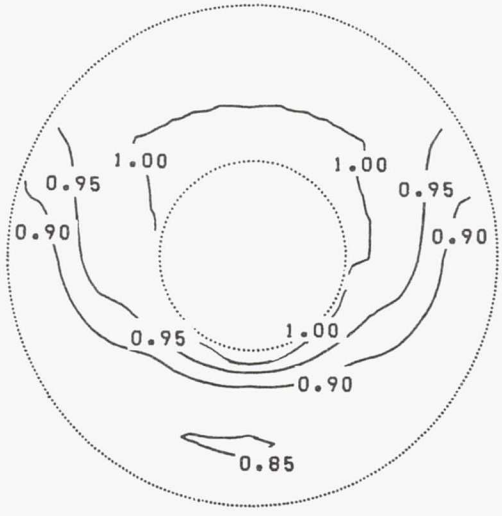

(d-3) Blowing mass flow ratio, W_j/W_c = 0.0201; diffuser pressure recovery, $P_{T2,\,avg}/P_{T1}$ = 0.931; distortion, $(P_{T2,\,max} - P_{T2,\,min})/P_{T2,\,avg}$ = 0.168.

(d) Discrete nozzle blowing on ramp side of diffuser.

Figure 27.—Continued.

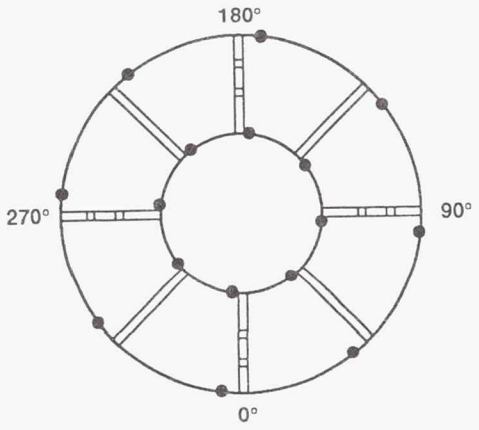

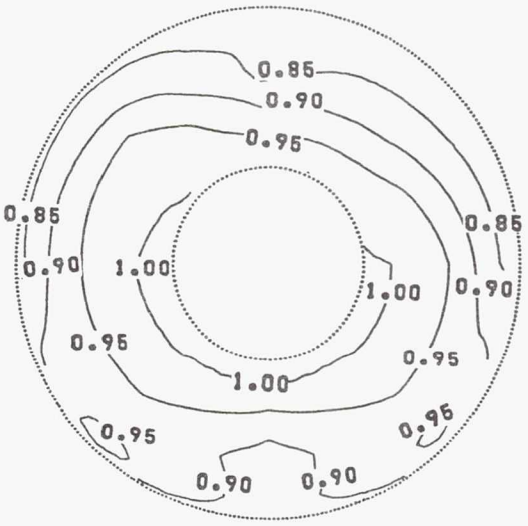

(e-1) Blowing mass flow ratio, $W_j/W_c = 0.012$; diffuser pressure recovery, $P_{T2, avg}/P_{T1} = 0.927$; distortion, $(P_{T2, max} - P_{T2, min})/P_{T2, avg} = 0.184$.

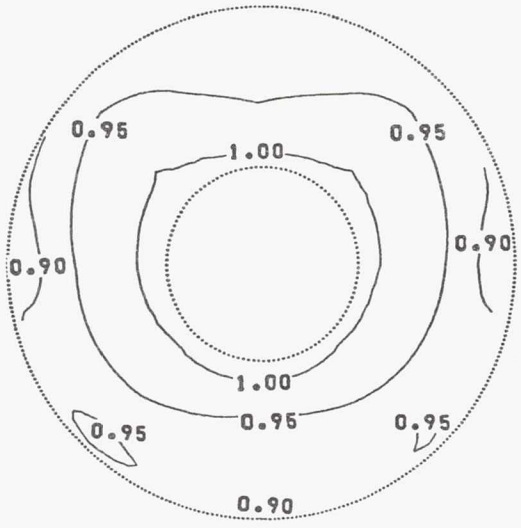

(e-2) Blowing mass flow ratio, $W_j/W_c = 0.031$; diffuser pressure recovery, $P_{T2, avg}/P_{T1} = 0.952$; distortion, $(P_{T2, max} - P_{T2, min})/P_{T2, avg} = 0.126$.

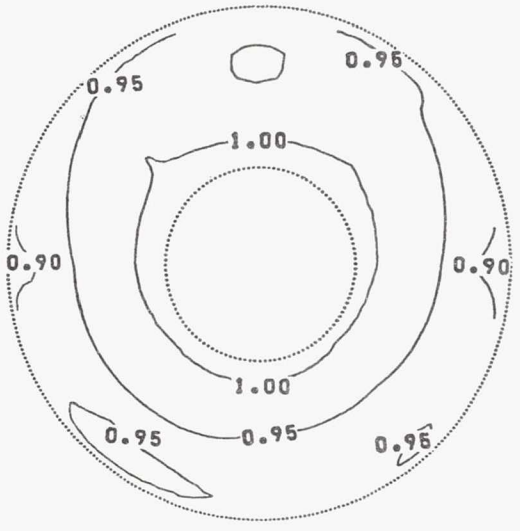

(e-3) Blowing mass flow ratio, $W_j/W_c = 0.045$; diffuser pressure recovery, $P_{T2, avg}/P_{T1} = 0.961$; distortion, $(P_{T2, max} - P_{T2, min})/P_{T2, avg} = 0.113$.

(e) Discrete nozzle blowing on diffuser ramp and cowl.

Figure 27.—Continued.

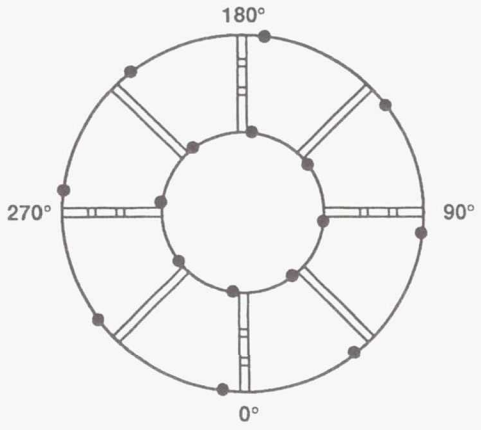

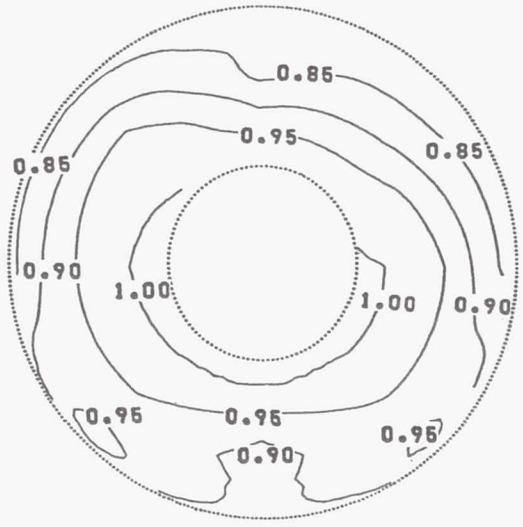

(f-1) Blowing mass flow ratio, W_j/W_c = 0.017; diffuser pressure recovery, $P_{T2,\,avg}/P_{T1}$ = 0.928; distortion, $(P_{T2,\,max} - P_{T2,\,min})/P_{T2,\,avg}$ = 0.184.

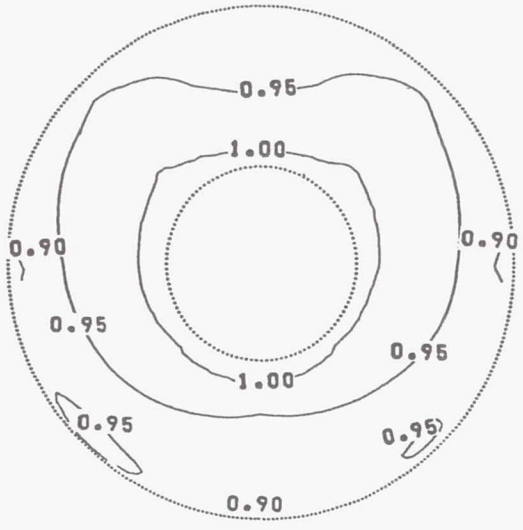

(f-2) Blowing mass flow ratio, W_j/W_c = 0.045; diffuser pressure recovery, $P_{T2,\,avg}/P_{T1}$ = 0.958; distortion, $(P_{T2,\,max} - P_{T2,\,min})/P_{T2,\,avg}$ = 0.107.

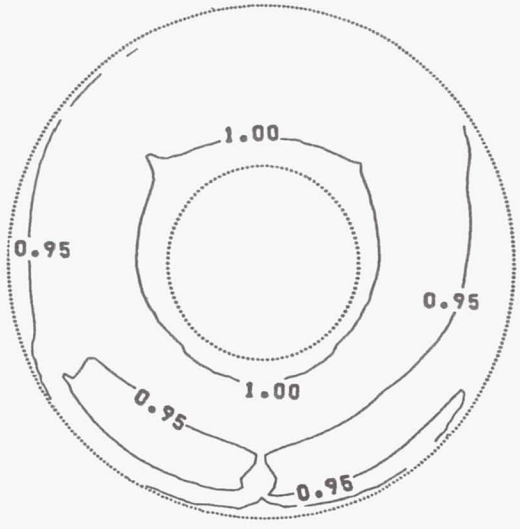

(f-3) Blowing mass flow ratio, W_j/W_c = 0.065; diffuser pressure recovery, $P_{T2,\,avg}/P_{T1}$ = 0.971; distortion, $(P_{T2,\,max} - P_{T2,\,min})/P_{T2,\,avg}$ = 0.087.

(f) Discrete nozzle blowing on all four walls of diffuser.

Figure 27.—Concluded.

REPORT DOCUMENTATION PAGE

Form Approved
OMB No. 0704-0188

1. AGENCY USE ONLY (*Leave blank*)	2. REPORT DATE	3. REPORT TYPE AND DATES COVERED
	March 1993	Technical Paper

4. TITLE AND SUBTITLE

Analytical and Experimental Studies of a Short Compact Subsonic Diffuser for a Two-Dimensional Supersonic Inlet

5. FUNDING NUMBERS

WU 505–62–71

6. AUTHOR(S)

Chanthy Iek, Richard R. Burley, and Albert L. Johns

7. PERFORMING ORGANIZATION NAME(S) AND ADDRESS(ES)

National Aeronautics and Space Administration
Lewis Research Center
Cleveland, Ohio 44135–3191

8. PERFORMING ORGANIZATION REPORT NUMBER

E–7111

9. SPONSORING/MONITORING AGENCY NAMES(S) AND ADDRESS(ES)

National Aeronautics and Space Administration
Washington, D.C. 20546–0001

10. SPONSORING/MONITORING AGENCY REPORT NUMBER

NASA TP–3247

11. SUPPLEMENTARY NOTES

Responsible person, Chanthy Iek, (216) 433–3897.

12a. DISTRIBUTION/AVAILABILITY STATEMENT

Unclassified - Unlimited
Subject Category 02

12b. DISTRIBUTION CODE

13. ABSTRACT ***(Maximum 200 words)***

An experimental study of a two-dimensional supersonic inlet with a short compact subsonic diffuser, length to exit diameter (dl/d) ratio of 1.25, was conducted to (1) investigate the impact of the short diffuser on inlet performance at low speeds and (2) assess the diffuser subsonic performance for a simulated diffuser flow corresponding to high-speed inlet conditions near the design flight Mach number of 2.2. For the low-speed testing, a drooped lip was employed to improve the inlet performance at a high angle of attack. For the simulated high-speed testing, air was blown through slots or discrete nozzles as an active boundary-layer control. The results from the low-speed performance test were compared with the results from a previous test program on the same inlet with a long subsonic diffuser ($dl/d \approx 4.5$). The comparison indicates that inlet recovery was not affected by the use of the short diffuser for either the baseline (no droop) or the drooped cowl lip configuration. However, the inlet baseline distortion for the short diffuser configuration was substantially higher than for the long diffuser. A comparison of the two configurations with a 70° drooped lip showed no significant difference in distortion. For the portion of the experimental program in which diffuser conditions for high-speed flight were simulated, diffuser-induced flow separation occurred. This separation was predicted from an analytical study that used the Hess potential flow panel method and the Herring two-dimensional boundary-layer analysis computer codes. The flow separated mainly on the diffuser ramp. Subsequent tests in which boundary-control systems were utilized showed that blowing with either slots or discrete nozzles could suppress the flow separation in the short subsonic diffuser, thereby substantially improving the diffuser performance.

14. SUBJECT TERMS	15. NUMBER OF PAGES
Two-dimensional V/STOL inlet; Short diffuser; Droop lips; Slot blowing BLC; Nozzle blowing BLC	68
	16. PRICE CODE: A04

17. SECURITY CLASSIFICATION OF REPORT	18. SECURITY CLASSIFICATION OF THIS PAGE	19. SECURITY CLASSIFICATION OF ABSTRACT	20. LIMITATION OF ABSTRACT
Unclassified	Unclassified	Unclassified	

NSN 7540-01-280-5500

Standard Form 298 (Rev. 2-89)
Prescribed by ANSI Std. Z39-18
298-102

NASA-Langley, 1993